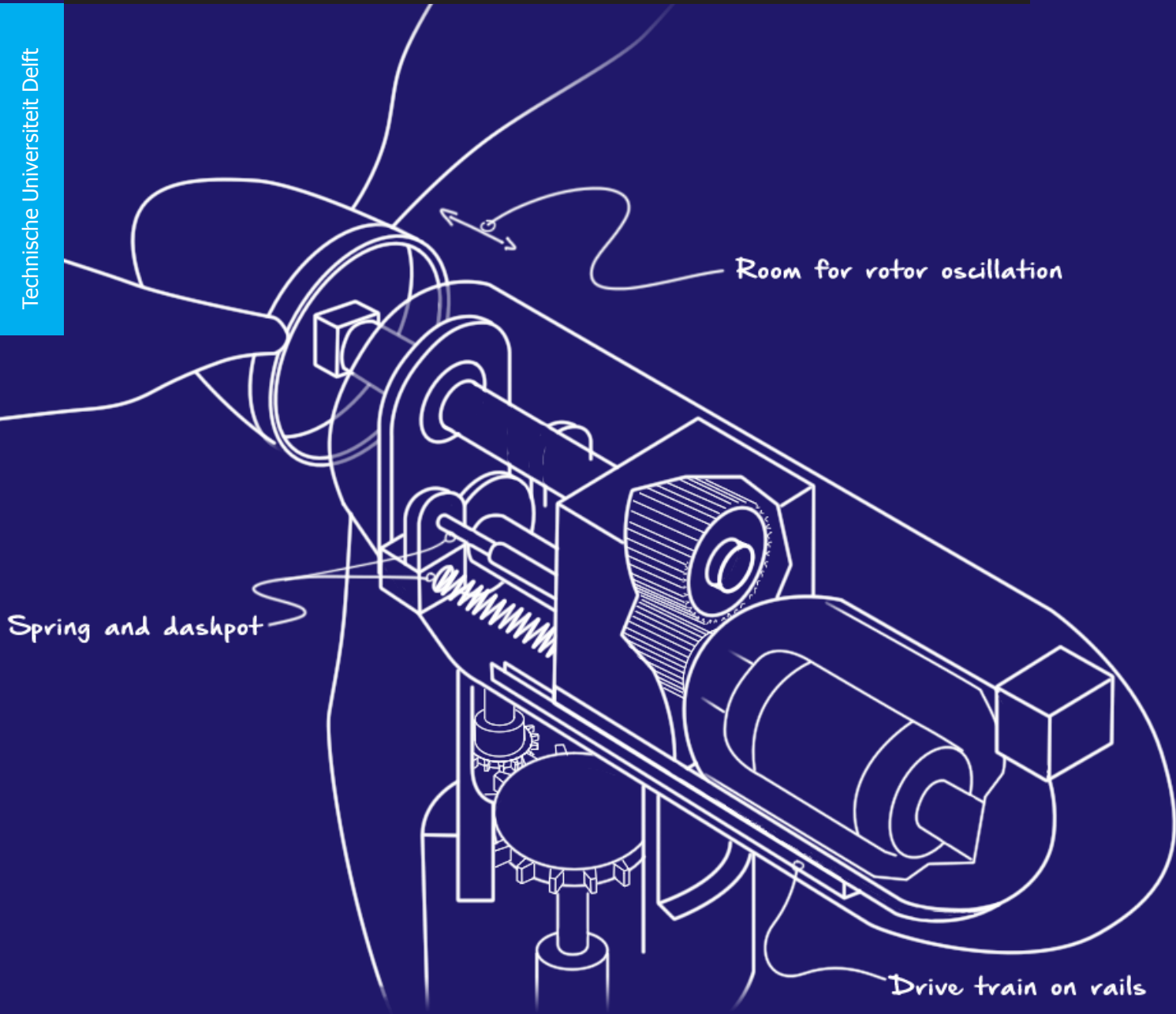


Dynamic analysis of two innovative tuned mass damper systems for a wind turbine using a 2-DOF model

A.F. Leiro

Technische Universiteit Delft



Dynamic analysis of two innovative tuned mass damper systems for a wind turbine using a 2-DOF model

by

A.F. Leiro

in partial fulfillment of the requirements for the degree of

Master of Science
in Sustainable Energy Technology

at the Delft University of Technology,
to be defended publicly on Tuesday February 13, 2018 at 10:30 AM.

Supervisor:	Dr. ir. M. B. Zaaijer	
Thesis committee:	Prof. dr. G. J. W. van Bussel,	TU Delft
	Dr. ir. H. F. Veldkamp,	TU Delft
	Ir. J. A. Melkert,	TU Delft

This thesis is confidential and cannot be made public until February 13, 2018.

An electronic version of this thesis is available at <http://repository.tudelft.nl/>.

Abstract

Reducing the cost of constructing wind turbines, as well as extending their design life, are two ways of reducing the cost of energy from wind. To achieve this, this project tested two innovative tuned-mass damper systems, which reduce resonance of the tower, and do so minimizing additional mass needed on the nacelle. These TMD systems allow the generator and full drive-train to oscillate with respect to the tower top. MATLAB was used to model these turbine-damper assemblies as simple 2-degree-of-freedom systems excited by thrust signals extracted from the FAST aeroelastic simulator. Furthermore, it was found that both tuned mass damper configurations have a net positive effect on the tower behaviour, both achieving double digit fatigue percentage reductions. It was also found that neither of these systems put significant burdens on acceleration-sensitive components, such as the generator and gear box. Two issues to constructing these devices may reside in their need for additional space for oscillations, as well as aggravated tip deflections in the case of the oscillating rotor-drive-train.

Acknowledgement

I would like to express my deep gratitude to Prof. Michiel Zaaijer and Dick Veldkamp for their unrelenting support of my project. Their ceaseless advice, immensely constructive comments and Socratic questioning of my assumptions have allowed me to focus my productivity and elevate the level of this report.

I am grateful towards the examination committee, including G.J.W. van Bussel and J.A. Melkert for taking the time to evaluate this document and challenge my assumptions and decisions during the defense.

Finally I would like to give a heartfelt thank you to my friends and family, whose support, through laughter and kindness, kept me going through the entire process.

*Andres Leiro
Delft, January 2018*

Contents

List of Figures	ix
1 Introduction	1
2 Objectives and research questions	5
3 Methodology	7
3.1 Baseline fatigue	7
3.2 Fatigue reduction using dampers	7
3.2.1 Configuration 1	8
3.2.2 Configuration 2	8
3.3 Calculating fatigue	9
3.3.1 Rainflow counting	10
3.3.2 Miner's rule	10
3.3.3 FDEL	10
4 Review of tuned mass dampers	13
4.1 Introduction to Tuned Mass Dampers	14
4.2 Modeling systems of 1 and 2 degrees of freedom	14
4.3 Dynamic Amplification Factor	16
4.4 Optimal Tuning	17
4.5 Optimizing the TMD system	18
4.6 Additional method for finding steady state response	19
4.7 Concluding remarks on TMDs in relation to other damping methods	20
5 Definition and modeling of the NREL 5MW turbine	23
5.1 Definition and Relevant Parameters	24
5.2 FAST	24
5.3 Modeling the turbine in MATLAB	24
5.3.1 Deriving the general stiffness	24
5.3.2 Modeling Wind	25
5.3.3 Modeling thrust force	25
5.3.4 Modeling aerodynamic damping	26
5.4 Modeling Loads on a Super-stiff Turbine	28
6 Validation Of the MATLAB Model	29
6.1 Steady state dynamic amplification factor as function of excitation frequency	29
6.2 Comparison of MATLAB and FAST	30
6.2.1 Stiffness adaptation	31
6.2.2 Motions above rated wind speed	32
6.2.3 Behaviour below cut-in wind speed	34
6.3 Behavior under FAST-given thrust excitation	35
6.4 Simulating Behaviour with Wind Excitation	36
6.5 Summary of MATLAB validation	38
7 Experimental Results	39
7.1 Values for Optimal Behavior	39
7.2 Behavior and Fatigue with Tuned Mass Dampers	39
7.2.1 Effect on Tower-top Motions	39
7.2.2 Effect on Tower Fatigue Life	40
7.2.3 Motions of the Dampers	44

7.3	Discussion	45
7.3.1	Fatigue reduction with TMDs	45
7.3.2	Comments on the Motions of the Absorbers	46
7.3.3	Construction	49
8	Conclusions and Recommendations for Future Work	53
8.1	Concluding Remarks	53
8.2	Recommendations for Future Work	54
	Bibliography	55
A	Motions and PSDs at All Wind Speeds	57
A.1	All motions for FAST and MATLAB thrust-excited simulations	57
A.2	All PSDs for FAST and MATLAB thrust-excited simulations	68
B	Modeling Using Wind Excitations	75
B.1	Failure of Simulations with Wind Excitation	75
B.1.1	Rotor point wind averaging	76
B.2	Loads on a Super-stiff Turbine	78
B.3	Additional examples of wind-excited simulations	78

List of Figures

1.1	World energy use by source. Source: EIA [1].	1
1.2	Average auction prices for solar PV and onshore wind. Source: IEA [2].	2
3.1	Drawing of Configuration 1: the generator oscillates with respect to the nacelle [3]. . .	8
3.2	Drawing of Configuration 2: the drive train oscillates with respect to the nacelle	8
3.3	Plot of the moment at the tower base as function of displacement from two FAST simu- lations.	9
3.4	Rainflow counting on a strain signal.	10
3.5	Weibull curve with $k=2$ and $a=8$	11
4.1	Dynamic amplification of a 1 degree-of-freedom system with different damping levels .	13
4.2	Diagram of a system with a TMD, as a 2 degree of freedom system	14
4.3	Thrust curves for several reference turbines	15
4.4	Displacements of a mass without and with TMD's of increasing mass, with a damping ratio of $\zeta_a = 2\%$	16
4.5	Dynamic amplification of a 1DOF system with $\zeta = 2\%$	16
4.6	Dynamic amplification of a system without and with a TMD	17
4.7	Optimal absorber parameters [4]	18
4.8	DAF with Warburton optimal and sub-optimal absorber parameters. $\mu = 0.02047$, $f_{opt} =$ 0.9799 $\zeta_{opt} = 0.0871$	18
4.9	Dynamic amplification with $\mu = 0.02047$, with Warburton optimal values and optimized values.	19
4.10	Dynamic amplification of a system with $\mu = 0.4864$ with Warburton optimal values and optimized values, as calculated with the Brown method.	19
4.11	Different damping systems can be used to protect structures. Source: Rezaee and Aly [5]	21
4.12	Damping effects of pitch and torque damping on tower fore-aft and side-side motions by Liu et al. [6]	21
5.1	Rendering of the NREL 5MW reference turbine	23
5.2	Power spectral density of a typical wind signal	25
5.3	Stepped wind signal	26
5.4	Thrust curve extracted from a stepped wind FAST simulation	26
5.5	Transient signal from which the damping at that wind speed is extracted by calculating the logarithmic decrement.	27
5.6	Original damping coefficient curve for the turbine FA motions at each wind speed. This curve was modified as shown in Chapter 6.	27
6.1	Steady-state dynamic amplification of the MATLAB turbine model with a TMD (Configu- ration 1), calculated according to Brown university formulas compared to the theoretical values by Ayorinde et al.	30
6.2	DAF of mass 1 in Configuration 2 as calculated with the Brown method and in the time domain.	30
6.3	Displacements from FAST and MATLAB of the turbine and 1DOF model under a stepped wind signal, with several aspects that need addressing.	31
6.4	Simulations on FAST and MATLAB of the turbine and 1DOF model excited under a stepped wind signal.	32
6.5	Detail of Figure 6.4	32
6.6	Thrust signals from FAST and produced by MATLAB under the same stepped wind signal	33

6.7	Rotor and generator powers from FAST, as the turbine transitions from partial-load to full-load at $t = 660s$.	33
6.8	Blade pitch angle from FAST, as the turbine transitions from partial-load to full-load at $t = 660s$.	33
6.9	Motion signal of the 1DOF system excited by a thrust signal extracted from FAST, compared to the motions of the FAST model under the same thrust signal.	34
6.10	Detail of Fig 6.9	34
6.11	Displacement of MATLAB model with previously calculated damping, excited by the thrust signal from a 7mps FAST simulation, compared to original motions from FAST	35
6.12	Original and improved damping curve fits for the MATLAB model	35
6.13	Motions of the thrust-excite MATLAB model with improved damping. The wind speeds are displayed in vertical lines.	36
6.14	Displacement of MATLAB model with new damping, excited by the thrust signal from a 7mps FAST simulation, compared to original motions from FAST.	36
6.15	PSD of the thrust excited MATLAB model at 5, 10, 15 and 20 [m/s], against those of FAST, plotted in dB.	37
6.16	PSDS of FAST and MATLAB thrust-excited signal compared to the 1-pt wind-excited signal, for a 10mps wind simulation (same as above)	37
6.17	Fore-aft motions of FAST and MATLAB thrust-excited signal for a 10mps wind simulation (same as Figure 6.16)	37
6.18	FDEL of FAST and MATLAB model before the addition of a TMD. The discrepancies are due to the deviating relationship between displacement and moment at the tower base.	38
7.1	Displacement of the MATLAB model turbine without and with TMDs at 10mps.	40
7.2	Detail of Figure 7.1.	40
7.3	Displacement of the MATLAB model turbine without and with TMDs at 20mps.	41
7.4	Power spectral densities of the MATLAB model turbine without and with TMDs at 10mps.	41
7.5	Power spectral densities of the MATLAB model turbine without and with TMDs at 20mps.	42
7.6	Fatigue equivalent loads for 20yr lifetime of the MATLAB model without and with TMDs.	42
7.7	Weibull distribution curve.	42
7.8	Damage according to Miner's rule for each load case with the TMD-less Configuration 1, and TMD Configurations 1 and 2.	43
7.9	Displacements of the tower top and generator in Configuration, 1 under 25[m/s] winds.	44
7.10	Displacements of the generator against the tower top in Configuration 1, under 25[m/s] winds.	45
7.11	Displacements of the tower-top and drive-train-damper of Configuration 2, under 25[m/s] winds.	45
7.12	Displacements of the rotor and drive train damper against the tower top in Configuration 2, under 25[m/s] winds.	46
7.13	Tower top displacements of Configurations 1 and 2, under 25[m/s] winds.	46
7.14	Close-up of Figure 7.13	46
7.15	Power spectral densities of the signals on Figure 7.13	47
7.16	Accelerations of the TMD-less tower top compared to the accelerations of the generator-absorber in Configuration 1. under 12[m/s] winds	48
7.17	Out of plane blade tip deflections at 12 [m/s].	48
7.18	Out of plane blade tip deflections at 25 [m/s].	48
7.19	Isolated drive train of a turbine. Shows likely attachment points for springs and dampers in red. The opposite ends of spring and dampers would attach to the nacelle frame [7].	49
7.20	Sketch of Configuration 2 with springs and dashpots attached to the nacelle frame on one end and the drivetrain platform on the other.	50

Nomenclature

ΔF_{EQ}	Fatigue damage equivalent load [Pa]
ΔF_{LEQ}	Lifetime fatigue damage equivalent load [Pa]
δ	Logarithmic decrement [-]
\dot{v}	First time derivative of speed, acceleration [$\frac{m}{s^2}$]
γ	Safety factor [-]
μ	Mass ratio between the absorber and main masses [-]
ω_a	First natural frequency of absorber mass [$[\frac{rad}{s}]$]
ω_F	Forcing frequency [$\frac{rad}{s}$]
ω_M	First natural frequency of main mass [$[\frac{rad}{s}]$]
σ	Stress [Pa]
ζ	Damping ratio [-]
d	Damage [-]
E	Young's modulus [Pa]
f	Tuning ratio [-]
l	Length [m]
m	Mass [kg]
M_y	Moment in y-direction [Nm]
R	Dynamic Amplification Factor [-]
R_i	Inner radius [m]
R_o	Outer radius [m]
t	Time [s]
U_{avg}	Average wind speed [$\frac{m}{s}$]
U_{ci}	Cut-in wind speed of the turbine [$\frac{m}{s}$]
U_{co}	Cut-out wind speed of the turbine [$\frac{m}{s}$]
U_r	Rated wind speed of the turbine [$\frac{m}{s}$]
v	Speed [$\frac{m}{s}$]
X	Maximum displacement [m]
c	Damping coefficient [$\frac{Ns}{m}$]
DAF	Dynamic amplification factor [-]
r	Forcing frequency ratio [-]

1

Introduction

The Working Group II of the United Nation's Intergovernmental Panel on Climate Change (IPCC), describe in their 2014 report on impacts, adaptation and vulnerability, how human and natural systems are experiencing disruptions due to changing weather conditions [8]. The report provides clear observations that can be attributed with high confidence (9/10 chance) to changing climate systems. These observations include shifting animal activity, melting of regions long covered by permafrost, and net negative effects on worldwide crop yields. The report also reveals the "significant" vulnerability of natural and human systems, mentioning that although a relatively low number of species extinctions can be confidently attributed to climate change, "natural global climate change at rates slower than current anthropogenic climate change caused significant ecosystem shifts and species extinctions during the past millions of years" [8]. Poor and marginalized human populations are especially at risk. To prevent catastrophic climate change it is essential to limit greenhouse gas emissions.

Energy consumption is increasing worldwide, as shown in Figure 1.1 by the US Energy Information Administration. Developing countries are becoming richer and the consumption of energy and material goods is growing. People's quality of life is improving because of this. But, almost all human activities requires energy, which is currently predominantly delivered through carbon intensive fossil fuels. Thus, higher consumption exacerbates the load society applies on the biosphere, as well as increasing pollution that causes health risks and climate change. To prevent irreparable climate change it is essential to curb greenhouse gas emissions by de-carbonizing the economy. This requires a rapid transition to renewable energies.

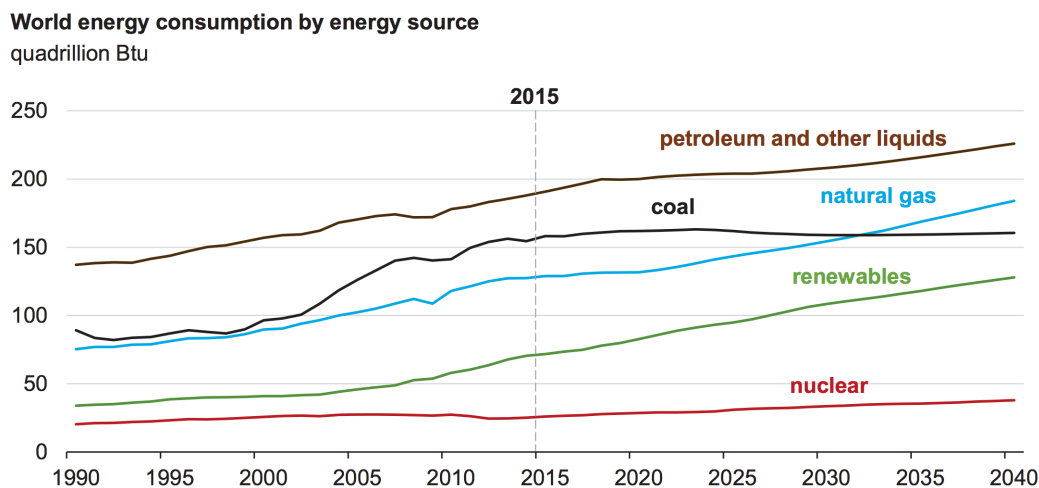


Figure 1.1: World energy use by source. Source: EIA [1].

Renewable energy sources can dependably and cheaply power the world. Wind, solar, biomass and hydro sources are growing in installed capacity, and their prices are dropping at rates faster than

expected. The International Energy Agency (IEA) had to overhaul its forecast of PV installed capacity growth for the next five years [9]. Figure 1.2 shows that bid prices per MWh for onshore wind and solar photovoltaics are projected to continue their downwards path. Furthermore, new and old methods for energy storage are being improved in order to ensure electricity supply needs are met even during low production periods, and provide grid stability usually provided by the rotating mass of generators. A very recent example of this is the Hornsdale Power Reserve at the Hornsdale Wind Farm in South Australia, a battery bank which has a capacity of 129 megawatt-hours. The Hornsdale Power Reserve has been hailed a success since its operations started on December 2017, having effectively smoothed out grid disruptions that have occurred since [10].

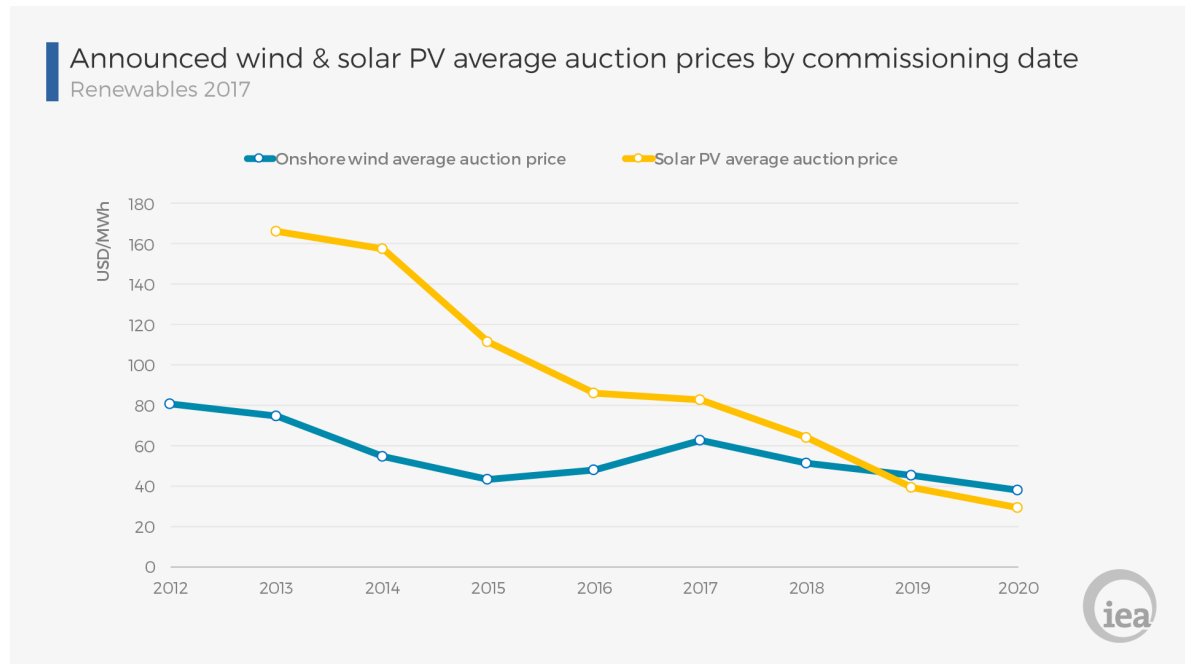


Figure 1.2: Average auction prices for solar PV and onshore wind. Source: IEA [2].

Wind energy is consistently proving itself as a reliable, affordable and sustainable source of electricity. In their 2017 Global Wind Statistics report, the Global Wind Energy Council reveal that in 2014, 2015 and 2016, more wind capacity had been installed than in any year before. According to the same document the world wind capacity is now a remarkable 486GW [11]. Assuming a 20% capacity factor, 486GW of installed capacity equals about 4% of the worlds total electricity consumption, which is 2.3TW, according to the IEA [12].

Wind power's affordability is also increasing, with projects awarded at prices as low as 5 Euro cents per kWh, which occurred when Vattenfall won a tender to build the Danish Kriegers Flak offshore project [13].

Despite these advancements, in the interest of continued sustainable development it is imperative to continue developing the industry's know-how, and thus reducing the cost of wind energy. Falling costs will ensure long term competitiveness of wind energy and motivate countries to support the technology, as well as private companies to invest in it.

Two options for reducing the cost of wind energy from a design standpoint, are to reduce the construction expenses for new wind turbines, and to extend the design life of the project by virtue of the fatigue life of the support structure. Both of these can be accomplished by reducing loads on the turbine's support structure.

Reducing loads on support structures can effectively be accomplished by reducing resonance of the structure's vibrations. In civil engineering, this is often accomplished with dampers. Using dampers of various kinds has been attempted many times in the past. However, in most cases, their use raises concerns of the additional mass and space requirements they entail, and how these affect the design [5]. This thesis aims to study the performances of two tuned-mass damper systems that make use of masses already in the turbine to reduce oscillations. These two dampers use the turbine's generator

mass and drive train mass as absorbers, respectively.

The next chapters describe in detail research objectives and questions, the methodology employed and results of the project. The report closes with concluding remarks on the effectiveness of the designs and recommendations for future research.

2

Objectives and research questions

This project aims to investigate fatigue loading on wind turbine towers. In particular, this thesis studied the reduction of fatigue loading through the use of tuned mass dampers (TMD's). Turbines with two innovative TMD systems were tested against a non-TMD turbine.

The two main objectives of the project are:

1. To establish a reference level for the fatigue loading
2. To find out how much fatigue loads may be reduced by using tuned-mass dampers

The objectives of the project lead to the following research questions:

1. In the interest of performing quick calculations, can a wind turbine with a tuned mass damper be modeled accurately enough as a two degree of freedom system?
2. Baseline fatigue of a wind turbine
 - What is the baseline unavoidable fatigue damage on a turbine tower base, assuming a constant dynamic amplification factor of 1 and only thrust forces acting on the rotor?
 - What is the lifetime fatigue on the turbine assuming instantaneous control response?
 - What is the increase in fatigue when the same turbine is modeled accounting for dynamic behavior of the tower?
3. What is the dynamic behavior of a wind turbine that uses its generator as a passive tuned mass damper?
 - What are the parametric values that will give the best possible dynamic behavior?
 - Is it feasible and practical to create a turbine with such a configuration?
 - What is the change in fatigue of this system compared to a turbine without a damper?
4. What is the dynamic behavior of a wind turbine that uses its entire drive train, namely its rotor, low and high-speed shafts, gearbox and generator as a single passive tuned mass damper?
 - What are the parametric values that will give the best possible dynamic behavior?
 - What is the effect of having an excited damper on the overall dynamic behaviour?
 - Is it feasible and practical to create a turbine with such a configuration?
 - What is the change in fatigue of this system compared to a turbine without a damper?

3

Methodology

This chapter provides a general explanation of the steps taken to answer the questions presented in the previous chapter. It introduces the assumptions that define the “baseline” or super-stiff fatigue, and provides a visual description of the tuned mass damper configurations tested to reduce fatigue on wind turbines.

3.1. Baseline fatigue

A horizontal axis wind turbine cannot operate without wind creating forces on the rotor. The forces acting on the blades of a wind turbine make the rotor turn, but also result in a thrust that pushes the turbine in the direction of wind flow. Varying wind speeds inherently mean that the forces on the rotor will vary. This variation in the thrust load leads to the emergence of fatigue damage.

The first aim of the project is to find to what extent the inevitable variation in the rotor thrust force during operation translates to fatigue damage of the support structure. This “baseline” fatigue calculation is a valuable tool that establishes the ultimate objective that turbine designers can work toward. Much like the Betz limit, which defines the single maximum percentage of energy that can be extracted from a moving fluid at 59.3%, this baseline fatigue is technically unattainable within the limits of cost-effective turbines. Still, it is a fundamental, unchanging property of each turbine model that can be very valuable for manufacturers.

Variations in the excitation force mean that the wind turbine is excited dynamically, as opposed to statically, and in practice this leads to larger displacements of the turbine. However, under the assumption that the turbine is always excited with a slowly varying force, with constant dynamic excitation of one, the resulting fatigue damage becomes baseline for a structure that is very stiff. This thesis aimed to find what this “super-stiff” fatigue is.

To obtain this limit, the assumption was made that the overall thrust variations on the turbine rotor can be emulated using a single wind signal that produces a single thrust signal on the hub. This thrust follows the turbine’s thrust curve, explained in Section 5.3.3. The thrust signal calculated from the curve at each point in time of a given load case was then used to find the stress at the tower base, which is the location we are interested in.

3.2. Fatigue reduction using dampers

The second part of the thesis tested new methods of reducing fatigue damage of the turbine’s support structure. The idea is to simulate turbines with tuned mass dampers, which have been investigated in the past, but in system configurations that do not require a significant addition of mass to the tower top. The systems use a wind turbine’s generator and the drive train as absorbers, respectively. These systems are henceforth called Configuration 1 and 2.

The question then is whether or not these systems are an effective method of reducing fatigue damage in the support structure of the turbine. To answer the question, the turbine is modeled as mentioned in the previous section, with an additional mass attached to the main mass, that represents the tuned mass damper. The dynamic behavior is tested under simulated wind conditions to assess their performance.

3.2.1. Configuration 1

Configuration 1 proposes a drive train with a telescoping high speed shaft, that can transfer torque whilst varying its length. Such a shaft allows the generator to slide back and forth on rails. This motion of the generator then allows it to absorb and dissipate vibrations of the nacelle in line with the wind.

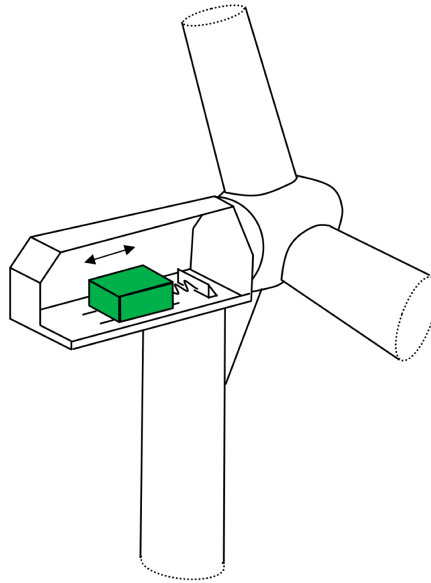


Figure 3.1: Drawing of Configuration 1: the generator oscillates with respect to the nacelle [3].

3.2.2. Configuration 2

The system that this report refers to as Configuration 2 describes a wind turbine in which all or part of the drive train can oscillate in translation with respect to the tower top. This configuration is interesting in that it separates the tower motions from most of the top mass, with the rotor itself acting as a TMD. If we include the rotor in the TMD, the strongest excitation forces are acting on the absorber itself, not on the tower main mass, which is the one we are attempting to protect. A diagram of the system can be seen in Figure 3.2. The motions of the damper in Configuration 2 are limited to the fore-aft direction for practical reasons.

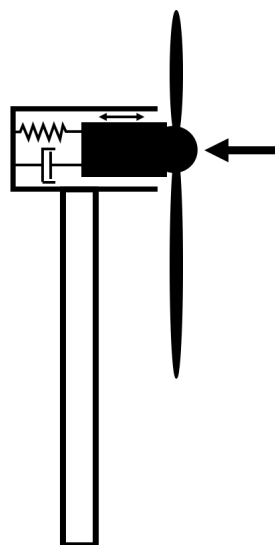


Figure 3.2: Drawing of Configuration 2: the drive train oscillates with respect to the nacelle

Both configurations are tested in the frequency and time domains, and their ultimate effectiveness is assessed based on the fatigue damage over a series of select load cases, specified in section 3.3.

3.3. Calculating fatigue

The ultimate goal of this project is to test whether the systems explained earlier in this chapter can extend the design life of wind turbine support structures. The operational life of a mechanical or structural component is defined by the number of cycles it can sustain until failure. The phenomenon that defines this number of cycles is called fatigue. This makes fatigue damage the key variable which the tuned mass damper configurations studied here aim to reduce.

To calculate a representative fatigue for wind turbine towers, the stresses at the tower base are used. These stresses are calculated from the moment that is either taken directly from FAST simulations, or calculated from the displacements of the models developed in MATLAB. To calculate the stress from the moment at the tower base we use the formula in Equation 3.1.

$$\sigma = \frac{M_y * R_o}{I} \quad (3.1)$$

Where σ is the stress at the tower base, which can be tensile or compressive. M_y is the moment and R_o is the outer radius at the tower base. I is the area moment of inertia, which is a geometric property given by:

$$I = \frac{\pi}{4}(R_o^4 - R_i^4) \quad (3.2)$$

In the MATLAB models used to model turbine motions, moments are not involved in the calculations. For this reason, an alternative way to calculate the moments is used. The assumption is made that there is a linear relationship between the displacement and the moment at the tower base. To find this relationship, the moments were plotted against the displacements at every time step for two FAST simulations, one at $6 \frac{m}{s}$ and one at $12 \frac{m}{s}$. From this the relationship was established as $M_y = x[m] * 1.57e5[kNm/m]$. This relationship is clear in Figure 3.3.

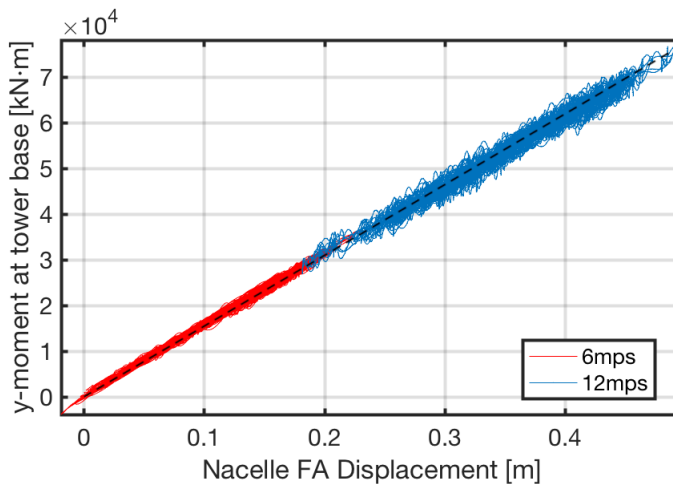


Figure 3.3: Plot of the moment at the tower base as function of displacement from two FAST simulations.

As can be seen in Figure 3.3, there is a seemingly linear relationship. The moment, however, deviates significantly from the dashed line, deviating up to 7% above or below. Because of the amount of load cycles over which these deviations occur, they are not negligible. Then, because we take this multiplication factor to be constant when in fact it is not, this procedure will introduce a discrepancy between the moment signals of FAST and MATLAB. Given the time limitations of the project, this discrepancy is unavoidable. However, as will be shown in the following chapters, the discrepancy does not render results invalid.

3.3.1. Rainflow counting

Rainflow counting is a well known method of characterizing and quantifying complex load cycle series into well defined load ranges and an amount of cycles for each load range. This characterization is necessary in order to identify fatigue damage to the structure using fatigue damage equivalent loads, which are explained later in this Chapter.

In an example, in Figure 3.4 a strain signal is given. These data are processed through a rainflow algorithm that identifies turning points in the signal and literally keeps count the range of every cycle.

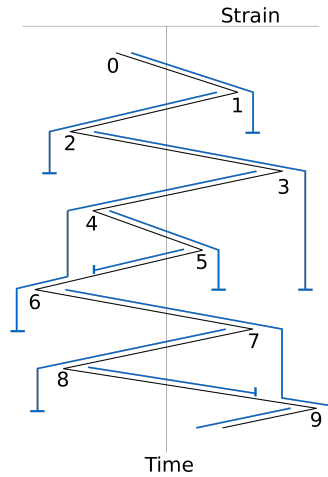


Figure 3.4: Rainflow counting on a strain signal.

The rainflow counting algorithm used in this project was taken from Mathworks File Exchange [14]. A more detailed explanation on how rainflow algorithms are used can be found in Downing & Socie, [15]

3.3.2. Miner's rule

A structural or mechanical component under long-term cyclic loading can fail under a stress load significantly inferior to its ultimate strength due to fatigue.

The method of calculating fatigue used in this project is simple. It is based on Miner's rule, which introduces the idea of partial damage and cumulative fatigue. This rule stipulates that for every load cycle experienced under the ultimate strength of the material concerned, a component receives a partial damage d_j ,

$$d_j = \frac{n_j}{N_j} \quad (3.3)$$

where n_j is the number of cycles endured at a given load range, compared to the maximum number of cycles that can be endured at this load range, N_j . Individual damages can be simply added up over separate simulations to accumulate fatigue damage. By Miner's rule, as long as the total damage remains under 1, the component will not fail.

3.3.3. FDEL

In this project, we use the fatigue damage equivalent load (FDEL) to calculate and compare the fatigue inflicted on the support structure of a turbine during each 10-minute simulation that both the FAST and MATLAB models are subjected to.

Fatigue damage equivalent loads are useful to easily compare the fatigue damage caused by complex loading cycles over long periods of time and large amounts of cycling. For a given 10 minute load simulation, this technique yields the stress magnitude that would cause the same amount of fatigue damage to the structure that the load case causes, if the structure were subjected to this equivalent load at a frequency of $1Hz$ over the length of the load case, which equals $N_{EQ} = 600$ times.

For a given load case, a time-domain stress signal is produced. Then, for that load case the resulting FDEL is:

$$\Delta F_{EQ,j} = \left(\frac{1}{N_{EQ}} \sum_{j=1} n_j \Delta F_j^m \right)^{\frac{1}{m}} \quad (3.4)$$

Where m is the slope of the SN curve that defines the fatigue behavior of the material. F_j and n_j are respectively, each of the load ranges present in the given stress signal, and the number of cycles counted for each identified load range. To calculate the FDEL we assume a slope $m = 3$, which is appropriate for welds such as those found at the base flanges of wind turbine towers. In Equation 3.4, the range characterization and counting of load cycles is done with the rainflow counting algorithm explained above.

Finally, to calculate the 20-year lifetime fatigue equivalent load at the wind turbine's tower base, we must make a choice of wind climate. Doing this we can compare the fatigue on different turbine designs under the exact same long term conditions. Making a choice of modeling under International Electrotechnical Commission Class II wind conditions [16], with a Weibull shape and scale factors of 2 and 8, respectively, using Equation 3.5 we end with the Weibull in Figure 3.5.

$$P_w(U) = \frac{k}{a} \left(\frac{U}{a} \right)^{(k-1)} \cdot \exp\left(- \left(\frac{U}{a} \right)^k \right) \quad (3.5)$$

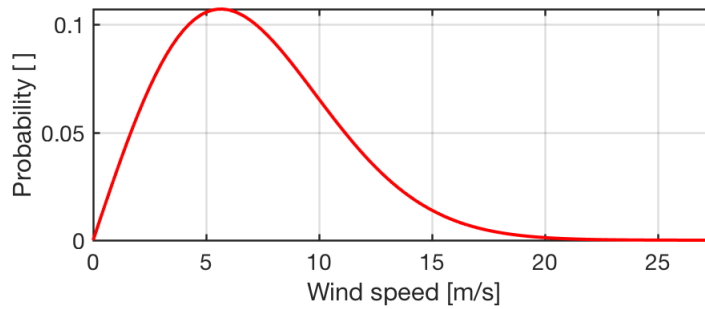


Figure 3.5: Weibull curve with $k=2$ and $a=8$.

We can then use this probability distribution to establish what percentage of turbine's lifetime the wind speed will be within specific limits, i.e. between 7.5 and 8.5 meters per second. The probability distribution found is shown in Table 3.1

Table 3.1: Weibull probability distribution for the curve shown in Figure 3.5

U [m/s]	P_w	U [m/s]	P_w
3.5-4.5	0.0974	14.5-15.5	0.0139
4.5-5.5	0.1057	15.5-16.5	0.0092
5.5-6.5	0.1068	16.5-17.5	0.0058
6.5-7.5	0.1017	17.5-18.5	0.0036
7.5-8.5	0.092	18.5-19.5	0.0021
8.5-9.5	0.0793	19.5-20.5	0.0012
9.5-10.5	0.0655	20.5-21.5	0.0007
10.5-11.5	0.0519	21.5-22.5	0.0004
11.5-12.5	0.0395	22.5-23.5	0.0002
12.5-13.5	0.029	23.5-24.5	0.0001
13.5-14.5	0.0205	24.5-25.5	0

Once these probabilities are established, the full, 20-year lifetime fatigue equivalent load can be calculated. This simple calculation involves using a modified version of Equation 3.4, shown below,

where p_{LC} is the Weibull probability that defines what percentage of the time each load case will occur over 20 years. This factor multiplies the fatigue equivalent load range found for each load case by the times that load case occurs in the turbine's lifetime. The lifetime factor calculation is shown in Section 7.2.2. This FDEL will be used to compare the effectiveness of the tuned-mass dampers studied in this project.

$$\Delta F_{LEQ} = \left(\sum_{LC=4}^{25} p_{LC} \Delta F_{LC}^m \right)^{\frac{1}{m}} \quad (3.6)$$

The damages done to the tower base are calculated using Equation 3.7, assuming a fatigue endurance limit of $\Delta F_D = 90 \text{ Mpa}$ at $N_D = 2E6$ cycles. In this case, N_{EQ} is taken to be the 20-year lifetime of the turbine in seconds.

$$D = \frac{N_{EQ}}{N_D} \left(\frac{\Delta F_{EQ}}{\Delta F_D} \right)^m \quad (3.7)$$

It's important to note that the fatigue damages calculated throughout the report will be somewhat conservative given that wind rose distributions were neglected. This means that all maximum stresses due to fore-aft tower motions are concentrated on a single location.

4

Review of tuned mass dampers

High and slender structures, such as skyscrapers and telecommunications towers, are susceptible to being excited by wind forces. Since the turbulence spectrum of wind contains all frequencies, the movements of a structure subjected to turbulent wind may be dangerously amplified if they are insufficiently damped. This is especially the case if the structure is excited near its first eigenfrequency, which for structural bodies is typically less than 1Hz. Figure 4.1 shows how the motions of a simple system are amplified depending on the amount of damping.

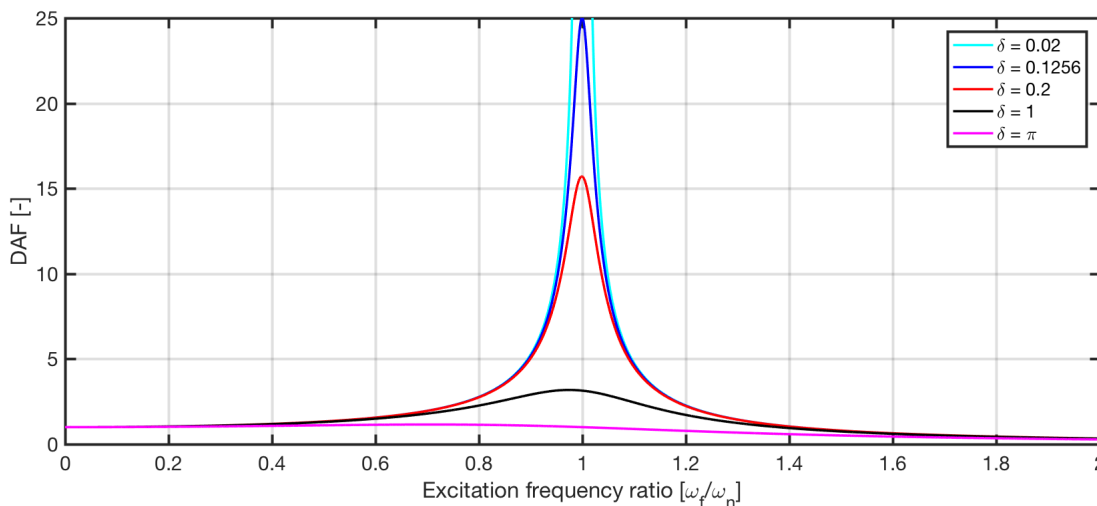


Figure 4.1: Dynamic amplification of a 1 degree-of-freedom system with different damping levels

The maximum amplification of a system at its natural frequency is given by:

$$R(f_e) = \frac{u_{dynamic}(f_e)}{u_{static}} \quad (4.1)$$

where u is the displacement, dynamic or static, and f_e is the forcing frequency.

Damping is defined by the logarithmic decrement δ . For example, if the structure is made of concrete, which is typically assumed to have a viscous damping of $\delta = 0.126$ [17] (damping ratio of 2%), the amplification will be $R = 25$. But, in a system with a higher logarithmic decrement, such as $\delta = 0.2$, the amplification will peak at $R = 15.7$. In wind turbines, the vast majority of damping comes from thrust changes wind varying wind speed. Comparatively, structural damping in wind turbines is insignificant. This means that it is important to have a system with as high a logarithmic decrement as feasible. It is possible to achieve this by coupling an auxiliary mass to the main system.

4.1. Introduction to Tuned Mass Dampers

Dampers are widely used to reduce vibrations of fatigue-sensitive structures. They are also used in structures meant to be used by humans to reduce unpleasant accelerations. Notable examples include the London Millennium bridge over the Thames, and the Taipei 101 in Taiwan's capital. Dampers are also used in long power lines and sometimes in automobiles and motorbikes. In recent decades, tuned-mass dampers (as well as other types of dampers) have gained interest in the field of wind energy to dampen vibrations of both the tower and the blades.

Tuned-mass dampers approach the problem of vibration based on the principle that *a moving auxiliary mass, attached to a larger mass, can absorb and dissipate its kinetic energy*. This effectively increases the logarithmic decrement of the large, main mass.

Tuned mass dampers work because with a relatively small mass the amplitude of motions of a structure can be significantly reduced, and their decay hastened. They can also be used to cheaply move the 1st mode of structures away from a dangerous frequency, that may be particularly excited by the environment or the operation of the component that the structure itself supports.

A diagram of a typical tuned mass damper can be seen in Figure 4.2. This system with two masses, each of which can move in a single direction is said to have two degrees of freedom (DOF), and can be modeled as a set of differential equations. This modeling is explained in the following section.

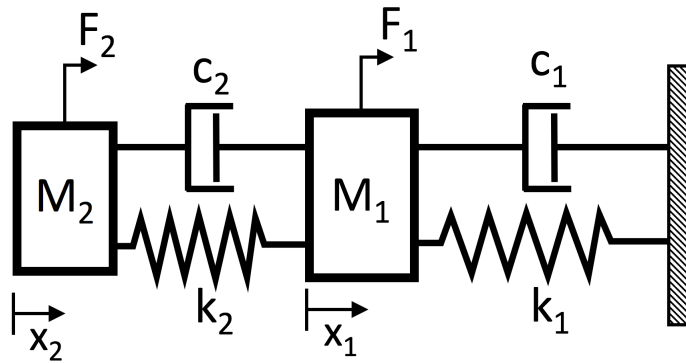


Figure 4.2: Diagram of a system with a TMD, as a 2 degree of freedom system

4.2. Modeling systems of 1 and 2 degrees of freedom

Any moving system, simple or complex, can be simplified or represented in an equivalent model of masses, springs and dampers. This is very useful for studying the dynamics of structures, vehicles, etc, since mass spring damper systems can be mathematically represented with relative ease. These mathematical representations can then be studied under specified initial conditions and excitation forces.

An obvious example of this is a wind turbine's nacelle, whose degrees of freedom can be simplified into a mere 1DOF system of a mass atop a mass-less spring, such as in Figure 4.3. This model is a useful representation if we assume that the first mode of the system accounts for most of the motions and consequent structural damage, which is the case for wind turbines. In such a model, the equivalent swinging mass of the tower is added to the point mass at the end of the spring. Similarly, all the masses atop the tower are accounted for in the point mass.

The forces that act on the turbine are represented as a force on the mass. These forces are thrust, which is a result of the lift and drag forces acting on the blades, and drag, which acts on the tower and the nacelle. Damping on the motions of the nacelle come from structural damping, mainly of the tower, and from aerodynamic damping caused by thrust force changes on the operating rotor that oppose its motion. The definition of these forces, stiffness and damping for our simulations is further explained in Chapter 5.

Given the model comprised of masses, springs and dampers, a mathematical expression can model the excitation forces and subsequent motions of the masses. In this case, for a single mass system, the mathematical expression takes the form of a single differential equation:

$$m_1 \ddot{x}_1 + c_1 \dot{x}_1 + k_1 x_1 = F_1 \quad (4.2)$$

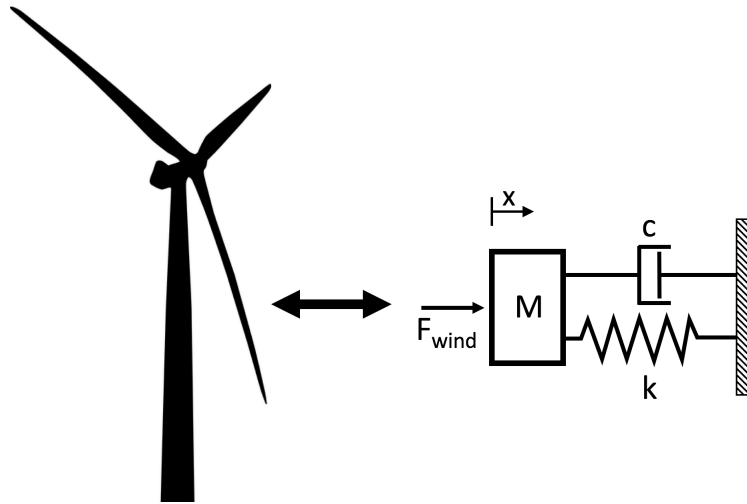


Figure 4.3: Thrust curves for several reference turbines

where \ddot{x} and \dot{x} are, respectively, the double and single time derivatives of the position, x , of mass m with respect to the origin. c and k are the damping coefficient and the spring stiffness, respectively. Each x variable, multiplied by its respective coefficient, equals a force, and these forces added are equal to the excitation force on the mass.

The mathematical expression for a more complex system requires a system of as many equations of motion, as there are degrees of freedom in the system. For a turbine with a tuned mass damper, an additional degree of freedom must be added to the system. So, for the 2 degree of freedom turbine-damper system, the mathematical expression would have the form shown in the matrix equation 4.3.

$$\begin{pmatrix} m_1 + m_2 & m_2 \\ m_2 & m_2 \end{pmatrix} \begin{pmatrix} \ddot{x}_1 \\ \ddot{x}_2 \end{pmatrix} + \begin{pmatrix} c_1 & 0 \\ 0 & c_2 \end{pmatrix} \begin{pmatrix} \dot{x}_1 \\ \dot{x}_2 \end{pmatrix} + \begin{pmatrix} k_1 & 0 \\ 0 & k_2 \end{pmatrix} \begin{pmatrix} x_1 \\ x_2 \end{pmatrix} = \begin{pmatrix} F_1 \\ F_2 \end{pmatrix} \quad (4.3)$$

This system of equations can be rewritten as:

$$\mathbf{M}\ddot{\mathbf{x}} + \mathbf{C}\dot{\mathbf{x}} + \mathbf{K}\mathbf{x} = \mathbf{F} \quad (4.4)$$

where \mathbf{M} , \mathbf{C} and \mathbf{K} represent the mass, damping and stiffness matrices, respectively. The use of these equations in MATLAB is explained in greater detail in Chapter 5.3.

The effectiveness of a tuned mass damper relies on it absorbing kinetic energy from the main mass. To model and assess a TMD two defining parameters are needed: the mass ratio, μ , which is the ratio between the absorber and main masses, and the damping ratio ζ of the auxiliary mass, which identifies how strongly its motions are damped. In Equation 4.6, $c_{critical}$ is the damping for a given system that brings the excited system to equilibrium with no oscillation, and δ is the logarithmic decrement.

$$\mu = \frac{m_a}{m_m} \quad (4.5)$$

$$\zeta = \frac{c}{c_{critical}} \approx \frac{\delta}{2\pi} \quad (4.6)$$

Figure 4.4 shows how a tuned mass absorber connected to a main mass via a spring and damper, as pictured in fig. 4.2, acts to reduce the vibrations of said main mass. In this figure, we can see the motions of a main mass with an initial displacement of 1 meter. Each of the curves shows the same main mass, but with a different size damper, so a different mass ratio μ . It is clearly visible that with an increasing mass ratio, the main mass reaches equilibrium faster. The motions of the absorber masses are hidden for clarity, but in all cases its initial position is also 1 meter from the origin.

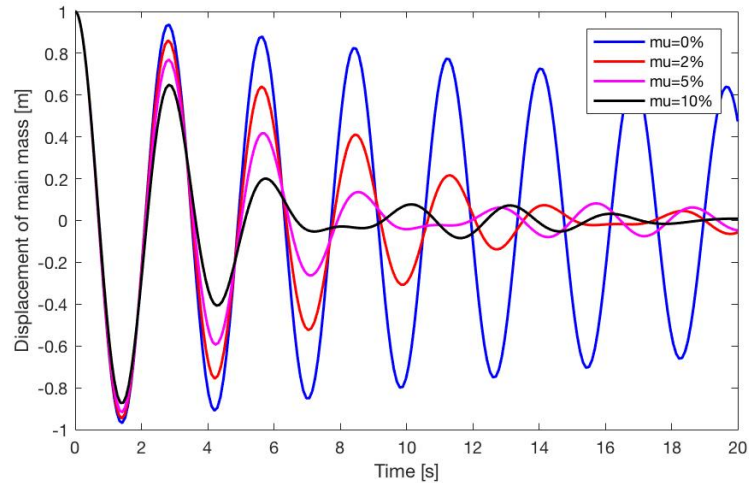


Figure 4.4: Displacements of a mass without and with TMD's of increasing mass, with a damping ratio of $\zeta_a = 2\%$

4.3. Dynamic Amplification Factor

The dynamic amplification factor defines the amplitude of the dynamic response of a system at a given excitation frequency, compared to the static response. A typical amplification curve can be seen in Figure 4.5. It shows the static and dynamic responses to the same magnitude excitation forces. The amplification factor is then plotted at each excitation frequency from these values. The static response has, of course, an excitation frequency of zero. For this reason, the dynamic responses at frequencies close to zero are equal to the static response, giving the DAF curve a value of one at frequencies near zero. At high frequencies, the dynamic response becomes smaller than the static response, and thus it falls towards zero, as does the DAF.

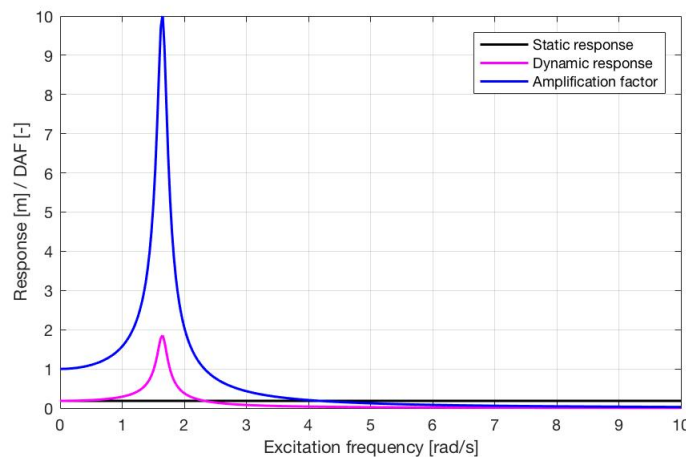


Figure 4.5: Dynamic amplification of a 1DOF system with $\zeta = 2\%$.

Figure 4.6 shows two dynamic amplification curves: for a single DOF system with no damper, and for a system with an absorber. The undamped curve has a peak, which occurs at the natural frequency of the system. If the system is undamped, the DAF will theoretically peak at infinity. For the system with a main mass and an absorber mass, the dynamic amplification is visibly lower, and the system has two peaks, at the natural frequencies of each degree of freedom. In this figure the frequencies are normalized.

To find the DAF factor of a system with two degrees of freedom, we use Equations 4.7 to 4.11, taken from Warburton and Ayorinde (1980). These equations reveal the dynamic amplification R of systems, which is a value that can only be studied when a system reaches steady state. This means

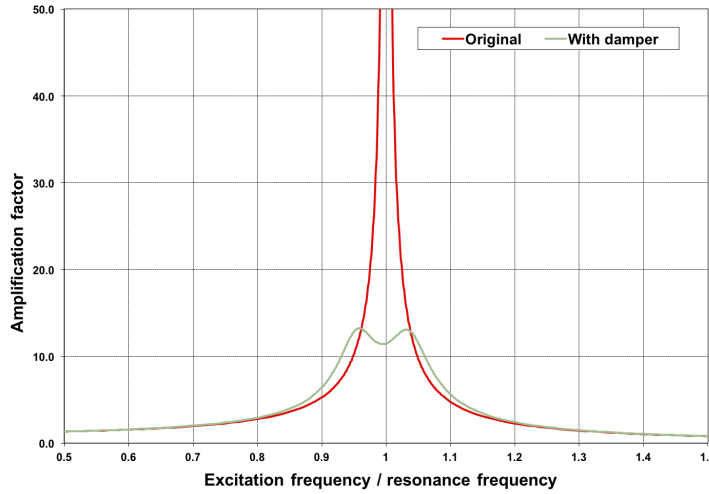


Figure 4.6: Dynamic amplification of a system without and with a TMD

that a complete study of the effectiveness of a tuned mass damper cannot be based solely looking at the DAF curves. This is why we utilize the equations of motion in a MATLAB solver, to study the dynamic amplification as well as the transient motions under irregular forces, such as wind.

$$R = \left[\frac{A + B}{C + D} \right] \quad (4.7)$$

$$A = f^2 - r^2 \quad (4.8)$$

$$B = 2\zeta_a r f \quad (4.9)$$

$$C = f^2(1 - r^2) - \mu f^2 r^2 - r^2(1 - r^2) - 4\zeta_m \zeta_a f r^2 \quad (4.10)$$

$$D = 2\zeta_a r f(1 - r^2 - \mu r^2) + 2\zeta_m r(f^2 - r^2) \quad (4.11)$$

Where R is the dynamic amplification factor, $f = f_a/f_m$ is the tuning ratio of undamped natural frequencies of the absorber and main mass, $r = \frac{\omega_F}{\omega_m}$ is the ratio between the forcing frequency and the main mass natural frequency, and ζ_m and ζ_a are the damping ratios of the main and absorber masses, respectively.

4.4. Optimal Tuning

In 1980, G.B. Warburton and E.O. Ayorinde published their research on finding optimal parameters for simple systems. Since then, it has been cited more than two hundred times. Based on equations 4.12 and 4.13, for a given mass ratio, Warburton and Ayorinde propose an optimal tuning ratio, f_{opt} , which defines the natural frequency and thus the stiffness of the absorber, and an optimal damping ratio, ζ_{opt} , for the absorber. The curves for the optimal parameters based on Warburton and Ayorinde [4] can be seen in Figures 4.7 a and b.

$$f_{opt} = \left(\frac{1}{1 + \mu} \right) \quad (4.12)$$

$$\zeta_{opt} = \sqrt{\frac{3\mu}{8(1 + \mu)}} \quad (4.13)$$

However, as we will see in the following section, these equations don't provide optimal parameters for the tuned mass damper when we consider a system in which the excitation force acts on the damper itself. This condition is relevant to study the behavior of Configuration 2.

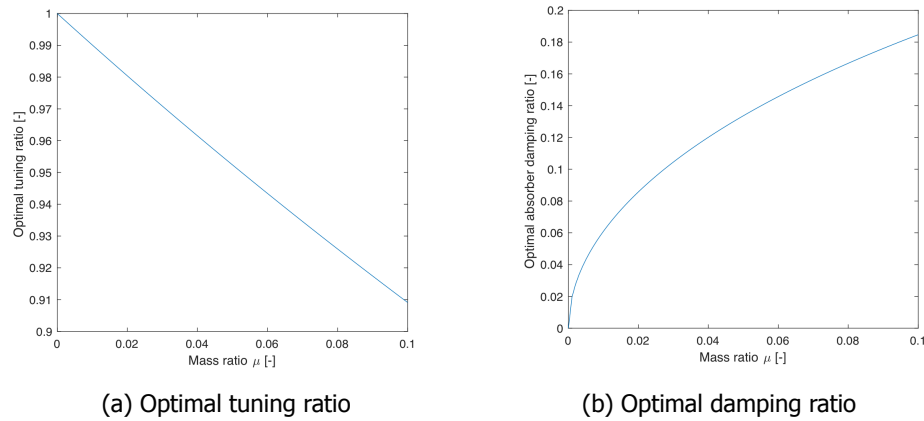


Figure 4.7: Optimal absorber parameters [4]

4.5. Optimizing the TMD system

If we utilize the formulas from Warburton and Ayorinde [4] to calculate the best performing parameters for a system in which $\mu < 1$, and the force acts on the main mass, the resulting parameter values produce a system with equal DAF peaks in the frequency spectrum. This is taken as the optimal behavior. As can be seen in Figure 4.8, the peaks of the DAF curve of a system with a mass ratio of 0.01 are lowest with the optimal tuning ratio and absorber damping. If the values are changed, in this case increasing and decreasing f and ζ by 1 percent, the heights of the peaks change, one rising and one falling, meaning that the system response is sub-optimal.

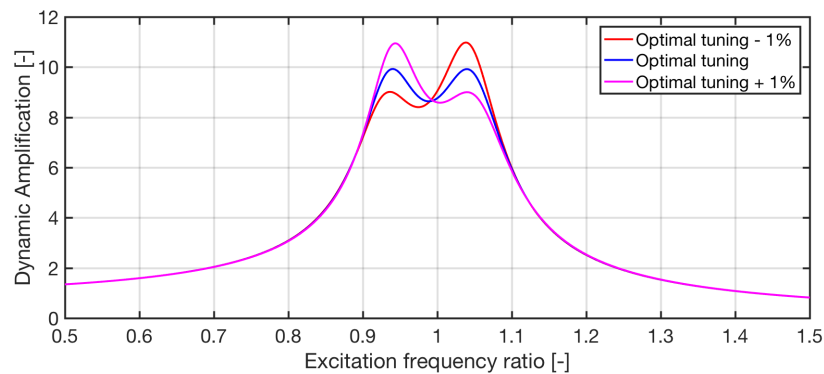
Figure 4.8: DAF with Warburton optimal and sub-optimal absorber parameters. $\mu = 0.02047$, $f_{opt} = 0.9799$, $\zeta_{opt} = 0.0871$

Figure 4.9 shows the same system as Figure 4.8, a system in which the excitation forces act on the main mass. We can see the same blue curve of the DAF resulting from the optimal values as given by Warburton [4]. An optimization procedure using MATLAB's `fminsearch` function, explained below, yields the same amplification behaviour. This curve with two equal peaks is of course the optimum.

In Configuration 2, the drive train is allowed to oscillate as a TMD. In this scenario, in which the excitation force is applied to the absorber mass (so, in equation 4.3 $F_1 = 0$ and $F_2 \neq 0$), we see in Figure 4.10 in blue that the formulas 4.12 and 4.13 don't give the most favorable behaviour. For this TMD system, a built-in MATLAB function was used instead. `fminsearch` allows the user to quickly find the minimum of a multivariable function. Using this function, for a given, fixed mass ratio, MATLAB can search the DAF at the natural excitation frequencies of each mass, varying the tuning ratio f by virtue of the absorber stiffness, and the damper coefficient c_a . The optimum is described as the minimum height of the two peaks, which makes the function output values that will give equal peaks, as seen in magenta in Figure 4.10.

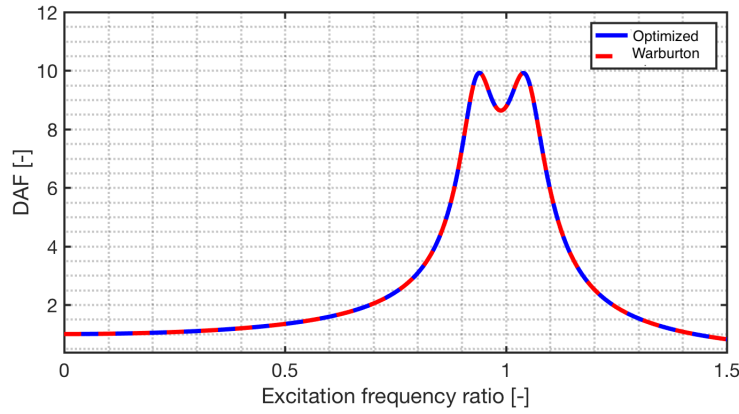


Figure 4.9: Dynamic amplification with $\mu = 0.02047$, with Warburton optimal values and optimized values.

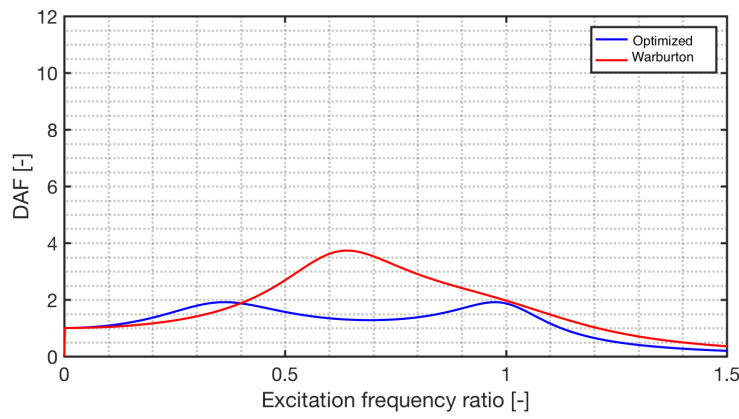


Figure 4.10: Dynamic amplification of a system with $\mu = 0.4864$ with Warburton optimal values and optimized values, as calculated with the Brown method.

4.6. Additional method for finding steady state response

In a system in which the absorber mass is excited instead of the main mass, such as our drive train-TMD, Warburton and Ayorinde's formulas cannot find optimal parameters. Furthermore, they cannot be used to find an accurate DAF as a function of excitation frequency. In this section, a second method is presented. It is used for the comparison and validation of the previously explained calculations of motion in the time and frequency domains for a 2DOF system. This method is taken from Brown University instructional material [18].

First, it is assumed that the system is excited by a sinusoidal force, acting on either mass 1 or 2. This force takes the shape of $F_i = f_i \cos(\omega t)$. For MATLAB to handle the second order differential equations needed to describe the 2DOF system, we introduce two new variables: v_1 and v_2 . With these, we turn the two second order equations of the system into 4 first order equations, equations 4.14 through 4.17, which can easily be handled in MATLAB.

$$m_1 \dot{v}_1 + (k_1 + k_2)x_1 - k_2x_2 + (c_1 + c_2)v_1 - c_2v_2 = f_1 \cos \omega t \quad (4.14)$$

$$m_2 \dot{v}_2 - k_2x_1 - k_2x_2 - c_2v_1 + c_2v_2 = f_2 \cos \omega t \quad (4.15)$$

$$\dot{x}_1 - v_1 = 0 \quad (4.16)$$

$$\dot{x}_2 - v_2 = 0 \quad (4.17)$$

These equations come together in the matrix equation shown in 4.18,

$$\begin{bmatrix} 1 & 0 & 0 & 0 \\ 0 & 1 & 0 & 0 \\ 0 & 0 & m_1 & 0 \\ 0 & 0 & 0 & m_2 \end{bmatrix} \begin{bmatrix} \dot{x}_1 \\ \dot{x}_2 \\ \dot{v}_1 \\ \dot{v}_2 \end{bmatrix} + \begin{bmatrix} 0 & 0 & -1 & 0 \\ 0 & 1 & 0 & -1 \\ (k_1 + k_2) & -k_2 & (c_1 + c_2) & -c_2 \\ -k_2 & k_2 & -c_2 & c_2 \end{bmatrix} \begin{bmatrix} x_1 \\ x_2 \\ v_1 \\ v_2 \end{bmatrix} = \begin{bmatrix} 0 \\ 0 \\ f_1 \\ f_2 \end{bmatrix} \cos \omega t \quad (4.18)$$

Using Euler's formula, shown in Equation 4.19, we convert the trigonometric cosine function to a complex exponential function. Then shortening the matrix equation we get Eq. 4.20 :

$$e^{i\omega} = \cos(\omega) + i\sin(\omega) \quad (4.19)$$

$$M\dot{y} + Dy = F(\exp(i\omega t) + \exp(-i\omega t))/2 \quad (4.20)$$

We assume that the solutions to each of the force terms on the right hand of the equation have the form $y = Y_0 \exp(i\omega t)$ and $y = \text{conj}(Y_0) \exp(-i\omega t)$, respectively. Substituting these into their respective parts of the main equation of motion, we get the equations we use to solve for Y_0 : $[i\omega M + D]Y_0 = f$ and $[-i\omega M + D]\text{conj}(Y_0) = f$. We have then the equation:

$$Y_0 = \frac{f}{i\omega M + D} \quad (4.21)$$

which we can solve for any given excitation frequency ω . Finally, the amplitude X_j of each mass is given by :

$$X_j = \sqrt{Y_{0j} \text{conj}(Y_{0j})} \quad (4.22)$$

Having the steady state amplitudes for each mass, their respective DAF is found by comparing these amplitudes to the static response of each mass, whose values are shown in Equations 4.23 through 4.25. This method is used in Chapter 6, where the validation is done.

For $F_1 \neq 0$ and $F_2 = 0$:

$$X_{1,static} = X_{2,static} = \frac{F_1}{k_1} \quad (4.23)$$

For $F_1 = 0$ and $F_2 \neq 0$:

$$X_{1,static} = \frac{F_2}{k_1} \quad (4.24)$$

$$X_{2,static} = \frac{F_2}{1} \quad (4.25)$$

$$\left(\frac{1}{k_1} + \frac{1}{k_2} \right)$$

4.7. Concluding remarks on TMDs in relation to other damping methods

In the efforts to reduce loads on wind turbines, scientists have studied several types of damping methods using masses, including TMDS, which are the focus of this thesis. These dampers include systems such as the pendulum damper, tuned mass damper, tuned sloshing damper, tuned liquid column damper, etc. They have been researched for use to reduce the vibrations of both tower and blades. Studying the effectiveness of all these systems is not within the scope of the project, and they are shown here for reference. Rezaee and Aly [5] provide a comprehensive description of these systems. Two of them can be seen in Figure 4.11.

In the past decade, methods of damping that use more creative mechanisms have emerged and entered the market. These include aerodynamic damping and damping by controlling the torque on the rotor. These methods only became available with the development of variable pitch and variable speed wind turbines, and are currently the subject of growing interest [19].

Blade pitch damping has the advantage that it can reduce fatigue in both the blade roots and the tower. This works by individually and collectively pitching blades depending on their azimuth, changing

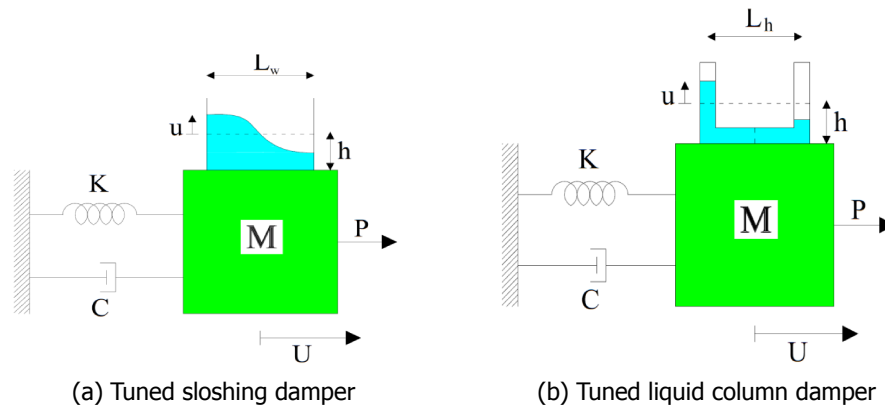


Figure 4.11: Different damping systems can be used to protect structures. Source: Rezaee and Aly [5]

their aerodynamic characteristics to reduce load fluctuations. Liu et al. [6] show that pitch damping can reduce loads on blades by up to 66.7%.

Damping using active torque control is widely used to reduce torsional fatigue damage in the drive train itself [19]. Controlling the torque on a generator's rotor has a reaction force on its stator, which is fixed to the nacelle and tower. This reaction force can be used to counter the lateral load fluctuations on the tower. Active torque control has been shown to reduce drive train loads by up to 64.3%, also by Liu et al. [6]. The load reductions on the tower base of the systems they tested are shown in Figure 4.12. Both these methods have the advantage of being able to dampen vibrations without requiring additional mass in a turbine, an attribute that this thesis also explores.

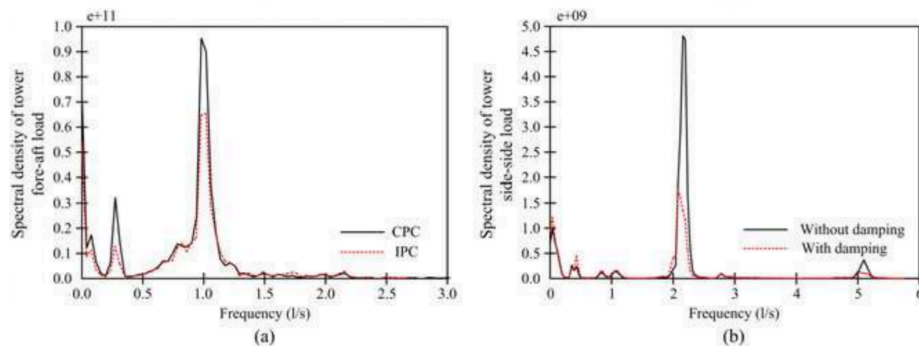


Figure 4.12: Damping effects of pitch and torque damping on tower fore-aft and side-side motions by Liu et al. [6]

By studying mass dampers, this thesis decided to take an arguably beaten path, given that tuned mass dampers have been studied numerous times. Despite all the research efforts invested, most methods of load reduction have been found unfeasible for different reasons, and they are still not widely used. This thesis, however, takes an approach that to this day remains un-investigated. Thus, whatever the outcome of this project's attempt, valuable knowledge will be produced.

One factor of concern in this project is the sensitivity to acceleration of certain components of wind turbines. Dueñas-Osorio and Basu [20] write about acceleration making sensitive components more prone to failure. These components include inverters, break systems and, of course, gearboxes and generators, the focus of this study. Specifically, for generators they predicted that they may become damaged if subjected to accelerations of more than $5 \frac{m}{s^2}$. A major consideration in this thesis is that if the accelerations required for effective damping are above this threshold, this may well be take away the whole purpose of the generator TMD.

5

Definition and modeling of the NREL 5MW turbine

In order to test the effectiveness of configurations 1 and 2, as well as to approximate the fatigue on the turbine under the assumption of an ideal super-stiff structure, we need to model a wind turbine as an equivalent mass-spring damper system with one degree of freedom, as shown in Figure 4.3. Then, onto this equivalent system we can attach the tuned mass dampers, and assess their behavior.

To create a simple system that is equivalent to a wind turbine in terms of its motions and responses to excitation, the complex mass and stiffness distributions of the wind turbine must be consolidated. Also, the different sources of damping must be reproduced. The mass consists of the rotor, nacelle and part of the tower. The stiffness, modeled by a massless spring, is the result of the tower acting as a displaced cantilever beam under loading, that tries to return to its original position. The damping of the turbine's fore-aft motions comes from different sources. Structural damping of the tower is present and equal in all directions of nacelle displacement and constant for all wind speeds. Aerodynamic damping results from the changes in thrust force on the rotor at the different wind speeds. These force changes oppose the motions of the rotor in the upwind and downwind directions

To validate the model a real turbine must be simulated. The 5MW reference turbine developed by the United State's National Renewable Energy Laboratory (NREL) fills this role. This reference turbine, shown in Figure 5.1, has been used widely in research and educational environments. It has been referenced and modified in scores of investigations, and much information is available on it. This makes it perfectly suitable to model and compare the possible benefits of the generator and drive-train tuned mass dampers.



Figure 5.1: Rendering of the NREL 5MW reference turbine

The following sections in this chapter take the reader through the derivation of the equivalent values for mass, stiffness and damping of the MATLAB model, as well as the representation of wind to generate excitation forces.

5.1. Definition and Relevant Parameters

Table 5.1: Relevant turbine parameters

Parameter	Value [unit]
Rated Power	5 [MW]
Hub height	90 [m]
Hub mass	56780 [kg]
Blade mass	17740 [kg]
Rotor mass	110000 [kg]
Generator mass	7500[kg]
Gearbox mass (assumed)	8000[kg]
Low speed shaft mass (assumed)	5000[kg]
Nacelle mass	240000[kg]
Tower mass	347460[kg]
Cut-in/out wind speeds	3/ 25 [m/s]
Rated wind speed	11.4 [m/s]

5.2. FAST

FAST is an open source software developed by the United States' National Renewable Energy Laboratory. It is an aeroelastic computer aided engineering tool that can be used to model wind turbines under many conditions ranging from onshore to offshore to freezing. FAST can design wind turbines, and it can be used to certify them by performing simulations in all necessary operational conditions, such as start-up, shut-down, extreme gusts or turbulence, etc.

This project made use of the graphical user interface for FAST developed by the TU Delft.

5.3. Modeling the turbine in MATLAB

As mentioned in Chapter 4, the project requires simulating the turbine as a model with one and two degrees of freedom, in a system of one or two second order differential equations, to test the effectiveness of the tuned mass damper configurations. This is done using the built-in MATLAB function ODE45.

To recreate the 5MW turbine as a simple system with a moving mass, in order to test its motions when using damper systems, we need to first establish the equivalent values for the mass, stiffness and damping of the system. We also need to insert an excitation force representative of the wind.

5.3.1. Deriving the general stiffness

The stiffness of the turbine was initially estimated by the formulas shown in this section and subsequently tuned during validation. We make the assumption that the turbine tower behaves like a cantilever beam. For a cantilever beam under a point load F at its free end, the deflection x at that location is given by:

$$k = \frac{F}{x} = \frac{3EI}{l^3} \quad (5.1)$$

Where E is the beam material's modulus of elasticity, and I is the length of the beam. I is the beam's area moment of inertia, a geometric property given by Equation 3.2 in Chapter 3. Given that the diameter and thickness of the tower changes linearly along its length, we take the values at the height of $45m$ as an average to calculate I . At this height the outer radius $r_o = 2.4465m$ with thickness $t = 0.3m$ give an $I = 1.3549m^4$. We take the steel's modulus of elasticity to be $E = 2.1e11 \left[\frac{N}{m^2} \right]$

Then, the stiffness for deflections at the tower top becomes:

$$k = \frac{3(2.1e11)(1.3549)}{90^3} \left[\frac{N}{m} \right] = 1.171e5 \left[\frac{N}{m} \right] \quad (5.2)$$

However, as will be shown in Section 6.2, the stiffness calculated here is underestimated. During validation, the stiffness is shown to lead to too large displacements. Consequently the deflections under the same thrust of the FAST turbine and MATLAB model are used to equalize the stiffness. The generalized mass for the entire turbine is found following beam theory. For the rotor and nacelle the mass is taken to be $347300kg$, plus the oscillating mass of the tower at $52900kg$, rendering $Mm = 400200kg$.

5.3.2. Modeling Wind

For stochastic wind simulations, wind is created from data in the shape of spectra that define the energy levels at different wind variation frequencies. A typical spectrum can be seen in Figure 5.2. To create a wind signal from this, a reverse Fourier transform is performed, which takes the energy at different frequencies in the spectrum to assign an amplitude to each frequency in the range. The sinusoidal signals produced are added to produce an artificial turbulent wind. FAST used this method to create wind signals.

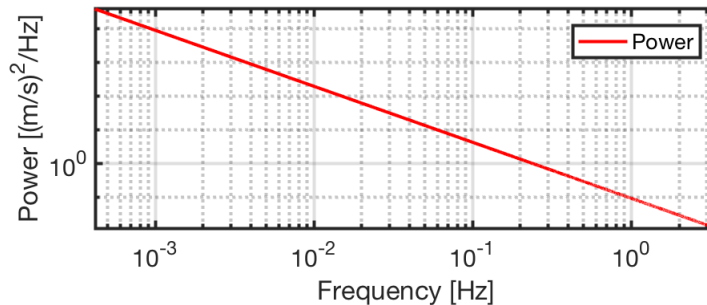


Figure 5.2: Power spectral density of a typical wind signal

For this project, we simply extracted from FAST the wind created in the file `turbsim.m`, the same wind file each load case simulation in FAST uses. The extraction produces a three-dimensional array of wind points over the rotor area for every point in time.

FAST simulations average wind over the rotating blades of the rotor, but not all wind data are sampled at all times. The rotors clearly only samples the wind velocities occurring at the locations where the blades are, ignoring all others. However, the MATLAB model has a limitation, that at every time step, only one wind speed can be sampled. This means that in order to emulate the overall thrust forces, a number of wind points over the rotor area must be chosen and averaged, such that at every time step the thrust is defined and the MATLAB model excited in as similar a way to the real turbine.

During validation it was found that using wind signals to excite the dynamics of the turbine does not yield an sufficiently similar behavior compared to the FAST turbine. This is further explained in Appendix B.

5.3.3. Modeling thrust force

To model the thrust as exactly as possible, a stepped wind simulation was carried out in FAST. The wind signal, which in this case is uniform across the rotor, increases in steps from below the cut-in speed of the turbine, to above cut-out. Figure 5.3 shows the signal over the simulation time.

The steps of this wind simulation are long enough that the turbine eventually comes to a semi-stationary position, in which the thrust slightly oscillates around an average. This stationary thrust at each speed was extracted and interpolated to create the thrust curve used in the MATLAB model. The thrust curve extracted from this simulation is shown in blue in Figure 5.4.

If the reader looks at the blue curve below cut-in wind speed, it is strange to see that the value of the thrust at $0 \frac{m}{s}$ wind speed is about $100kN$. This force is caused by the upwards tilt of the rotor, which adds a gravity effect to the thrust. This added force acts vertically, and is constant through all

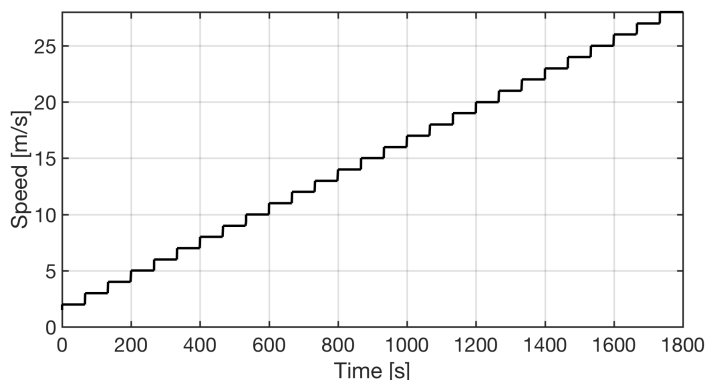


Figure 5.3: Stepped wind signal

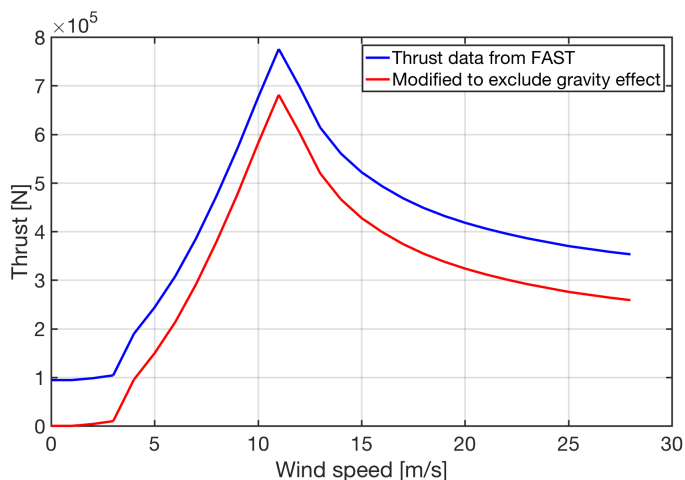


Figure 5.4: Thrust curve extracted from a stepped wind FAST simulation

operational speeds of the turbine. Because this component of the thrust force has no effect in the turbine's fore-aft motions, we remove it from the thrust signal as an offset of 94.25 kN . This leaves us with the red curve, which is used in MATLAB. This curve is used as a MATLAB function handle representing the force on the rotor, whether on mass 1 or 2, at each time step of the simulation. The modification allows the MATLAB model to coincide with the FAST turbine in having a deflection of zero at zero wind speed.

A thrust force signal is also extracted from each simulation of the real turbine in FAST. An adaptation to the MATLAB model was written, so this signal could also be readily used to test its behavior and compare it to the behavior of the real turbine. In the fatigue calculations of the turbine without and with tuned-mass dampers, these thrust signals from FAST were used instead of wind signals.

5.3.4. Modeling aerodynamic damping

Damping of a wind turbine in the fore-aft direction changes depending on the speed of the wind, as an effect of changing thrust, as well as the controller pitching the blades. In the MATLAB turbine model, damping on the turbine can only be described by the variable c . This means that all damping phenomena, structural and aerodynamic, must be condensed into this variable.

To do this, the same stepped wind simulation in FAST that was used in section 5.3.3 was used to extract the damping on the turbine. The instant jump in wind speed provides an excitation similar to a single strike on the system. A strike excites all modes of the turbine, and from the decay of the displacements after the "strike" we can calculate the overall damping on the turbine at the speed the wind jumps to.

Calculating the damping from the decay of the motions after an excitation requires calculating the

logarithmic decrement. The logarithmic decrement, denoted δ , is defined as the natural logarithm of the ratio between two consecutive peaks in the motion of a system. It's formula is shown in Equation 5.3, where $x(t)$, the displacement at time t , is divided by the displacement after exactly one period, T .

$$\delta = \ln\left(\frac{x(t)}{x(t+T)}\right) \quad (5.3)$$

Figure 5.5 shows the motions of the turbine in FAST after a jump in the wind speed. The stationary position of the turbine at every wind speed is taken to be zero. Then, the peaks of the signal are isolated, and an exponential curve is fitted on them. From this curve the logarithmic decrement is then extracted. The transient signal here shown was flipped for visual clarity, but the damping data remains unaffected.

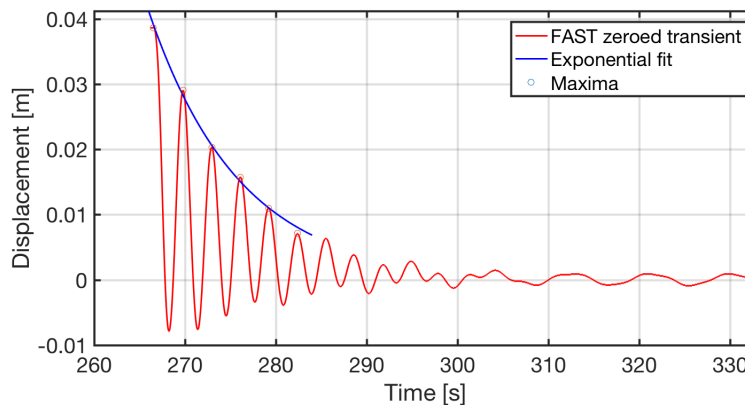


Figure 5.5: Transient signal from which the damping at that wind speed is extracted by calculating the logarithmic decrement.

The turbines motions above rated wind speed, as seen in Figure 6.5 in the next Chapter, have a moving average and thus a meaningful exponential curve cannot be easily fit though their peaks. In this case the distances from peak to trough were calculated for consecutive oscillations. The logarithmic decrement was then calculated from the decrease in these distances.

Because the excitation on the turbine below cut in wind speed is too small to create motions from which damping can be extracted, the structural damping ratio is assumed to be 2 percent. This gives a damping coefficient of $3.2842E04 \frac{N}{m/s}$. This value is introduced to the data gathered above for all wind speeds below cut-in. However, motions below cut-in wind speed are not relevant for this project.

The resulting damping coefficients were then interpolated into a curve seen in Figure 5.6. The curve was made into MATLAB function handle to be used in the time simulations, defined given the wind speed at each time step. We see that the sharp fall in damping at $12 \frac{m}{s}$ indicates the pitch control of the turbine switching on.

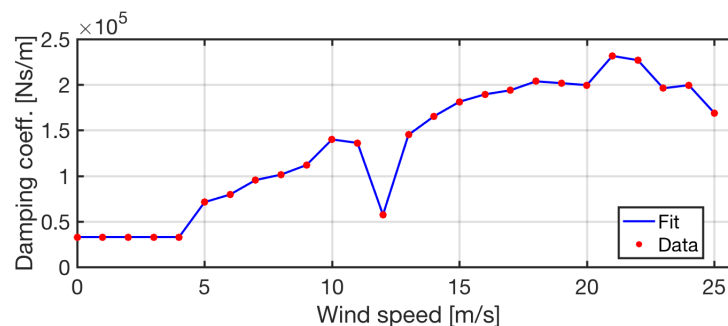


Figure 5.6: Original damping coefficient curve for the turbine FA motions at each wind speed. This curve was modified as shown in Chapter 6.

It was found during validation, that the damping values derived here do not result in good enough correspondence between FAST and MATLAB. Improvements are discussed in chapter 6.

5.4. Modeling Loads on a Super-stiff Turbine

In this section the approach is explained to attempt and answer the research question of what is the baseline fatigue in a turbine that has a constant dynamic amplification of 1, and whose control system responds instantly to changes in wind speed. Given that we use MATLAB to calculate this, however, this approximation is valid as a comparison to other calculations in the MATLAB model. In order to find this baseline MATLAB fatigue, we do not need to construct and validate a model. The simple procedure of calculating loads from wind signals on this turbine is explained in this section.

This modeling does not require any actual simulations, and is based on a simple calculation. In this method, the wind signals of each load case are ran through the thrust transfer function, which was calculated in Section 5.3.3 of this chapter. The moment on the tower base, is then found by simply multiplying the thrust calculated at each time step by the height of the tower, 90 meters. This is finally used to find the stress signals which are fed to the fatigue equivalent load MATLAB scripts to find the lifetime fatigue damage.

This model uses the coherence given by averaging 18 wind signals over the turbine's rotor. Given that in the project's time frame no better way to model wind sampling could be found, the fatigue damage equivalent load calculated in this method cannot be compared to the FAST or MATLAB modelled turbines. In fact, because of the 18 point averaged signal's low relative turbulence, we expect that the fatigue damage equivalent load will be lower than expected. Section B.2 shows the resulting fatigue equivalent loads. Due to time limitations, this is the best approximation offered to a "super-stiff" turbine.

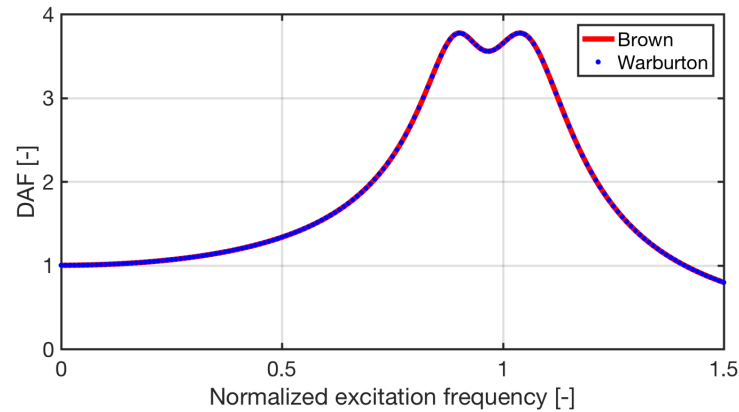


Figure 6.1: Steady-state dynamic amplification of the MATLAB turbine model with a TMD (Configuration 1), calculated according to Brown university formulas compared to the theoretical values by Ayorinde et al.

To do this, the force is modeled as nonzero on mass 2, and simulations are run at different excitation frequencies for enough time for the system to reach steady state. From these steady-state motions we extract the maximum displacement at each excitation frequency. With these, the DAF is calculated in the same way as in Section 4.6.

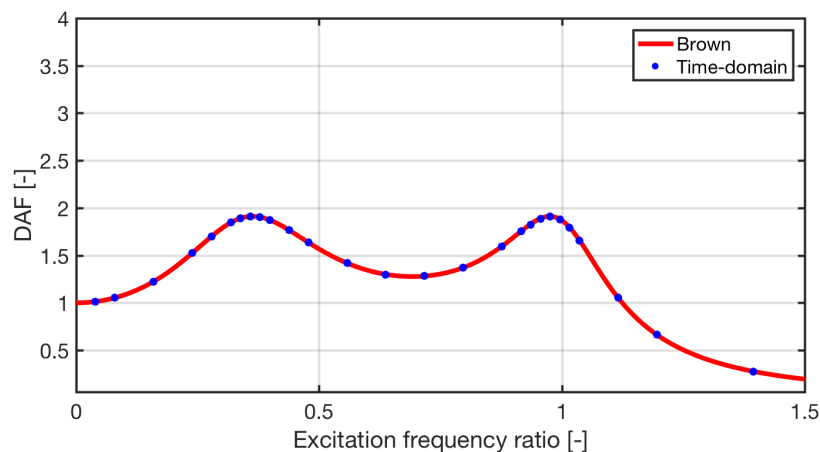


Figure 6.2: DAF of mass 1 in Configuration 2 as calculated with the Brown method and in the time domain.

6.2. Comparison of MATLAB and FAST

In this section, the behaviour of the MATLAB model in the time domain is put to the test. As mentioned in the introduction to this chapter, this was done by exporting wind and thrust data from FAST simulations. The wind and thrust data from each FAST simulation were introduced into the MATLAB model to excite the turbine. Then, the responses of the MATLAB model are put against those of the FAST model.

In addition to visually comparing the amplitudes of the motions in the time domain, to compare between the real turbine and the MATLAB model the power spectral densities of their respective motions were plotted. The PSDs are obtained by performing a Fourier transform on the motion signals. PSD graphs show the amount of energy of the systems at each frequency, and are a fundamental tool to expose the phenomena that dictate the complex motions of the models. Finally, as explained in Chapter 3, the FDELs of each 10 minute simulation are compared with those of FAST.

At this point in the project, the final decision had not been made to model the turbine in MATLAB using thrust signals instead of wind. This will be elucidated in the following sections.

In the first time simulation, The MATLAB model is excited by a wind signal uniform through the turbine's rotor. The wind signal is a step function, the same signal seen in Figure 5.3. This simulation

allows us to visualize and compare several aspects of the models at the same time. At each speed, the constant thrust means the turbine will oscillate around a specific equilibrium point, which can be used to test and confirm the stiffness of the turbine. Similarly, the shape of the decreasing oscillations is used to ensure the logarithmic decrements are the same as those calculated in Section 5.3.4.

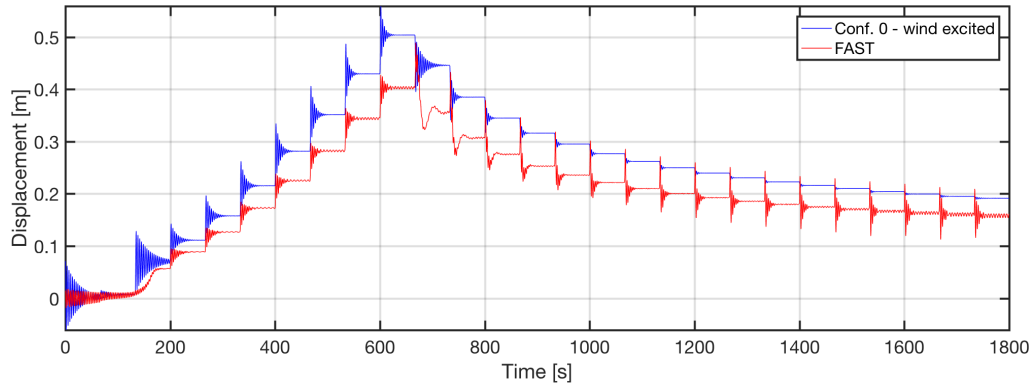


Figure 6.3: Displacements from FAST and MATLAB of the turbine and 1DOF model under a stepped wind signal, with several aspects that need addressing.

We see in Figure 6.3 that there are several discrepancies that must be explained and addressed:

- Discrepancy in the equilibrium points that is largest at rated wind speed
- Clear difference in shape of transient motions above rated wind speed
- Discrepancy in the damping below cut-in wind speed

In the partial load region, amplitudes of the motions are larger for the MATLAB model, although they appear to decay in the same way, which suggests the damping is approximately correct. The other discrepancies mentioned above are addressed in the next sections.

6.2.1. Stiffness adaptation

The mismatch in the resting positions at each wind step seen in Figure 6.3 increases towards rated wind speed. We know from Chapter 5 that the thrust on the rotor is maximum at U_{rated} . We also know the deflection of a spring with a stiffness k under a force F is given by Hooke's Law:

$$x = \frac{F}{k} \quad (6.1)$$

The discrepancy of the displacement of two springs subjected to the same force will increase linearly with the magnitude of that force. This suggests that there is a mismatch in the stiffness of the models, and thus that the generalized stiffness found in Chapter 5 is not representative of the real turbine.

To test and fix this discrepancy we calculate the ratio of the displacements at their highest points, which is: $\frac{x_{FAST}}{x_{MATLAB}} = 0.7995$. Since the thrust force is the same on both systems, we know that:

$$F_{thrust} = x_{MATLAB}k_{MATLAB} = x_{FAST}k_{FAST} \quad (6.2)$$

Then, the ratio between the displacement of the FAST model and the MATLAB model is the same as the ratio of the stiffness of the MATLAB model and that of the FAST model. In other words,

$$\frac{x_{FAST}}{x_{MATLAB}} = \frac{k_{MATLAB}}{k_{FAST}} = 0.7995 \quad (6.3)$$

Thus,

$$k_{FAST} = k_{MATLAB} \cdot 1.2508 \quad (6.4)$$

Inserting this stiffness discrepancy factor into the MATLAB model results in the response seen in Figure 6.4, which is a notable improvement from the response seen in Figure 6.3. The resting positions at each wind step are all but equalized.

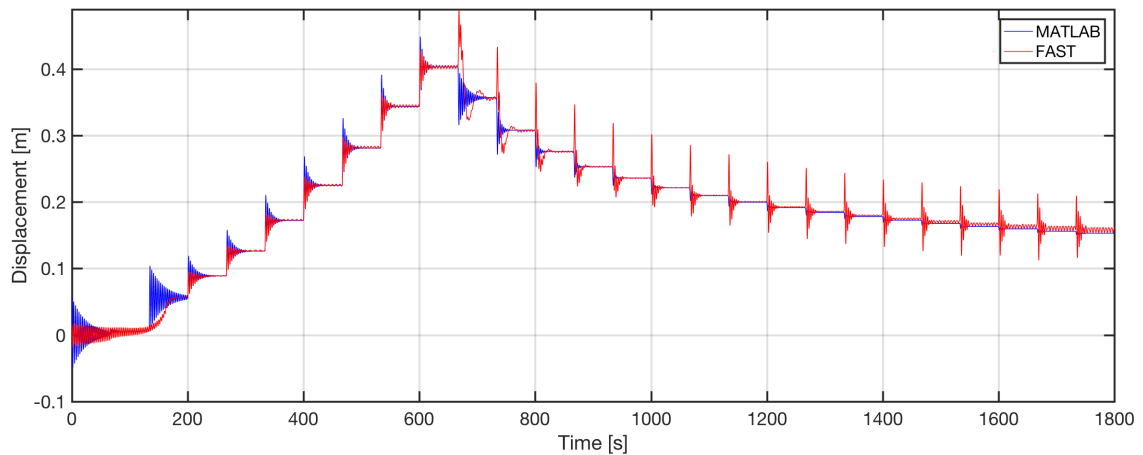


Figure 6.4: Simulations on FAST and MATLAB of the turbine and 1DOF model excited under a stepped wind signal.

Still, if we look closer at the motions beyond rated wind speed, as in Figure 6.5 we see clearly that at $t = 660s$, when the wind speed rises from $11 \frac{m}{s}$ to $12 \frac{m}{s}$, although both systems come to rest at the same location, the shape of the motions are very different.

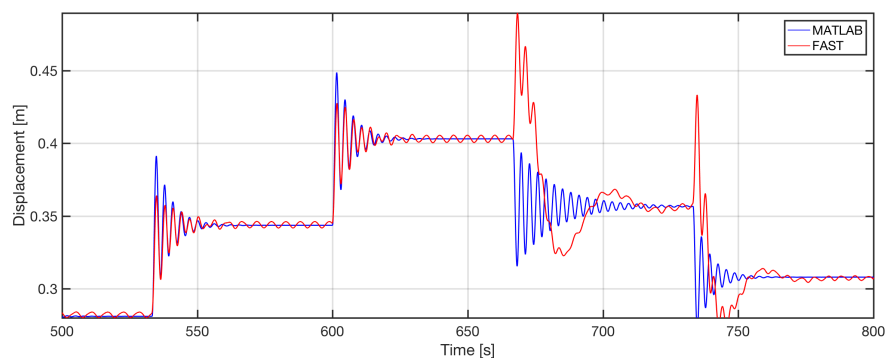


Figure 6.5: Detail of Figure 6.4

6.2.2. Motions above rated wind speed

Up until now the MATLAB simulations have been based on the assumption that the model can be accurate enough by using wind as a source of excitation. Here however, we see why this is not the case. The source of the difference in the motions above rated becomes clear when we look at the thrust signals from FAST and MATLAB. As can be seen in Figure 6.6, the MATLAB-generated thrust changes in a step-wise fashion, simply following the changes in wind. The thrust from the FAST simulation, however, oscillates and has large peaks at the beginning of each wind step above U_{rated} .

The state of the turbine is subject to the speed of the control algorithms and mechanisms that are designed to maintain constant power above rated wind speed. These controls have, of course, a lag time. If we look at the rotor power, generator power, and blade pitch curves of the FAST simulation in Figures 6.7 and 6.8, we see that the control system of the turbine cannot immediately act to adjust for sudden changes in wind speed.

This lag causes spikes in the thrust when the wind increases, spikes that are not present in the MATLAB thrust signal. This means that in MATLAB the turbine mass is merely released to a lower thrust state, while the FAST turbine is "struck" by wind at the same time as the controller kicks in to adjust torque and pitch accordingly, causing the motions we see in Figure 6.5.

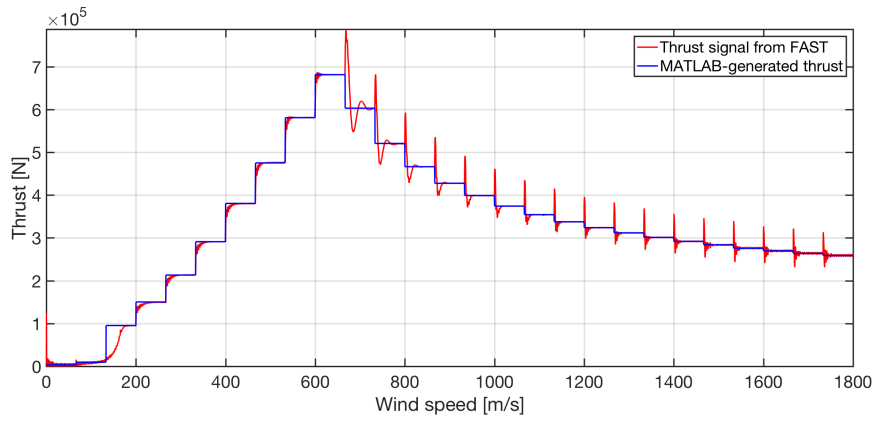


Figure 6.6: Thrust signals from FAST and produced by MATLAB under the same stepped wind signal

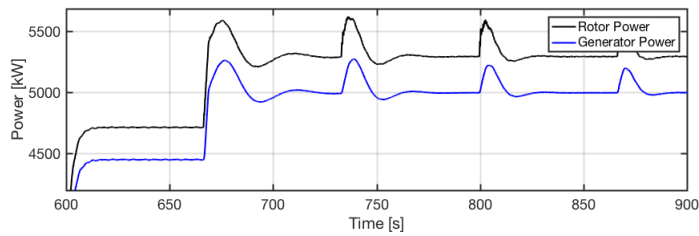


Figure 6.7: Rotor and generator powers from FAST, as the turbine transitions from partial-load to full-load at $t = 660s$.

If we run the MATLAB model with the FAST-generated thrust instead of the MATLAB-wind-generated one, we get the response seen in Figure 6.9. Seen against the response of the FAST turbine, the response follows very well the real turbine. We see that below rated speed the transient motions have similar amplitudes, but the decay is slower for MATLAB. The motions above U_{rated} have similar decays, and we see in the detail Figure 6.10 that the transient at $t = 660s$ follows better that of the real turbine, although with higher amplitudes.

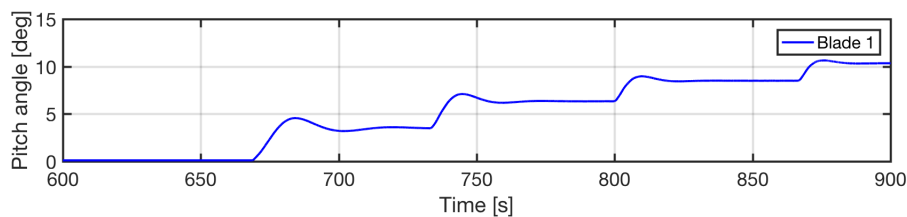


Figure 6.8: Blade pitch angle from FAST, as the turbine transitions from partial-load to full-load at $t = 660s$.

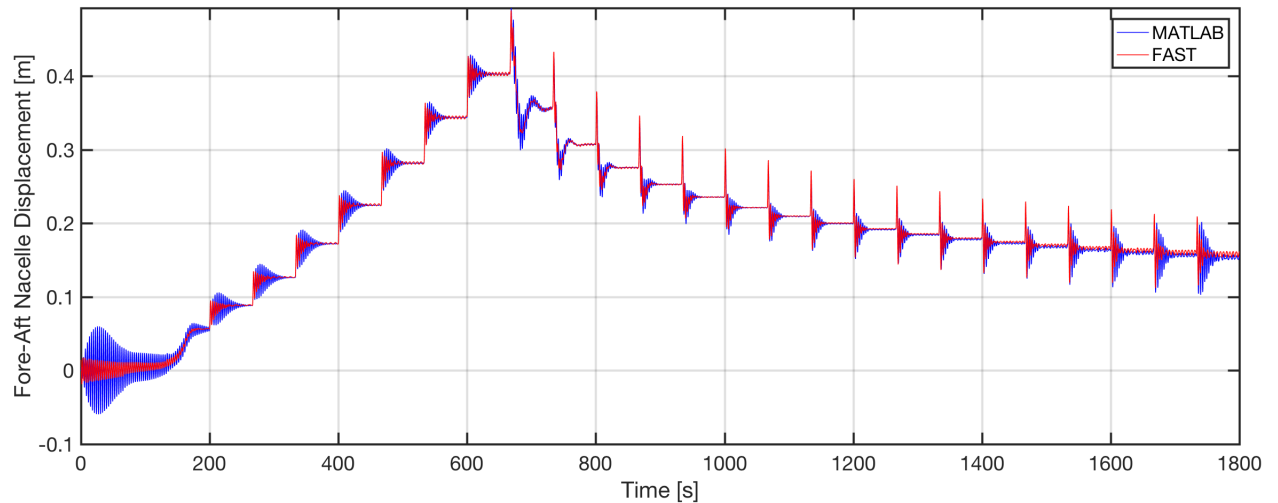


Figure 6.9: Motion signal of the 1DOF system excited by a thrust signal extracted from FAST, compared to the motions of the FAST model under the same thrust signal.

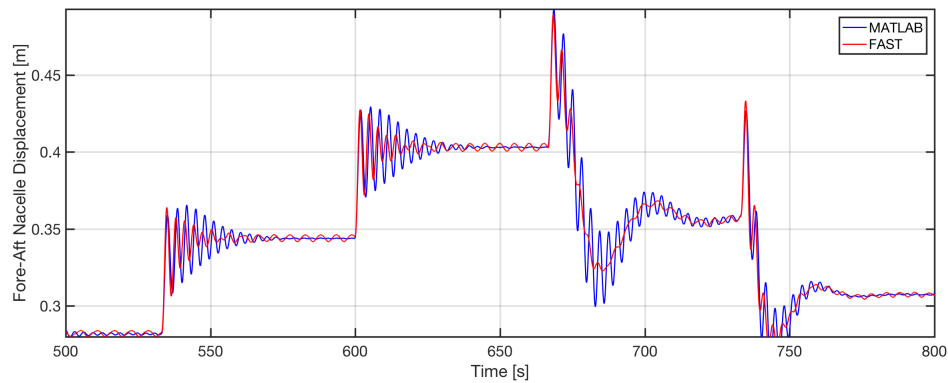


Figure 6.10: Detail of Fig 6.9

Given the results of this section, it becomes clear at this point in the project that to give the most accurate representation of the real turbine in MATLAB, without the implementation of artificial control emulators, the model must be excited using thrust signals from FAST. From this point in the report onward, all MATLAB simulations shown are performed using thrust signals from FAST, with the exception of Figure 6.16.

6.2.3. Behaviour below cut-in wind speed

For the purposes of this project the turbine is not modeled below cut-in wind speed. Thus, achieving satisfactory behavior of the model below this speed is thus not necessary, but for the sake of completeness this section offers an explanation of the MATLAB model's behaviour.

It is clear from Figures 6.4 and 6.9 that below the cut-in wind speed, the damping of the MATLAB model is not representative of the real turbine. If we look at Figure 6.4, the damping chosen in section 5.3.4 based on structural damping seems too high in the first 100 seconds, and not high enough when the turbine starts up at around 150s.

However, when the thrust curve from FAST in Figure 6.6 is inspected, we see that around $t = 140s$, while the MATLAB-generated thrust jumps as expected, the FAST thrust rises following an "S" shape. The instant change in thrust "strikes" the MATLAB model, creating a transient motion similar to those of the turbine at higher wind speeds. The FAST model's thrust rises slowly enough that the motion reflects quasi-static excitation, simply following Hooke's law. That is why we see the MATLAB model perform much better during start-up in Figure 6.9, when it is excited by the thrust signal from FAST.

6.3. Behavior under FAST-given thrust excitation

Here the MATLAB model is tested by exciting it with the thrust signal exported from FAST, as done for the stepped wind signal. It is clear from Figure 6.11 that this approach emulates the real turbine well. This is especially the case in the full-load region, where the turbine's speed control dominates the shape of motions.

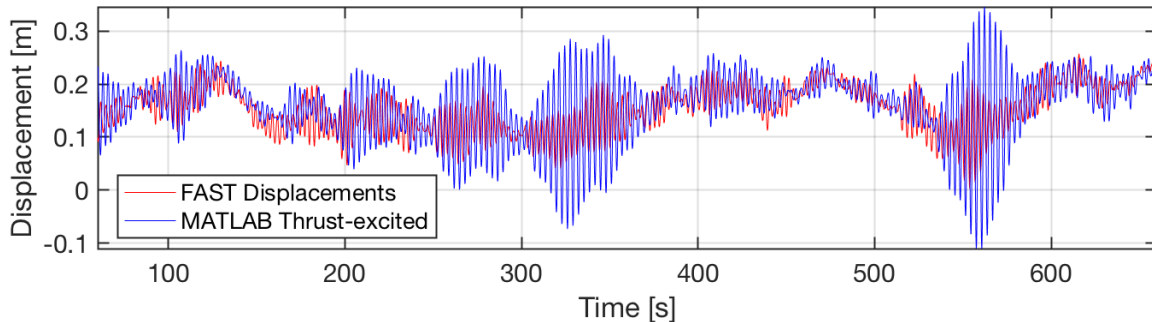


Figure 6.11: Displacement of MATLAB model with previously calculated damping, excited by the thrust signal from a 7mps FAST simulation, compared to original motions from FAST

Looking at Figure 6.11 again we see that some of the time the amplitudes of the MATLAB model largely exceed those of the real turbine. A similar behavior is visible in Figure 6.9. This suggests that the damping found with the method in Section 5.3.4 may have been underestimated.

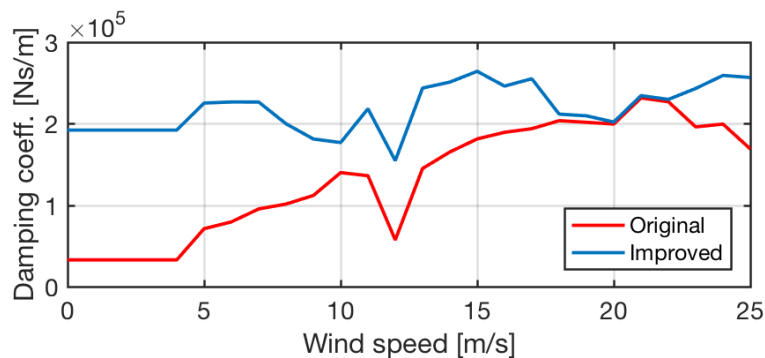


Figure 6.12: Original and improved damping curve fits for the MATLAB model

To solve this, an iterative method was used to visually "tune" the damping to achieve similar decay in motions at each wind speed of the stepped wind simulation. Constant factors increased the value of the damping at each speed, and the power spectra of motions at each wind speed confirmed the accuracy of the model. This procedure resulted in a damping curve fit that is higher than the original. Both are shown in Figure 6.12.

The motions resulting from the new damping values under the stepped wind signal can be seen in Figure 6.13. This curve has behaviour that is visibly better than any other mentioned up to this point, as motions both below and above rated wind speed decay in almost exactly the same way.

With this adaptation in damping, the motions of the thrust-excited MATLAB model under the forces of the same $7 \frac{m}{s}$ simulation become much more similar. This can be seen in Figure 6.14.

The power spectra of the motions under turbulent wind, as excited by respective thrust signals, are shown in Figure 6.15 for wind speeds of 5, 10, 15 and 20 meters per second. We can observe in the spectra the expected peaks at the first natural frequency of the turbine, as well as smaller peaks for other excitations of the turbine, such as 3P around 1Hz.

Note that the spectra are plotted in decibels, which is a logarithmic unit. If we plot the spectra linearly at any of these speeds, such as in Figure 6.16, it becomes clear that any peaks in power at frequencies above 0.5Hz are negligible. Also, when comparing this spectrum to that of the same simulation excited by a wind signal, the improvement is very apparent.

When we plot the motions in Figure 6.17 the improvement is easy to understand visually.

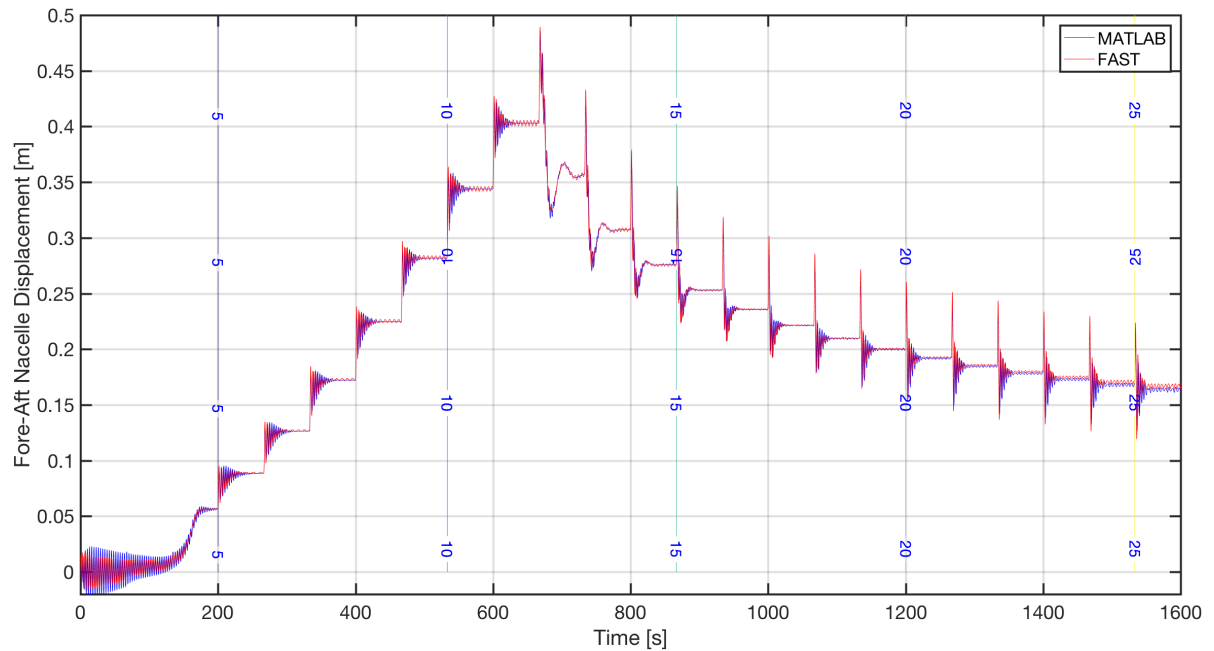


Figure 6.13: Motions of the thrust-excite MATLAB model with improved damping. The wind speeds are displayed in vertical lines.

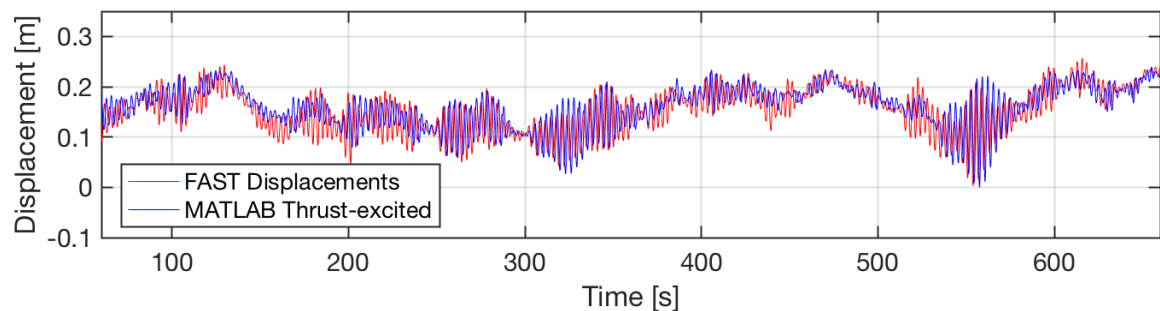


Figure 6.14: Displacement of MATLAB model with new damping, excited by the thrust signal from a 7mps FAST simulation, compared to original motions from FAST.

As a final point of comparison, the FDELs of each simulation are compared. As mentioned before, these are the final points of comparison of behaviors between FAST and MATLAB. We see in Figure 6.18 that there is good correspondence.

We can see in Figure 6.18, that the fatigue damage equivalent loads are within the correct range of those of FAST. The discrepancies that can be seen are caused by the imperfect relation between motions and moment at the tower base, likely caused by excitations of the turbine's second and higher modes. This has been explained in Section 3.3. Given the scope and time limitations of the project this issue is not addressed. As mentioned before, the comparison between the MATLAB model without and with the TMD configurations remains valid. These comparisons will be shown in Chapter 7.

6.4. Simulating Behaviour with Wind Excitation

Deriving thrust from the wind signal was attempted. However, as mentioned in Chapter 3, it appeared to be impossible to get realistic thrust time series with simple approximations. The failed validation procedure for wind excitations is thus not included in the report, instead shown in Appendix B.

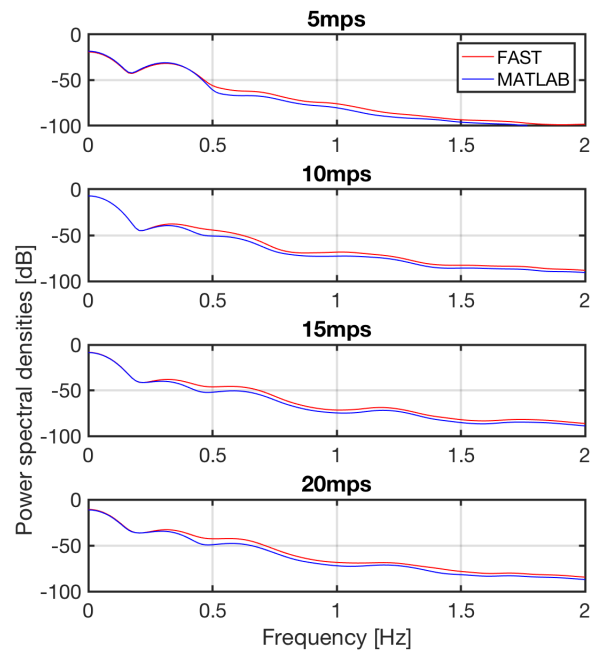


Figure 6.15: PSD of the thrust excited MATLAB model at 5, 10, 15 and 20 [m/s], against those of FAST, plotted in dB.

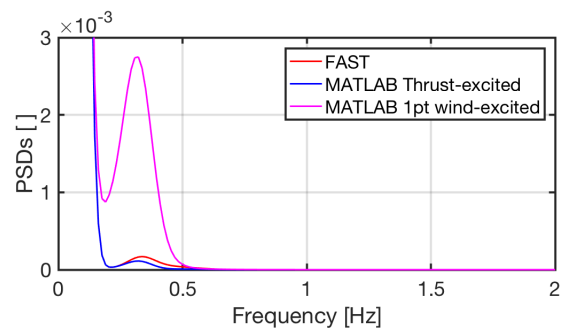


Figure 6.16: PSDs of FAST and MATLAB thrust-excited signal compared to the 1-pt wind-excited signal, for a 10mps wind simulation (same as above)

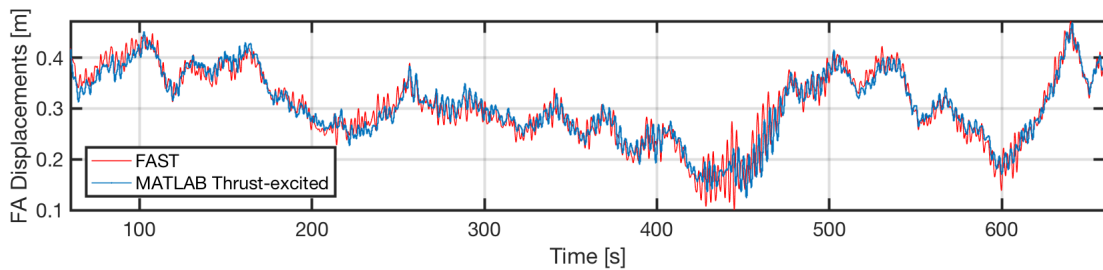


Figure 6.17: Fore-aft motions of FAST and MATLAB thrust-excited signal for a 10mps wind simulation (same as Figure 6.16)

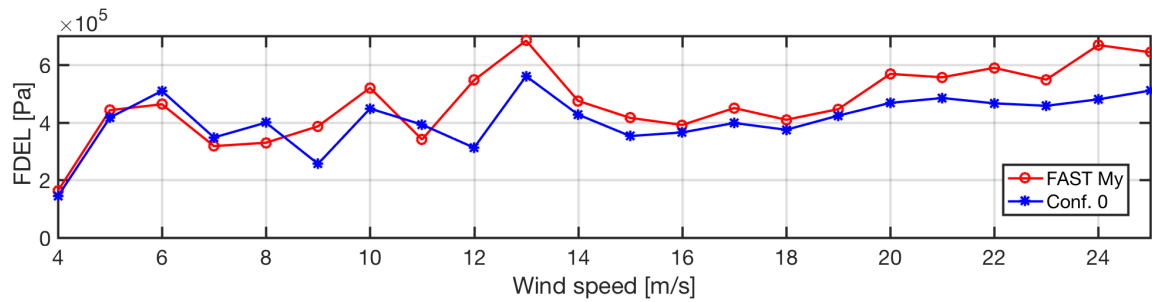


Figure 6.18: FDEL of FAST and MATLAB model before the addition of a TMD. The discrepancies are due to the deviating relationship between displacement and moment at the tower base.

6.5. Summary of MATLAB validation

This Chapter shows that for the purpose of modeling the excitations and resulting dynamic behavior to the best possible correspondence with the real turbine, the thrust signals extracted from FAST must be utilized.

The MATLAB model that gives the most suitable approximation has an equivalent mass of $3.99E05Kg$. The model has an adapted linear stiffness estimated at $1.69E06 \frac{N}{m}$ and an undamped first natural frequency of $3.28Hz$. The NREL report defining the reference turbine [21] gives the first natural frequency of the tower fore-aft motions as $3.24Hz$, which is very close to MATLAB approximation. The damping on the MATLAB model is variable, as was explained in Section 5.3.4 with the modification shown in Figure 6.12, which significantly increased the damping coefficient at most wind speeds.

The need to model the turbine's control system was eliminated with the decision to use thrust signals from FAST to excite the MATLAB model. This greatly simplifies the representation of wind forces on the rotor, because it means that the control algorithms affecting forces are already included in the signal. Furthermore, when exciting the MATLAB model with thrust, smaller but not insignificant load signatures that are sampled by the rotor are also introduced, such as 1 and 3P excitations.

A consideration that must not be ignored when modeling in MATLAB with thrust excitations is that the thrust is changing independently of the motions. This means that in some situations, if the direction of thrust change aligns with the direction of motion, instabilities might arise. However, given the artificial adjustments done to the damping, whatever instability is in fact present is mostly muffled. **This may explain the rather large increase in damping required from that calculated.**

As will be discussed in Section B.1, wind excited models are deemed inadequate to draw meaningful results and conclusions. For this reason, the only use given to wind signals seen in the Appendix is the calculation of the lifetime fatigue equivalent load under the assumption of constant $DAF = 1$.

Assessing the performance of the models modified and validated in this Chapter, the MATLAB thrust-excited model can be judged to be equivalent in the respects that are relevant to this project. With this, we can move on to use this model to implement and test the tuned-mass dampers, and, doing so finally delve into the research questions.

7

Experimental Results

7.1. Values for Optimal Behavior

The report showed in Chapter 4 and Section 6.1 that the optimal parameter values for Configuration 1 are given by the Warburton & Ayorinde equations. Similarly, these sections show how the optimal values for Configuration 2 were found using a MATLAB optimizer. The values found with these methods are shown in Table .

Table 7.1: Optimal damper values for Configurations 1 and 2. *Damping of the Conf. 2 absorber is subject to changes in aerodynamic damping, and thus is not constant.

Configuration 1 - Optimal Values			Configuration 2 - Optimal Values		
Variable	Unit	Value	Variable	Unit	Value
f_{opt}	-	0.9799	f_{opt}	-	0.3835
c_a	Ns/m	2.84E+03	c_a^*	Ns/m	1.9E+05 to 2.5e+05
k_a	N/m	3.32E+04	k_a	N/m	1.21E+05

Note that truly optimal values cannot be achieved in Configuration 2. Because the damper is itself the drive train including rotor, its damping coefficient will be variable and dependent on the wind speed and control system, following the values on Figure 6.12. Still, as shown later in this chapter, implementing it results in good fatigue reduction.

7.2. Behavior and Fatigue with Tuned Mass Dampers

7.2.1. Effect on Tower-top Motions

Displacements

Looking at the motions of the tower top with and without tuned mass dampers, the difference is visible. In Figure 7.1, the motions of the TMD-less MATLAB model, which we call Configuration 0, are shown in red in both sub-figures. These displacements are for a 10 minute simulation at $U_{avg} = 10 \frac{m}{s}$. Also plotted in blue on top of both, we see the motions of the tower when Configurations 1 and 2 are implemented, respectively. We see that the red peaks of Configuration 0 are more visible against the smaller motions of Conf. 2.

Comparing instead motions of the turbine simulated at $U_{avg} = 20 \frac{m}{s}$, shown in Figure 7.3, we see that similar to the previous figure, the motions of the turbine with a drive-train-damper, Configuration 2, has in general smaller oscillations than that with the oscillating generator. The motions of the TMD-less turbine, shown in red, are clearly more visible.

These results we see in these displacement signals repeat themselves over the operational speed range of the turbine. In all cases the displacements of Configuration 2, with the oscillating drive train, show the smallest amplitudes and smoothest behavior. The displacements for all simulations of the operational speed range are shown in Appendix A, for space.

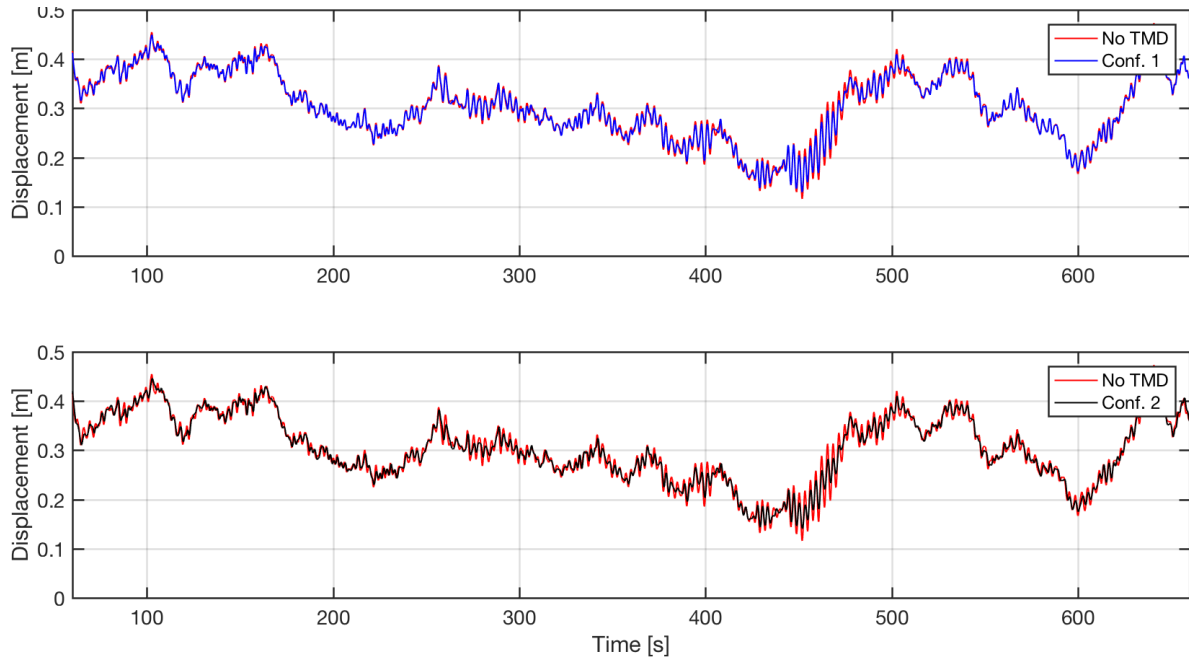


Figure 7.1: Displacement of the MATLAB model turbine without and with TMDs at 10mps.

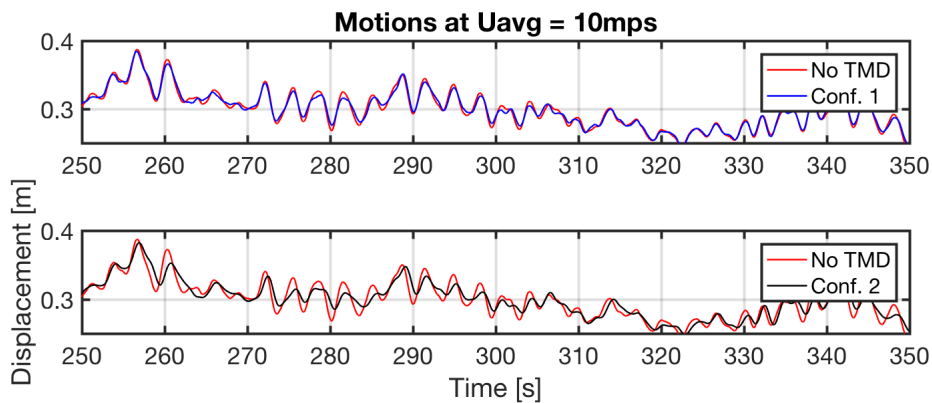


Figure 7.2: Detail of Figure 7.1.

Power Spectral Densities

In Figure 7.4, we see that although the motions are not so visibly reduced with the generator-TMD, the power at the first natural frequency is, in fact, significantly reduced. With the implementation of Configuration 2, which allows for the rotor to oscillate minimizing energy transfer to the support structure, the power reduction is even more marked.

For the PSDs of simulations at $U_{avg} = 20 \frac{m}{s}$, shown in Figure 7.5, we see a similar change.

Similar to the previous section, the power spectral densities at all other wind speeds are shown in Appendix A for space.

7.2.2. Effect on Tower Fatigue Life

FDEL of Each Speed Load Case

Here, we plot the FDELs of the TMD-less Configuration 0 MATLAB model, as we did in the previous chapter, against the equivalent loads from the same simulations on the models of our two TMD systems. These can be seen in Figure 7.6.

The reduction in the equivalent load is evident. In Table 7.2, the average load reduction over the entire operational range of the turbine is -2% for the generator-TMD, and -13% for the drive train-TMD. It may seem the effect of using the turbines 8 ton generator is not as positive as was expected,

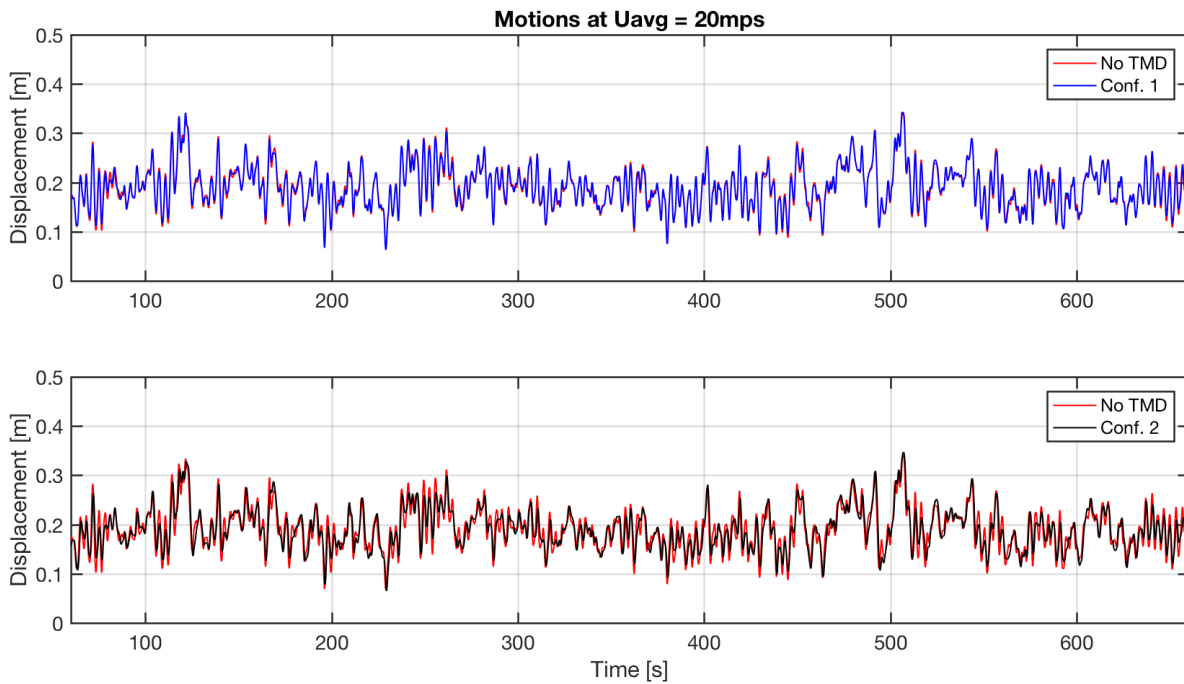


Figure 7.3: Displacement of the MATLAB model turbine without and with TMDs at 20mps.

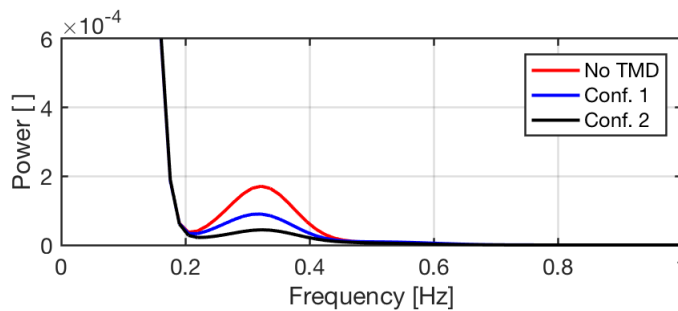


Figure 7.4: Power spectral densities of the MATLAB model turbine without and with TMDs at 10mps.

but this average assumes equal probability for all wind speeds, which is not the case.

Lifetime FDEL

If we take, as an example a location with a wind climate characterized by a Weibull curve with a scale factor $k = 2$ and shape factor $a = 8$, shown in Figure 7.7, we can estimate the overall effect these systems have, in the reduction of FDEL, over the lifetime of a turbine. In Figure 7.7 we calculate the probability for each load case, or the probability that the average wind speed is within the bin $0.5 \frac{m}{s}$ below or above every velocity integer. These bins are of course $1 \frac{m}{s}$ wide, making the area under the curve of each bin equal to its height.

Given the probability distribution in Figure 7.7, we can find the total amount of time in seconds that the wind will be within a specific bin. With this amounts of time, a factor is calculated for each bin by dividing each quantity, which are in seconds, by 600s or 10m: the length of each simulation performed. Table 3.1 shows these factors. They will be used to multiply the number of load cycles at each load range for each 10-minute simulation. This total number of load ranges and cycles is be added up to a final, 20-year lifetime fatigue damage equivalent load for comparison between systems.

Using these data, we simply introduce the lifetime factor into our FDEL calculation MATLAB script. When the stress signals for each load case are produced and rainflow-counted, n_j is multiplied by this factor in Equation 3.4 for each load range in each load case. Thus the total number of cycles at each stress range for each wind speed load case is accounted.

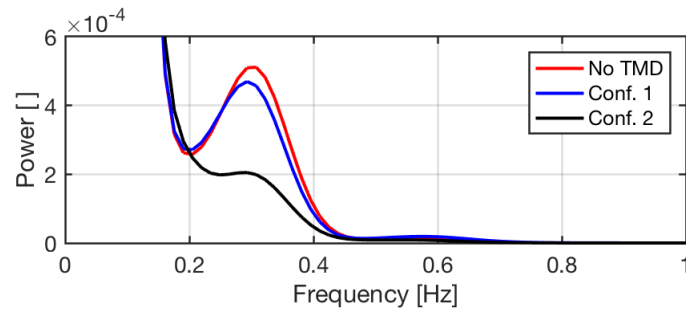


Figure 7.5: Power spectral densities of the MATLAB model turbine without and with TMDs at 20mps.

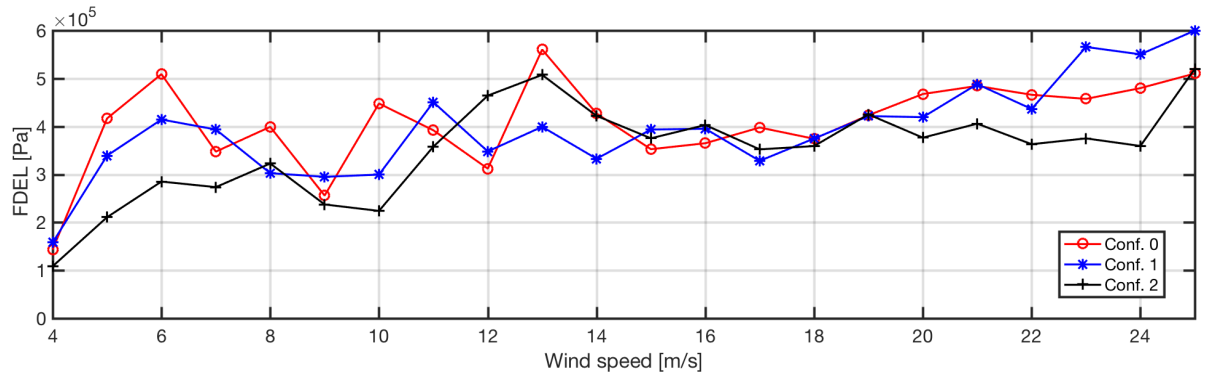


Figure 7.6: Fatigue equivalent loads for 20yr lifetime of the MATLAB model without and with TMDs.

As explained in Section 3.3, the fatigue equivalent load ranges counted in all load cases must be added inside the summation sign, before being elevated to the power of 1 over the SN slope, $m = 3$, as Equation 3.6 shows. In the end the final FDELs and their decrease using Configurations 1 and 2 are shown in Table 7.3.

In Table 7.3 it becomes clear that the tuned mass damper configurations are very effective in reducing fatigue damage over a turbine's operational range. The fatigue equivalent load for the FAST displacement-calculated stresses, and Configuration 0, the MATLAB turbine model without an absorber, are shown for comparison to the FAST moment signal-calculated fatigue. Configuration 1, with its oscillating 8 ton generator is able to reduce the overall fatigue by 12%. Fatigue equivalent load is even more reduced when implementing Configuration 2 with its the oscillating rotor and drive train, with an overall reduction of over twenty percent.

The actual damage done to the turbine's tower at each load case and over its lifetime is shown in Table 7.4 and Figure 7.8. The percentages shown are compared to the total damage of the MATLAB model with no TMD. We can see that although the damage is greater for the TMD configurations in some load cases, Configuration 1 provides noticeable improvement while Configuration 2 shows even more promise.

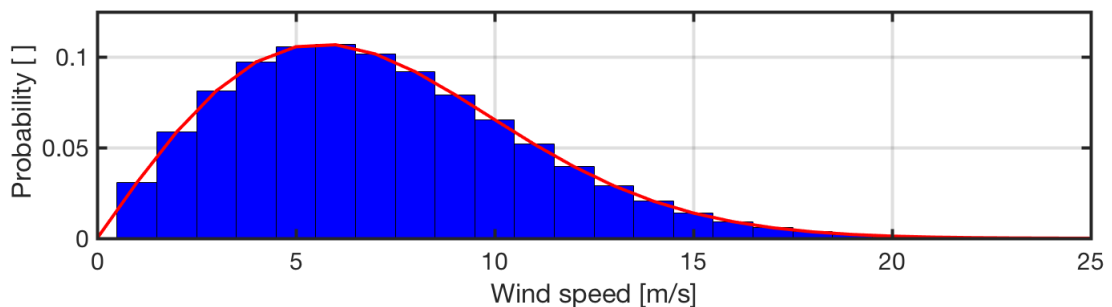


Figure 7.7: Weibull distribution curve.

Table 7.2: 1Hz FDEL of tower base fatigue for Configurations 1 and 2, as compared to the TMD-less MATLAB model.

Uavg[m/s]	Pw	1 Hz Equivalent Load Range [Pa]			Rel. damage [%]	
		Conf. 0	Conf. 1	Conf. 2	Conf. 1	Conf. 2
4	0.0974	1.4E+05	1.6E+05	1.1E+05	10	-24
5	0.1057	4.2E+05	3.4E+05	2.1E+05	-19	-49
6	0.1068	5.1E+05	4.1E+05	2.9E+05	-19	-44
7	0.1017	3.5E+05	3.9E+05	2.7E+05	13	-21
8	0.092	4.0E+05	3.0E+05	3.2E+05	-24	-19
9	0.0793	2.6E+05	3.0E+05	2.4E+05	15	-7
10	0.0655	4.5E+05	3.0E+05	2.2E+05	-33	-50
11	0.0519	3.9E+05	4.5E+05	3.6E+05	15	-9
12	0.0395	3.1E+05	3.5E+05	4.6E+05	12	49
13	0.029	5.6E+05	4.0E+05	5.1E+05	-29	-9
14	0.0205	4.3E+05	3.3E+05	4.2E+05	-22	-1
15	0.0139	3.5E+05	3.9E+05	3.8E+05	12	6
16	0.0092	3.7E+05	4.0E+05	4.0E+05	8	10
17	0.0058	4.0E+05	3.3E+05	3.5E+05	-17	-11
18	0.0036	3.7E+05	3.7E+05	3.6E+05	0	-4
19	0.0021	4.2E+05	4.2E+05	4.3E+05	0	0
20	0.0012	4.7E+05	4.2E+05	3.8E+05	-10	-19
21	0.0007	4.8E+05	4.9E+05	4.1E+05	1	-16
22	0.0004	4.7E+05	4.4E+05	3.6E+05	-6	-22
23	0.0002	4.6E+05	5.7E+05	3.8E+05	24	-18
24	0.0001	4.8E+05	5.5E+05	3.6E+05	15	-25
25	0	5.1E+05	6.0E+05	5.2E+05	18	2

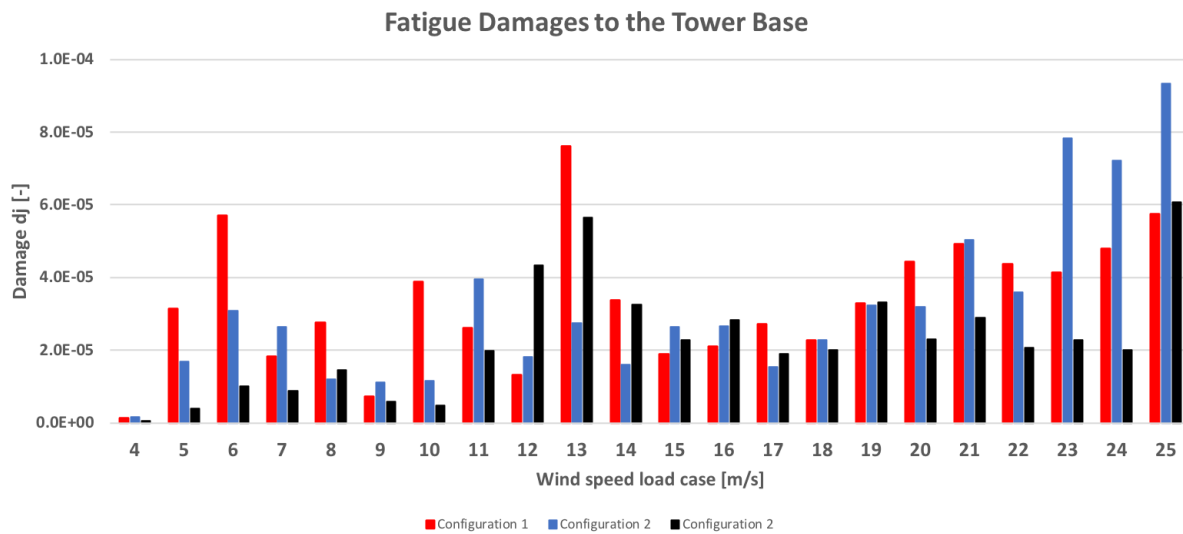


Figure 7.8: Damage according to Miner’s rule for each load case with the TMD-less Configuration 1, and TMD Configurations 1 and 2.

Table 7.3: Calculation of the 20-year lifetime FDELs for FAST (from moments and motions signals) and for each of the MATLAB configurations

Lifetime Fatigue Equivalent Loads - No TMD		
Source	20yr FDEL [Pa]	Diff. wrt FAST My [%]
FAST My	3.988E+05	-
FAST Disp	3.874E+05	-3
MAT Conf. 0	3.743E+05	-6

Lifetime Fatigue Equivalent Loads - With TMD		
Source	20yr FDEL [Pa]	Diff. wrt Conf.0 [%]
MAT Conf. 1	3.299E+05	-12
MAT Conf. 2	2.896E+05	-23

Table 7.4: Fatigue damage for each load case, and their percentage in relation to the total lifetime fatigue damage D of MATLAB Configuration 0.

Fatigue damage						
U_{avg}	Configuraton 0		Configuraton 1		Configuraton 2	
	d_j	% of D	d_j	% of D	d_j	% of D
4	1.29E-06	0.00	1.71E-06	0.00	5.55E-07	0.00
5	3.13E-05	0.04	1.69E-05	0.02	4.05E-06	0.01
6	5.71E-05	0.08	3.08E-05	0.04	1.00E-05	0.01
7	1.82E-05	0.02	2.64E-05	0.04	8.85E-06	0.01
8	2.75E-05	0.04	1.20E-05	0.02	1.45E-05	0.02
9	7.26E-06	0.01	1.11E-05	0.02	5.79E-06	0.01
10	3.89E-05	0.05	1.16E-05	0.02	4.86E-06	0.01
11	2.61E-05	0.04	3.96E-05	0.05	1.98E-05	0.03
12	1.31E-05	0.02	1.82E-05	0.02	4.33E-05	0.06
13	7.61E-05	0.10	2.75E-05	0.04	5.65E-05	0.08
14	3.37E-05	0.05	1.59E-05	0.02	3.25E-05	0.04
15	1.90E-05	0.03	2.64E-05	0.04	2.29E-05	0.03
16	2.10E-05	0.03	2.67E-05	0.04	2.83E-05	0.04
17	2.72E-05	0.04	1.53E-05	0.02	1.89E-05	0.03
18	2.27E-05	0.03	2.28E-05	0.03	2.00E-05	0.03
19	3.28E-05	0.04	3.24E-05	0.04	3.32E-05	0.05
20	4.42E-05	0.06	3.19E-05	0.04	2.31E-05	0.03
21	4.92E-05	0.07	5.03E-05	0.07	2.89E-05	0.04
22	4.38E-05	0.06	3.60E-05	0.05	2.07E-05	0.03
23	4.14E-05	0.06	7.83E-05	0.11	2.28E-05	0.03
24	4.78E-05	0.06	7.21E-05	0.10	2.01E-05	0.03
25	5.75E-05	0.08	9.34E-05	0.13	6.08E-05	0.08
D	7.37E-04	1.00		0.95		0.68

The reader must remember that these numbers are comparative. Given that the slope and fatigue strength steel are not part of these calculations, and given that non-operational states of the turbine were not taken into account, this project cannot offer the exact fatigue damage at the end of a 20-year life.

7.2.3. Motions of the Dampers

Configuration 1

The motions of the generator with respect to the main mass are quite important. They determine how much space must be kept free in the nacelle to allow for unobstructed oscillations. This in turn will drive the design of the nacelle, or, if the motions are too large, nullify the feasibility of the system.

In Figure 7.9 we plot the motions of Configuration 1 under wind at $25 \frac{m}{s}$. The speed is shown in Section 7.2.2 to have the highest fatigue, and thus oscillations.

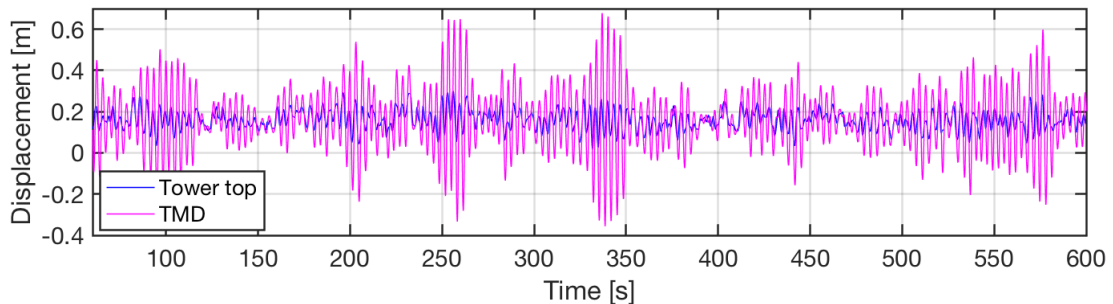


Figure 7.9: Displacements of the tower top and generator in Configuration, 1 under 25[m/s] winds.

The most important distances, however, are those between the generator and its center of equilibrium within the nacelle. Because the displacements in Figure 7.9 are shown with respect to an origin irrespective of the motions, it is difficult to see the distance between the generator and its equilibrium point. As shown in Figure 3.2, the origins of each mass in the MATLAB model are independent of each other. Then, to show the distance between the masses with respect to time, we subtract the displacement of the TMD by that of the tower top. This way, when the TMD is further downwind than the tower-top, the difference is positive. These displacements are shown in Figure 7.10 for the same load case. The generator's largest displacement from its equilibrium point is slightly higher than 0.47m, in both directions.

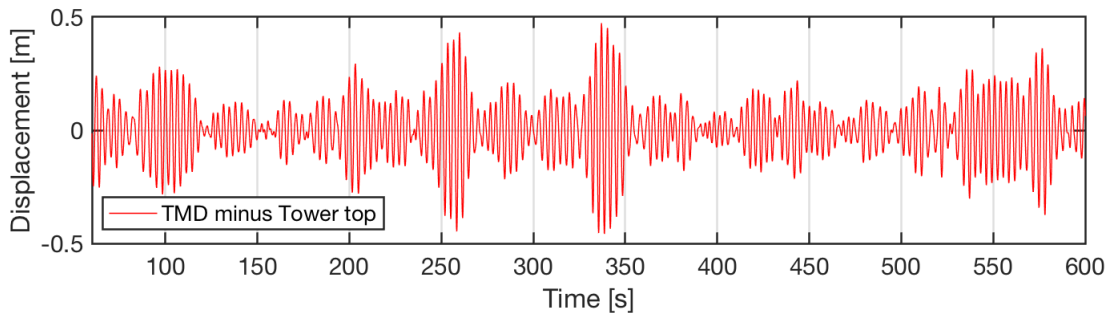


Figure 7.10: Displacements of the generator against the tower top in Configuration 1, under 25[m/s] winds.

Configuration 2

An important consideration for a turbine's nacelle and rotor design is the blade's maximum tip deflection. If the rotor fore-aft displacements with respect to the tower exceed this clearance, blade-tip collision may cause catastrophic failure of the turbine and its tower.

The displacements of the tower top and drive train are shown with respect to a single origin in Figure 7.11. We see that given the high stiffness of the tower and relatively lower, ideal stiffness of the drive train, the two components are separated by more than 2 meters most of the time.

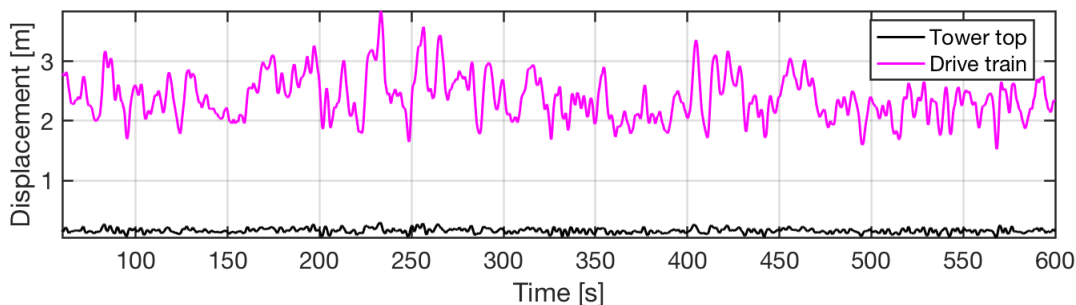


Figure 7.11: Displacements of the tower-top and drive-train-damper of Configuration 2, under 25[m/s] winds.

Just as in Section 7.2.3, we plot the distance between displacements of the tower and TMD, shown in Figure 7.12. In this case, it is clear that the distances are much larger, reaching as much as 3.5 meters.

7.3. Discussion

7.3.1. Fatigue reduction with TMDs

Configuration 1 was able to reduce fatigue by 12%, while Config. 2 boasted a remarkable 23% reduction as compared to the FAST turbine. Particularly for Configuration 2, the results are compelling. Having the drive train, rotor included, be able to oscillate with respect to the tower allowed to prevent the vast majority of kinetic energy from being transferred to the support structure. This remarkable reduction in fatigue damage equivalent load achieved using Configuration 2 begs the question: why is it so effective? It seems this system can be seen as analogous to the suspension system on a motor

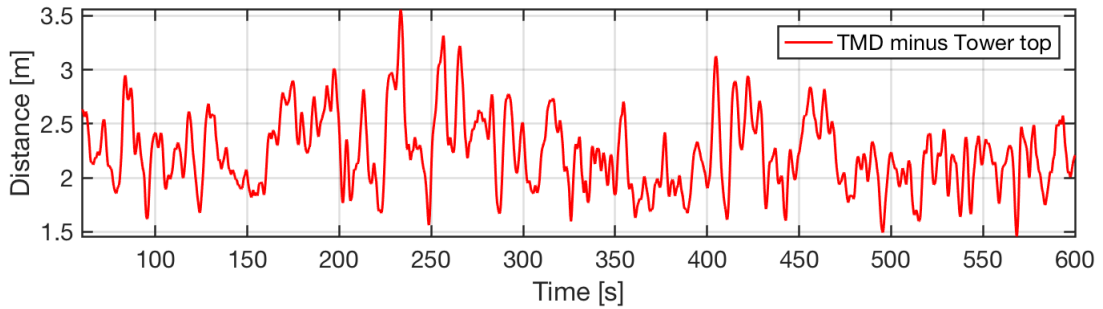


Figure 7.12: Displacements of the rotor and drive train damper against the tower top in Configuration 2, under 25[m/s] winds.

vehicle, that can effectively reduce the impacts felt by the driver from excitations caused by the road on, incidentally, the drivetrain of the vehicle.

Figures 7.13 and 7.14 compare the displacements of the tower top when Configuration 1 is implemented (blue) as well as Configuration 2 (in black, dashed). In Figure 7.14 we can clearly see that the amplitudes of the tower top in Configuration 2 are comparatively smaller.

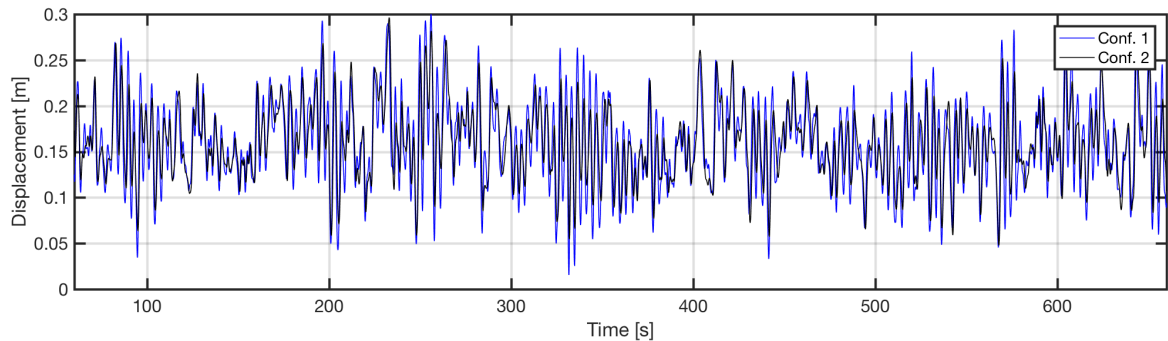


Figure 7.13: Tower top displacements of Configurations 1 and 2, under 25[m/s] winds.

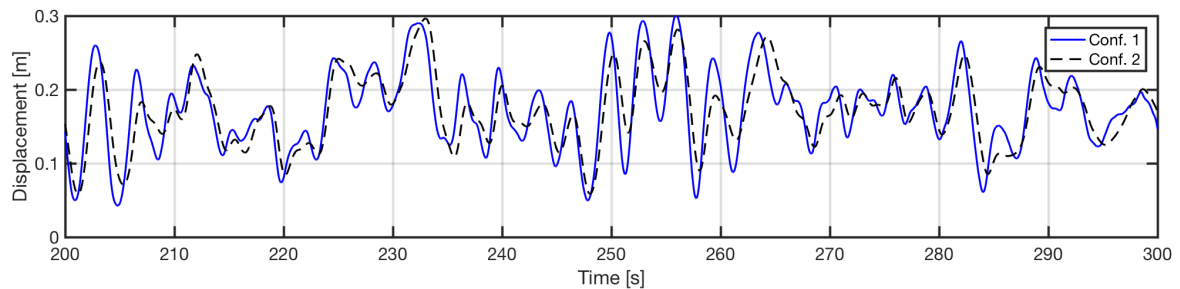


Figure 7.14: Close-up of Figure 7.13

The smaller amplitudes of Configuration 2 become even more clear to see when the power spectral densities of the signals are plotted together. In addition to the lower peak for Configuration 2 at the natural frequency of the system of 0.3Hz, we see other, much smaller peaks for excitations such as the 3P excitation, which occur at 0.6Hz at rated rotor speed. These PSDs are shown in Figure 7.15.

It must be reiterated that these results are not meant to give an exact percentage of fatigue reduction or the possible extension of structural design life, but instead to prove that these systems in fact work.

7.3.2. Comments on the Motions of the Absorbers

Configuration 1 - Nacelle spatial limitations and generator accelerations

If the systems we have thus studied are to be deemed effective in reducing fatigue damage on the support structure, we must study their effect on the tower-top motions. However, an equally important

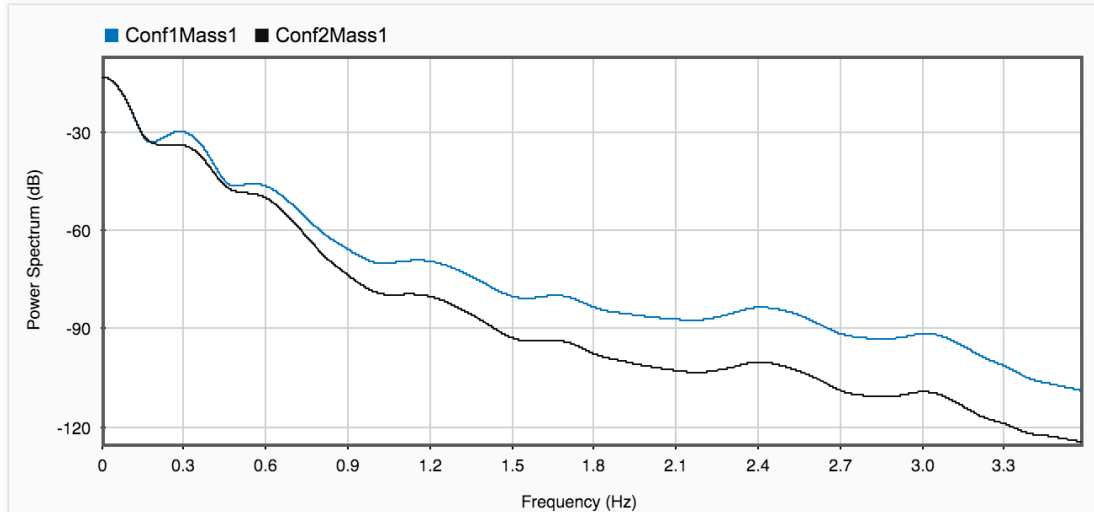


Figure 7.15: Power spectral densities of the signals on Figure 7.13

aspect to proving the feasibility of these tuned-mass dampers depends on whether the motions of the dampers themselves are within an acceptable range.

For example, the generator-TMD in Configuration 1 will, clearly, move with respect to the rest of the nacelle to dampen tower motions. We saw the in Chapter 7, Figure 7.10, that the motions of the generator have amplitudes of up to 0.5 meters in both up and down-wind directions. This additional space requirement would mean turbine nacelles would have to be made at least 1 meter longer.

This does not seem like an unfeasible design change, but space in nacelles are at a premium, and this design change would incur a non-insignificant cost surge in the production of the turbines.

Another concern if this system is to be implemented, is the increased vulnerability to damage and failure of the generator. Given that it is constantly oscillating, it will be subjected larger accelerations. As explained in Section 4.7, Dueñas-Osorio and Basu [20] mention that accelerations higher than $5 \frac{m}{s^2}$ can be detrimental to the life of components such as generators, inverters and other electrical and mechanical controls.

Using simple Newtonian physics in Equation 7.1, we can analytically calculate the maximum accelerations of the generator-TMD. The equation says that,

$$a_2 = (2\pi f_2)^2 \cdot x_{max} = (2\pi \cdot 0.3244Hz)^2 \cdot 0.5m = 2.1 \left[\frac{m}{s^2} \right] \quad (7.1)$$

where a_2 , f_2 are the acceleration and natural frequency in Hz of the TMD mass, and x_{max} is its maximum displacement from a point of equilibrium, which is taken from Figure 4.4.

In Figure 7.16 we see the tower top accelerations, as simulated in MATLAB, of the turbine without a tuned mass damper, plotted against the accelerations of the generator-TMD. It is clear from the figure that the accelerations of the generator increase up to three-fold in amplitude, as compared to those of the entire rotor-nacelle assembly in the original TMD-less MATLAB model. Nonetheless, they remain below the analytically calculated $2 \frac{m}{s^2}$, and they remain far below the danger threshold of $5 \frac{m}{s^2}$.

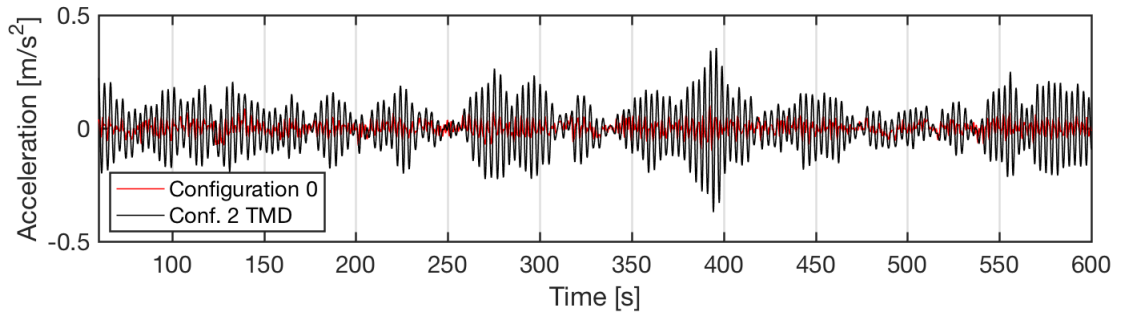


Figure 7.16: Accelerations of the TMD-less tower top compared to the accelerations of the generator-absorber in Configuration 1. under 12[m/s] winds

Configuration 2 - Tip clearance

Identifying the blade tip clearance at almost exactly 8 meters during idling, we can assess if there exists danger of tip collision during operation of the rotor, both rotating and performing fore-aft oscillations to dampen tower motions.

From our FAST simulations, the tip deflection at each point in time can be found. At rated wind speed, when the thrust on the blades is at it's highest, we expect to see the highest tip deflections. These are shown in Figure 7.17. At this speed, the downwind displacements of the nacelle often reach more than 5 and even 6 meters with respect to the displacements of the tower top. We can be certain that the fore-aft displacements of the rotor in addition to tip deflections, which max at about 7 meters, will cause a collision to occur.

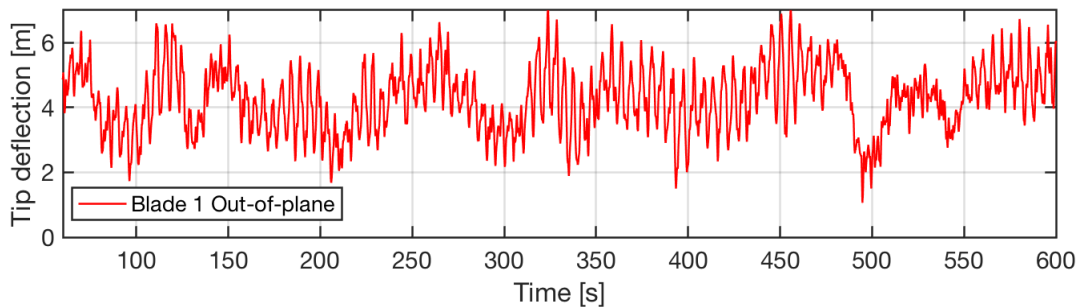


Figure 7.17: Out of plane blade tip deflections at 12 [m/s].

At $25 \frac{m}{s}$, when the rotor damper presents very high amplitudes as seen in Chapter 7, the tip deflections are not as high as in Figure 7.17. As shown in Figure 7.12, at this speed the fore-aft displacements of the rotor reach up to 3.5 meters with respect to its equilibrium point at the center of the tower. With the tips oscillating with maximum deflections reaching up to 4 meters, shown in Figure 7.18, collisions are not guaranteed to occur.

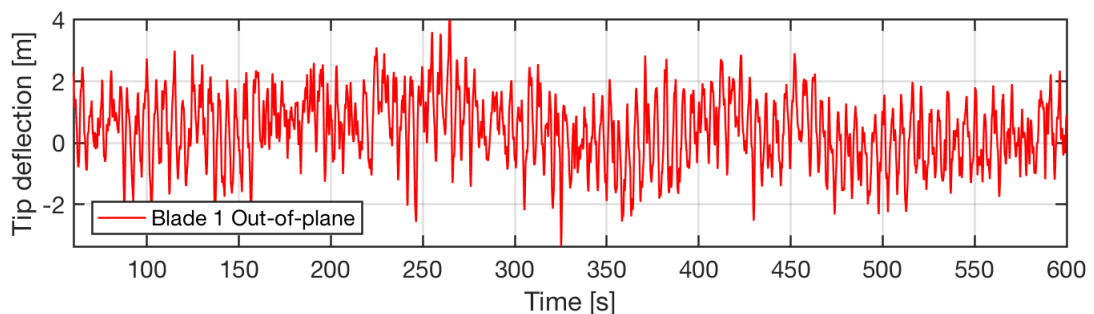


Figure 7.18: Out of plane blade tip deflections at 25 [m/s].

However, the tip deflections must be combined with the IEC 61400-1 standard [16] required safety

factors for tip deflection, which are $\gamma_f = 1.25$ as load factor, and a material factor of $\gamma_m = 1.1$. With these included the final deflection of the tips is an unacceptable 10.3 meters. Increasing the overhang, pre-bending, coning or shaft tilt to increase clearance by a few meters will incur an increased cost, but it is not an unreasonable modification to such a large turbine.

Another possible solution to this would be to have a variable center of equilibrium. This would mean that during idling, the turbine's drive train rests with its center of mass closer to the center of the tower. Then, during operation while the drive-train damper is being pushed downwind, its equilibrium point, defined by the TMD spring's anchor point, could move matching the average thrust forces on the rotor. This is a very complicated system, however, and it could potentially be prohibitively costly to design and test.

7.3.3. Construction

In both configurations the dashpots and springs can be attached on one end to either the front or back of the nacelle frame. The other end would attach to the TMD, being either the generator or the entire drive train, onto clamps that are used to attach the generator or gear box to the frame on which they rest.

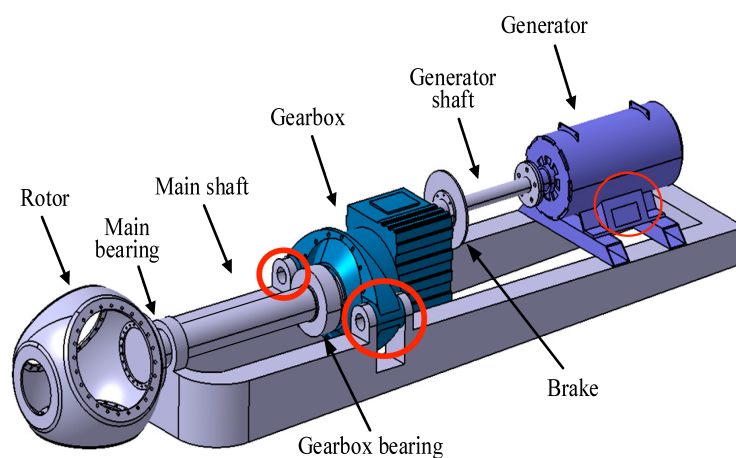


Figure 7.19: Isolated drive train of a turbine. Shows likely attachment points for springs and dampers in red. The opposite ends of spring and dampers would attach to the nacelle frame [7].

As shown in Figure 7.20, the tuned mass damper configuration 2 has a platform on which the entire drive train oscillates. The springs and dashpots are attached to the gearbox clamps and the nacelle frame on each end

In such mounting configurations the springs and dashpots would allow for elongations and contractions of a few meters. These elongations are fundamental given the displacements seen in the previous sections

Configuration 1

For a turbine to function correctly, it is necessary for the rotor to transfer torque to the generator at all times during operation. Thus, allowing the generator in Configuration 1 to oscillate with respect to the rest of the nacelle requires the shaft between the gearbox and generator, usually referred to as the high-speed shaft (HSS), to extend and retract in length as the generator moves back and forth, while transferring torque to actuate the generator.

From Section 7.3.2 we know that the motions of the generator would require 0.5 meters on each side of the equilibrium point. The scope of this thesis does not include an economic feasibility analysis. We can, however tentatively, suggest that if the 12% reduction in fatigue could reduce around 10% on tower costs, this reduction could conceivably justify paying for the additional costs of the nacelle and extensible shaft.

Configuration 2

The construction of a turbine with an oscillating drive train would require an additional frame to be mounted on the main nacelle frame, on which the bearings, gears and generator are attached. It of

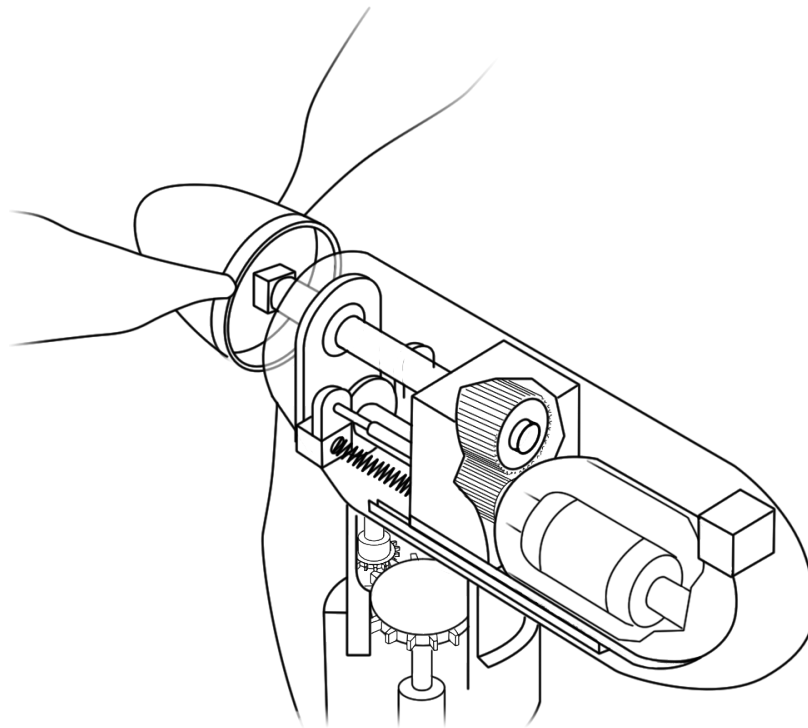


Figure 7.20: Sketch of Configuration 2 with springs and dashpots attached to the nacelle frame on one end and the drivetrain platform on the other.

course would also require a longer, and thicker low speed shaft, given that it must protrude from the nacelle with enough distance to retract when the rotor gets pushed. In addition, the large amplitudes of displacement of the drive-train-damper present a difficult design issue. It is not impossible to construct a nacelle that will allow for 3-meter amplitudes, but it may be prohibitively costly.

A possible solution for this is to de-optimize the system, by increasing the stiffness of the springs attaching tower and drive train. It should be possible to find an optimal compromise between tower fatigue reduction and rotor fore-aft oscillations. As was shown in Figure 4.8, by moving the stiffness and damping of the tuned-mass damper away from the optimal, the dynamic amplification of the main mass can be slightly increased, while that of the damper decreases. Given that configuration 2 offers great fatigue reduction, this could conceivably lead to finding a larger "optimal" DAF for the tower, that would prevent construction costs of the damper becoming too costly.

8

Conclusions and Recommendations for Future Work

8.1. Concluding Remarks

Answering the first research question, this project has shown that yes, within the scope of requirements of this project, modeling of a wind turbine as a simple one or two degree-of-freedom system is perfectly feasible and accurate enough. However, this is true only when the forces on the model are exactly those experienced by the real turbine, as is the case when using the thrust excitations from FAST. When using wind signals over the turbine's blades averaged to a 1-point wind signal in order to excite the simple model, the performance was comparable to the real turbine, but not similar enough to draw conclusions about long-term fatigue.

To find the baseline fatigues as calculated on "super stiff" and zero-control-lag models, and thus answer the second set of research questions, wind had to be used in order to excite the turbine in FAST and MATLAB. As explained in Section 5.3.2 and Appendix B, both of these attempts failed. Although in all likelihood it is possible, within the time frame this project was not able to model an un-moving, super stiff tower in FAST. Similarly, since in MATLAB modeling wind excitations failed, which was necessary to bypass control lags above U_r , the "super stiff" turbine calculations were deemed unfit for inclusion in the report. The simulations for the MATLAB stiff turbine are shown in Appendix B.

The third research question involved testing the dynamic behavior of Configuration 1, which allows the generator to oscillate in the fore-aft direction and act as a tuned-mass damper. The parameter values that resulted on optimal behavior for this configuration were found using formulas from Warburton and Ayorinde [4], and are a tuning ratio of $f_{opt} = 0.9799[-]$, and an absorber damping coefficient and stiffness of $c_{a,opt} = 2.84E03[Ns/m]$ and $k_{a,opt} = 3.32E04[N/m]$, respectively. The practicality of this system was assessed based on the displacements and accelerations it requires to perform optimally. It was found that with maximum deflections of about 0.5 meters in both directions, the turbine's nacelle would require roughly 1 additional meter in length. In terms of accelerations, the generator-TMD stayed well below the dangerous acceleration threshold of $5[m/s^2]$. The last and most important sub-question regarding Configuration 1 asked what is its effect in fatigue over a 20-year production period. This system was compared to the original MATLAB turbine model and found to offer a 12% reduction in fatigue damage equivalent load.

The last of the main research questions is similar to the previous but, but it is concerned with the rotor-and-drive-train tuned mass damper, Configuration 2. The values that produced optimal behaviors for this configuration were found using a MATLAB optimizer, and are a tuning ratio of $f_{opt} = 0.3835[-]$, and an absorber stiffness of $k_{a,opt} = 1.21E05[N/m]$. Because this TMD includes the rotor, the damping coefficient is of course variable, dependent on the aerodynamic forces on the rotor. For this reason, it cannot be optimized. It thus varies between $1.9e + 05$ and $2.5E05[Ns/m]$.

The second sub-question concerning Configuration 2 asked what the effect of having a system in which the tuned-mass damper is excited instead of the main mass. What was shown in Chapter 7, in Figure 7.14, is that with the optimal values shown above, once the tower reaches a quasi-static resting position at each load case, perturbations from this position are smaller compared to Configuration 1.

This makes sense, given that the tower itself is excited mostly by its own drag, whereas the rotor, no longer anchored to the tower, receives the vast majority of forces on the turbine.

As discussed in Section 7.3.3, if Configuration 2 were to be implemented on a turbine, no shaft needs to become extensible. However, the entire drive train would need to be mounted on a secondary frame on top of the main nacelle frame. Furthermore, attention would have to be paid to the deflection of the blade tips. To avoid tip collision, coning and pre-bending of the rotor would have to be increased.

Finally, the change in dynamic behavior for this configuration was shown to improve the fatigue damage over the turbine's design life. The reduction in fatigue equivalent load was calculated to be 23% as compared to the TMD-less MATLAB model.

Overall, the implementation of the dampers caused significant reductions in fatigue damage. These reductions could lead to a reduction of safety factors and thus material costs for the turbine. Alternatively, a more consequential outcome would be an extension of the design life of the support structure, leading to welcome reductions in leveled production costs for new projects, which would continue to make wind energy more competitive. It is the hope of the writer that research into wind turbines will continue to increase the cost-effectiveness, reliability, and of course market penetration of wind energy.

8.2. Recommendations for Future Work

This project made the decision to model a wind turbine in such a way that made it easy and quick to run simulations. Modeling as a simple 1DOF system also made it very easy to vary parameters and influence its behaviour. Furthermore, this approach offered unparalleled simplicity to incorporate auxiliary masses to act as tuned-mass dampers, and study the effects these had on the model's dynamic behavior.

Perhaps not so unexpectedly, this simplification also introduced some unwanted difficulties in achieving satisfactory correspondence between the developed model and a real turbine. In the end the project concludes that simplifying complex systems for easy mathematical modeling incurs complications, and limitations to the models must be accepted and accounted for. Future projects that attempt to perform complex or numerous simulations to investigate motions on a simplified model of a wind turbine, must implement artificial ways to model control mechanisms such as pitching and torque.

An uncertainty remains in regards to modeling excitation forces on the turbine using a single force signal. As explained in the discussion in Section 7.3, using averaged wind signals over the rotor area result in behavior that matches the behavior of the FAST model. A future project investigating rotors aerodynamics using computational fluid dynamics should be able identify whether forces over the rotor can be turned into a single equivalent point force signal using only wind data for equivalent behavior.

This project did not delve into the economic aspects of possible implementations of the TMDs investigated. Calculating cost increases in terms of material and design required to implement these systems are beyond the scope of this project, but could be investigated in a project with a larger focus on economics of wind turbine design. These increases in cost should of course be compared to the possible cost reductions in terms of support structure construction or possible extended design lives.

Bibliography

- [1] EIA, *International Energy Outlook 2017 Overview*, U.S. Energy Information Administration **IEO2017**, 143 (2017), arXiv:EIA-0484(2013) [DOE] .
- [2] I. E. Agency, *Market Report Series: Renewables 2017 Analysis and Forecasts to 2022*, International Energy Agency **104**, 20142 (2017).
- [3] O. Altay, F. Taddei, C. Butenweg, and S. Klinkel, *Vibration mitigation of wind turbine towers with tuned mass dampers*, *Advances in Industrial Control* , 337 (2014).
- [4] G. B. Warburton and E. O. Ayorinde, *Optimum absorber parameters for simple systems*, *Earthquake Engineering & Structural Dynamics* **8**, 197 (1980).
- [5] M. Rezaee and A. M. Aly, *Vibration control in wind turbines for performance enhancement: A comparative study*, *Wind and Structures* **22**, 107 (2016).
- [6] H. Liu, Q. Tang, and Y. Chi, *Vibration reduction strategy for wind turbine based on individual pitch control and torque damping control*, ... *Transactions on Electrical ...* (2016), 10.1002/etep.2201.
- [7] P. Qian, X. Ma, and D. Zhang, *Estimating Health Condition of the Wind Turbine Drivetrain System*, *Energies* **10**, 1583 (2017).
- [8] IPCC, *Summary for Policymakers, Climate Change 2014: Impacts, Adaptation and Vulnerability - Contributions of the Working Group II to the Fifth Assessment Report* , 1 (2014), arXiv:arXiv:1011.1669v3 .
- [9] N. Cunningham, *The era of expensive renewables is over and that's more bad news for fossil fuel producers*, *Business Insider* , 1 (2017).
- [10] D. Mcconnell, *Tesla 's Battery in Australia Is Surpassing Expectations*, *Renewable Energy World* , 1 (2018).
- [11] Global Wind Energy Council, *Global Wind Statistics 2016*, (2017).
- [12] I. E. Agency, *Key World Energy Statistics*, Tech. Rep. (International Energy Agency, 2017).
- [13] Vattenfall, *Vattenfall wins tender to build the largest wind farm in the Nordics*, (2016).
- [14] A. Nieslony, *Rainflow Counting Algorithm*, (2002).
- [15] S. D. Downing and D. F. Socie, *Simple rainflow counting algorithms*, *International Journal of Fatigue* **4**, 31 (1982).
- [16] International Electrotechnical Commission, *Wind turbines – Part 1: Design requirements*, Tech. Rep. (INTERNATIONAL ELECTROTECHNICAL COMMISSION, 2005).
- [17] K. Hesameddin, A. Irfanoglu, and T. J. Hacker, *Effective Viscous Damping Ratio in Seismic Response of Reinforced Concrete Structures*, 6th International Conference on Advances in Experimental Structural Engineering (2015).
- [18] Brown University, *Introduction to vibration of systems with many degrees of freedom*, (2013).
- [19] Z. Zhang, S. R. K. Nielsen, F. Blaabjerg, and D. Zhou, *Dynamics and Control of Lateral Tower Vibrations in Offshore Wind Turbines by Means of Active Generator Torque*, *Energies* **7**, 7746 (2014).
- [20] L. Dueñas-Osorio and B. Basu, *Unavailability of wind turbines due to wind-induced accelerations*, (2008).

-
- [21] J. Jonkman, S. Butterfield, W. Musial, and G. Scott, *Definition of a 5-MW reference wind turbine for offshore system development*, Tech. Rep. February (National Renewable Energy Laboratory, 2009).



Motions and PSDs at All Wind Speeds

A.1. All motions for FAST and MATLAB thrust-excited simulations

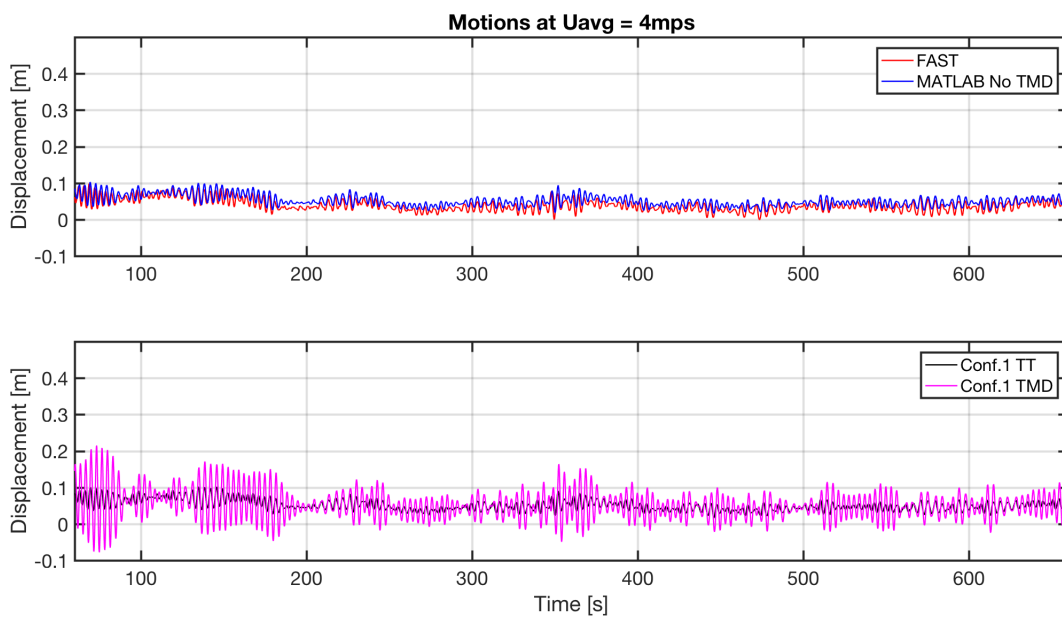


Figure A.1: Displacements of FAST and MATLAB Configuration 0 and Configuration 1 at 4mps wind.

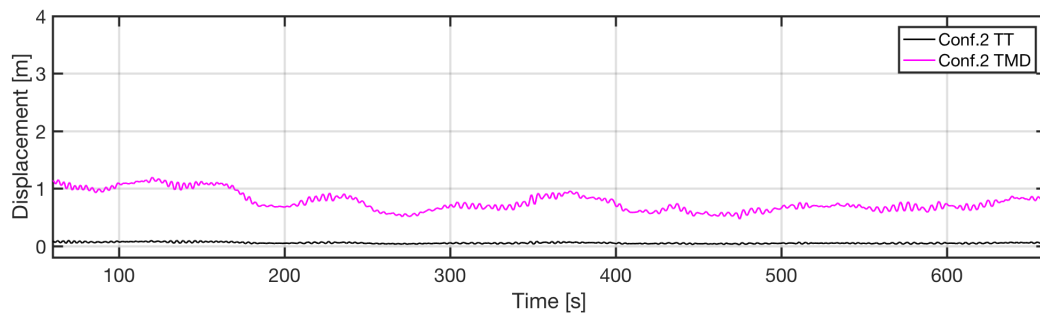


Figure A.2: Displacement of MATLAB Configuration 2 at 4mps wind.

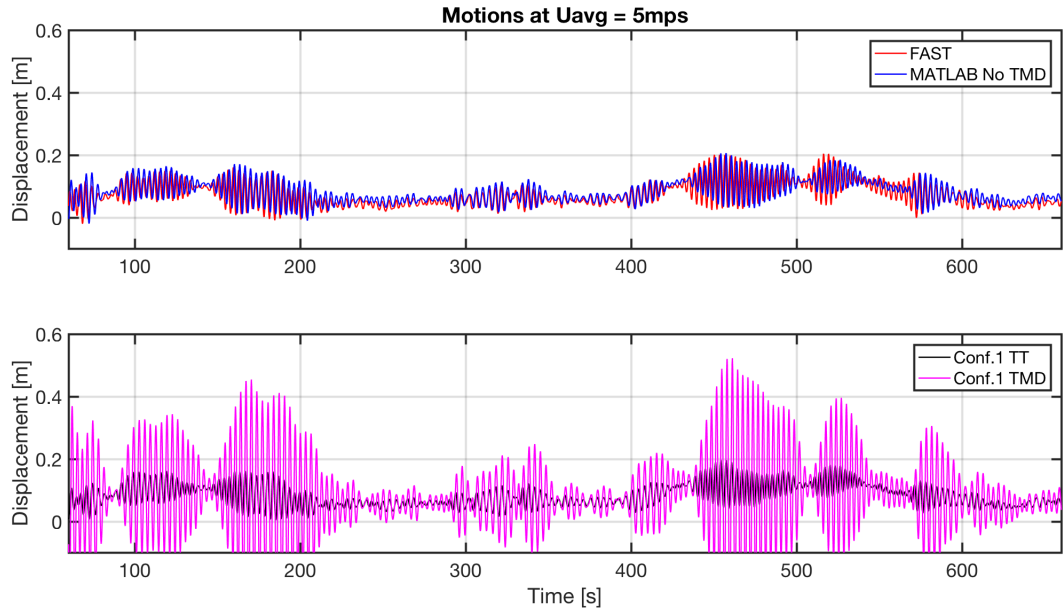


Figure A.3: Displacements of FAST and MATLAB Configuration 0 and Configuration 1 at 5mps wind.

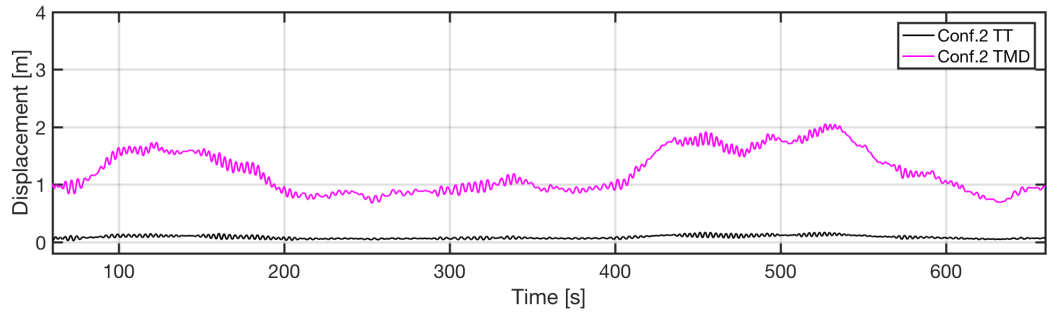


Figure A.4: Displacement of MATLAB Configuration 2 at 5mps wind.

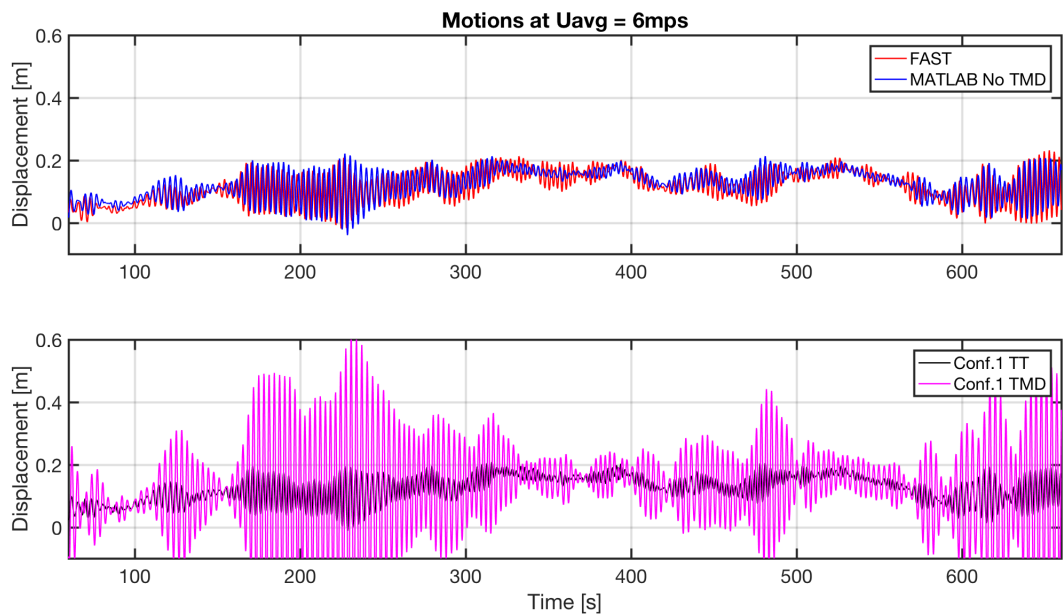


Figure A.5: Displacements of FAST and MATLAB Configuration 0 and Configuration 1 at 6mps wind.

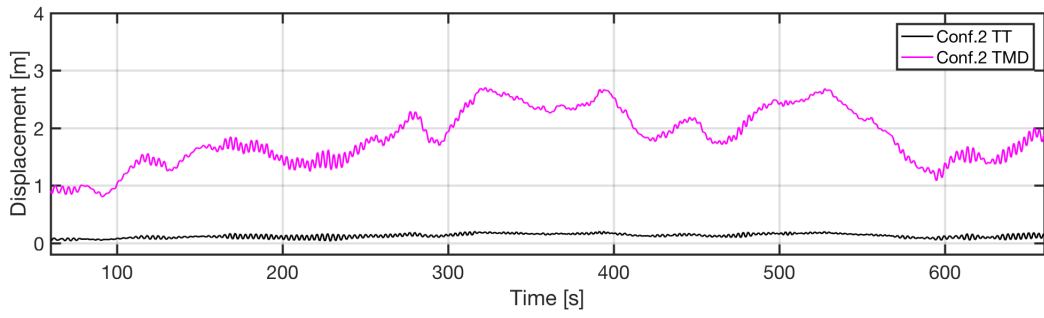


Figure A.6: Displacement of MATLAB Configuration 2 at 6mps wind.

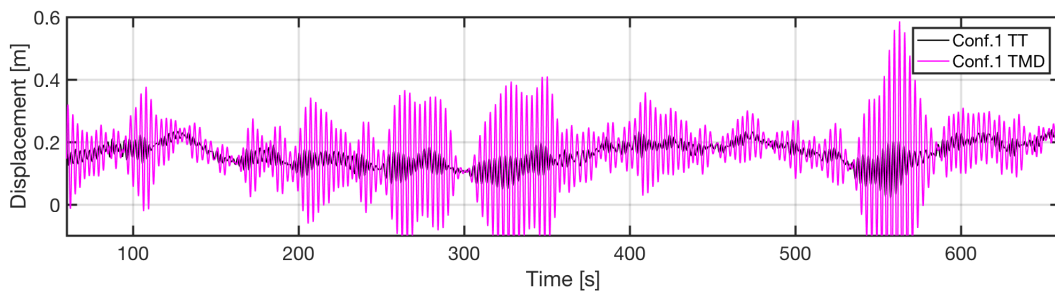
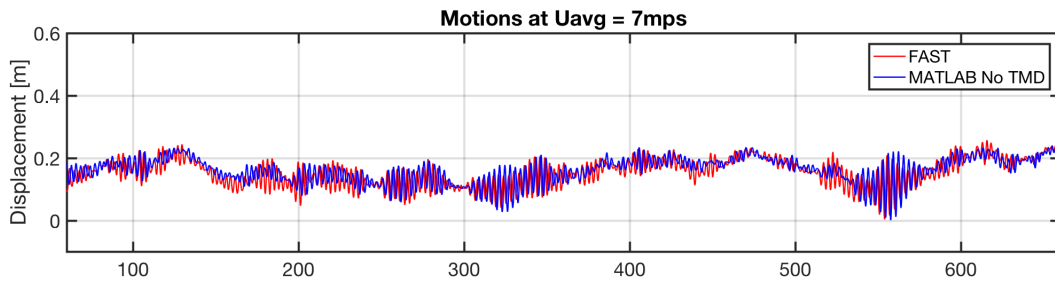


Figure A.7: Displacements of FAST and MATLAB Configuration 0 and Configuration 1 at 7mps wind.

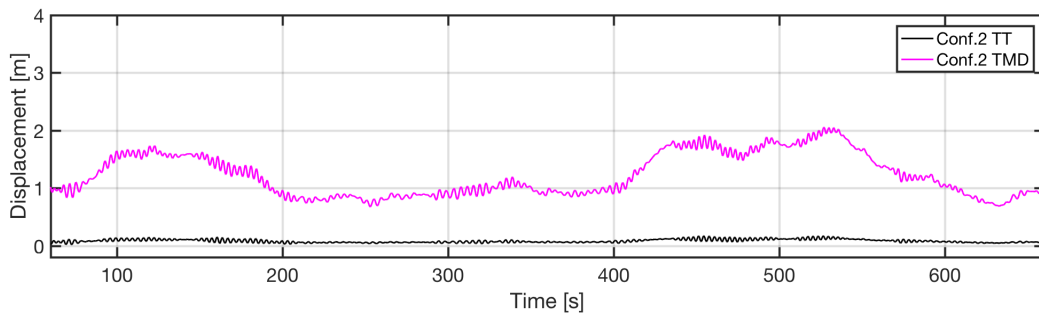


Figure A.8: Displacement of MATLAB Configuration 2 at 7mps wind.

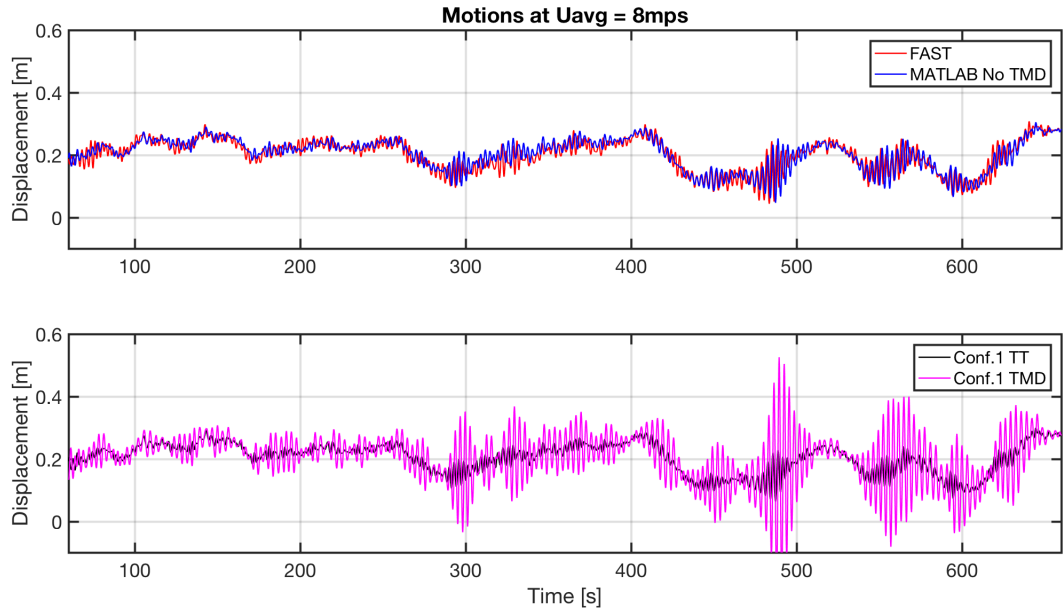


Figure A.9: Displacements of FAST and MATLAB Configuration 0 and Configuration 1 at 8mps wind.

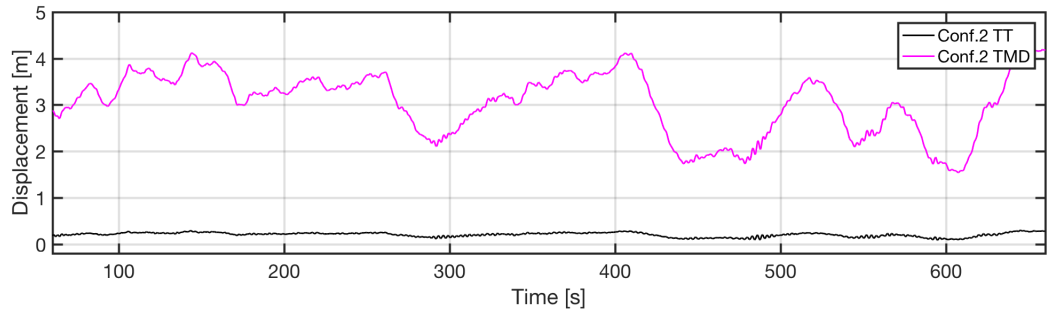


Figure A.10: Displacement of MATLAB Configuration 2 at 8mps wind.

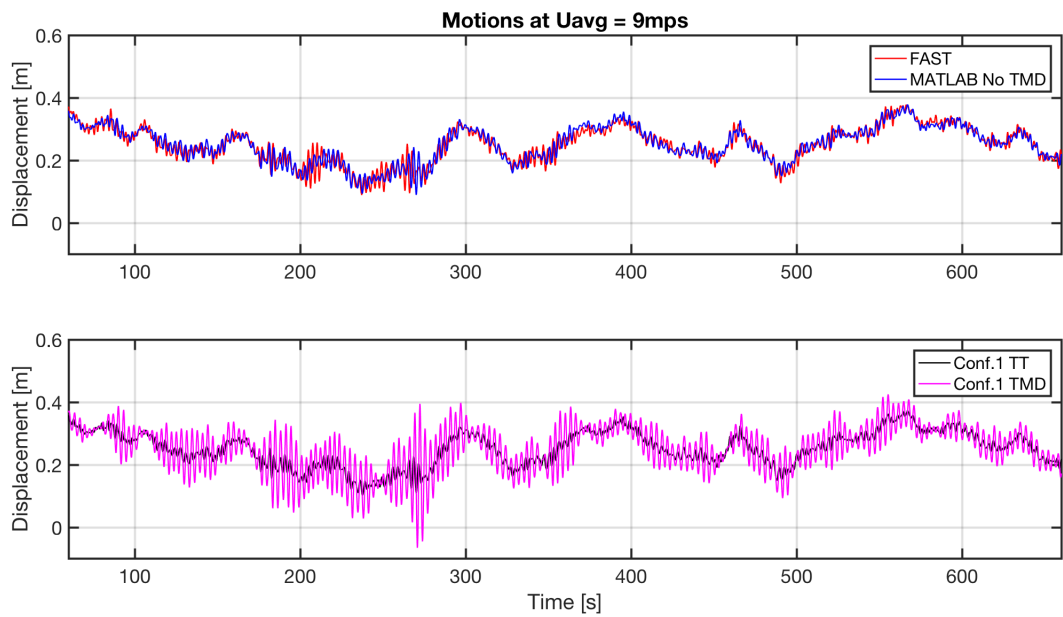


Figure A.11: Displacements of FAST and MATLAB Configuration 0 and Configuration 1 under 9mps wind.

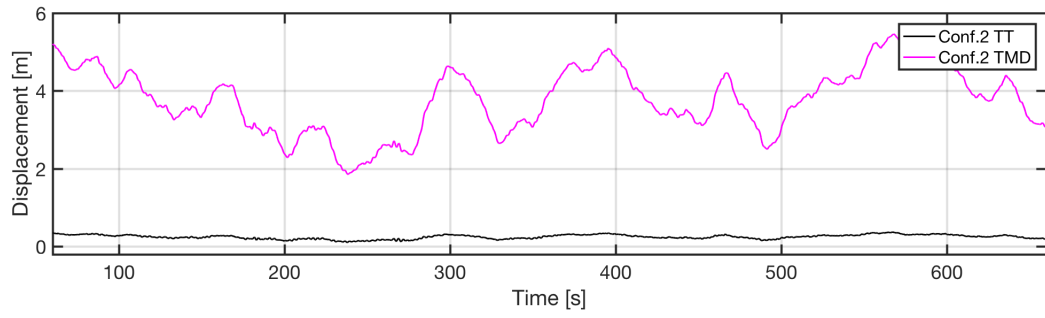


Figure A.12: Displacement of MATLAB Configuration 2 under 9mps wind.

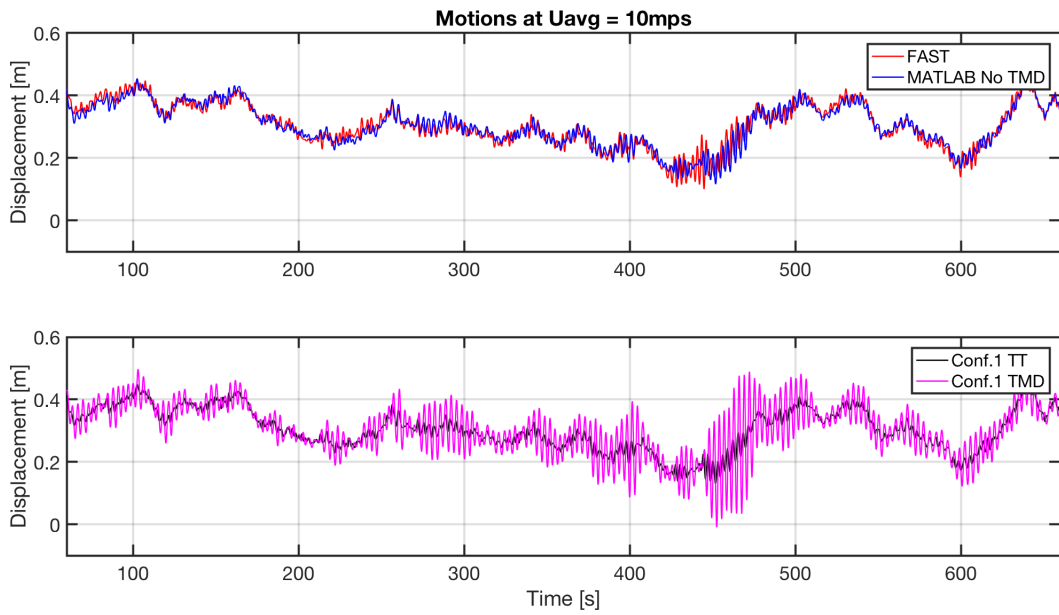


Figure A.13: Displacements of FAST and MATLAB Configuration 0 and Configuration 1 under 10mps wind.

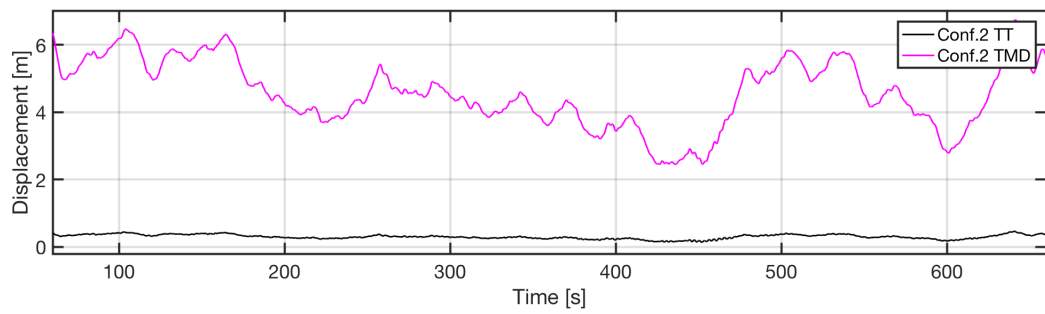


Figure A.14: Displacement of MATLAB Configuration 2 under 10mps wind.

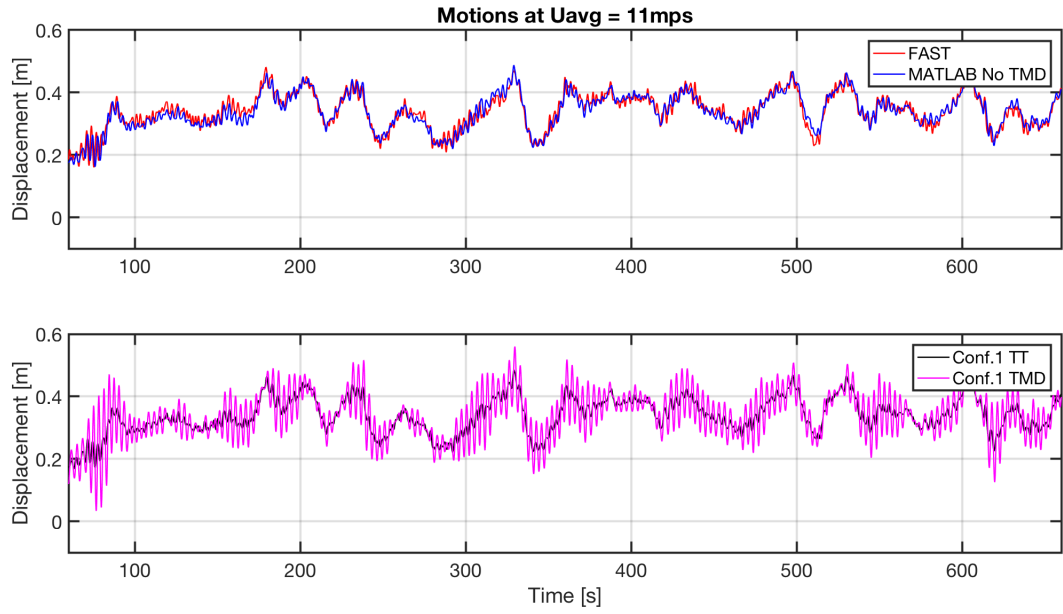


Figure A.15: Displacements of FAST and MATLAB Configuration 0 and Configuration 1 under 11mps wind.

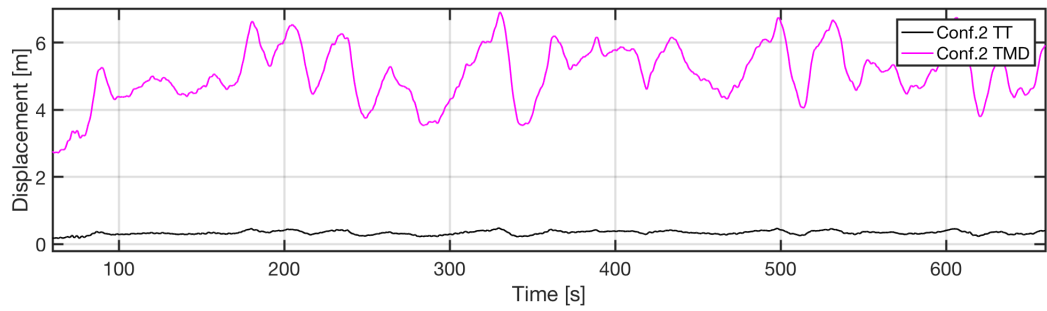


Figure A.16: Displacement of MATLAB Configuration 2 under 11mps wind.

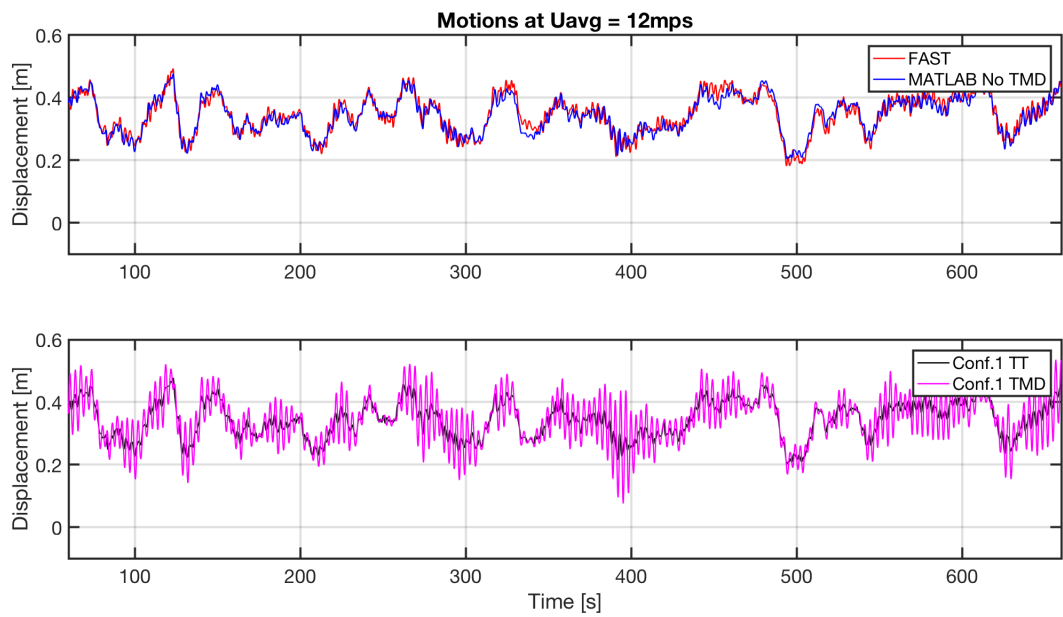


Figure A.17: Displacements of FAST and MATLAB Configuration 0 and Configuration 1 under 12mps wind.

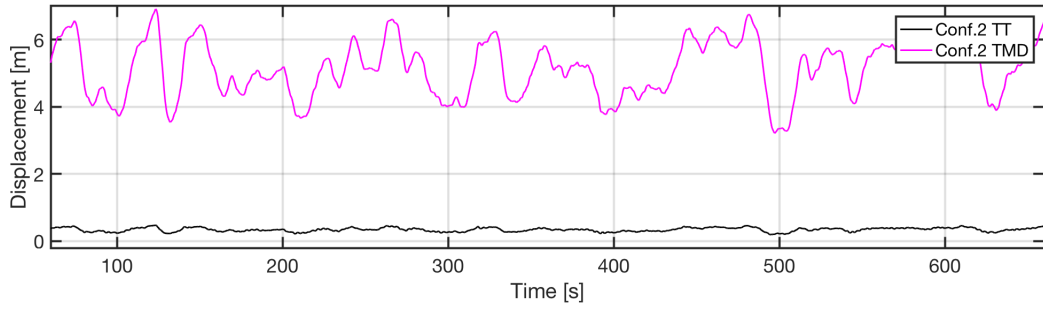


Figure A.18: Displacement of MATLAB Configuration 2 under 12mps wind.

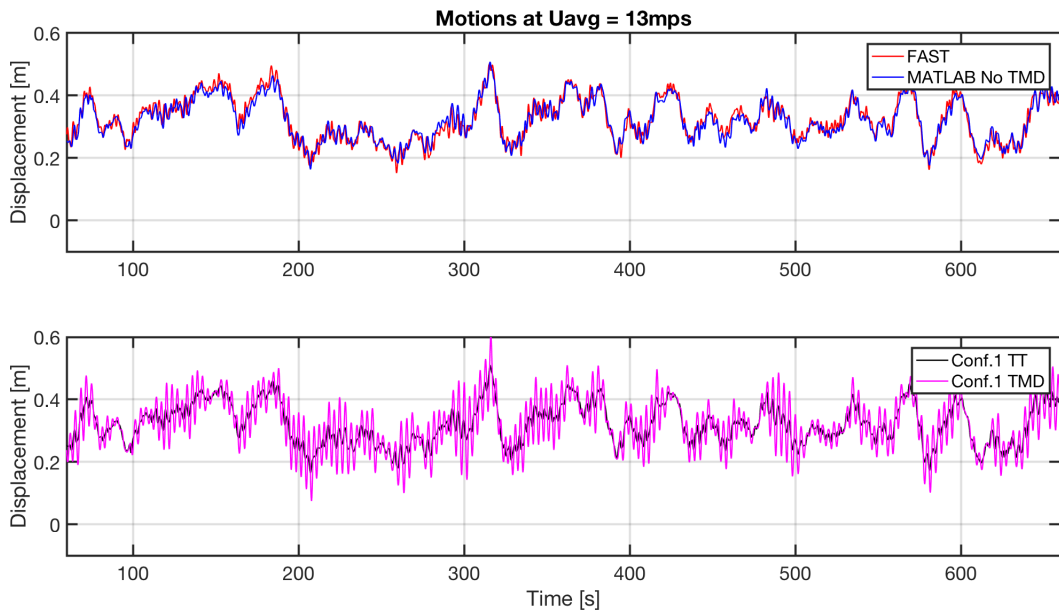


Figure A.19: Displacements of FAST and MATLAB Configuration 0 and Configuration 1 under 13mps wind.

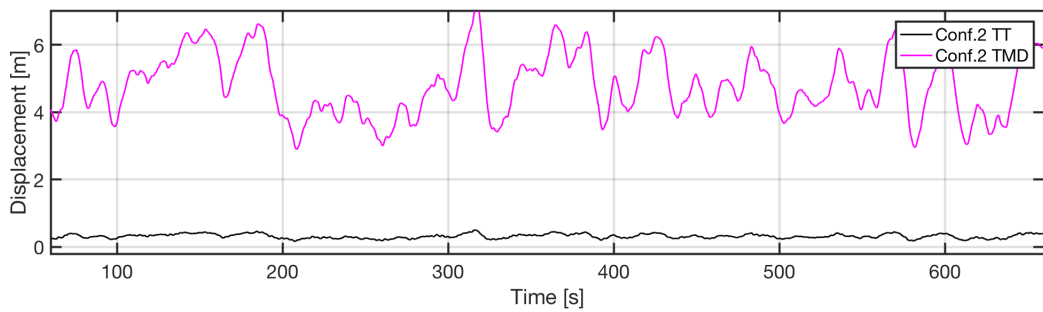


Figure A.20: Displacement of MATLAB Configuration 2 under 13mps wind.

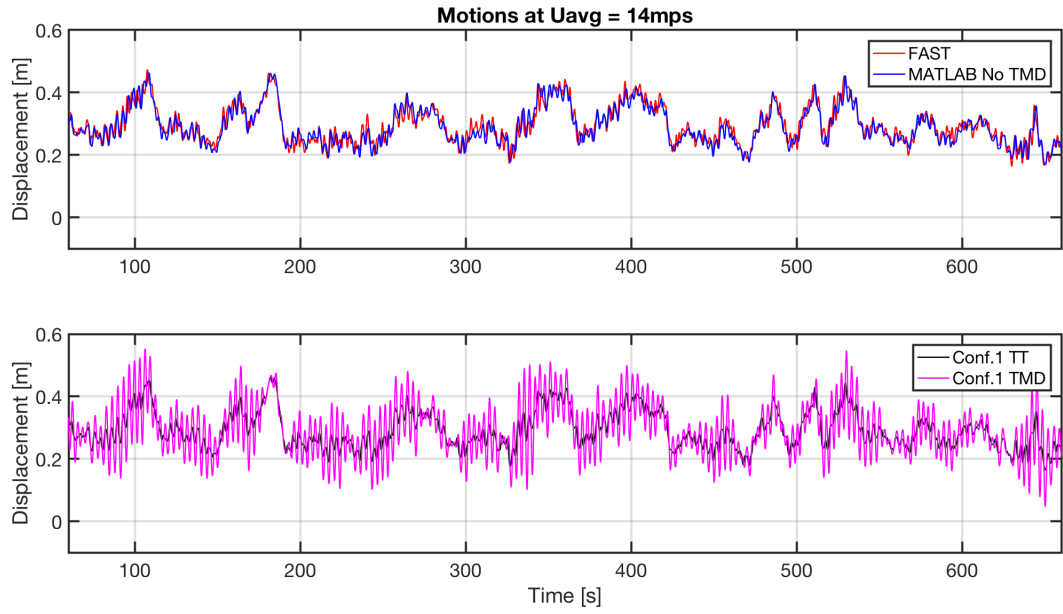


Figure A.21: Displacements of FAST and MATLAB Configuration 0 and Configuration 1 under 14mps wind.

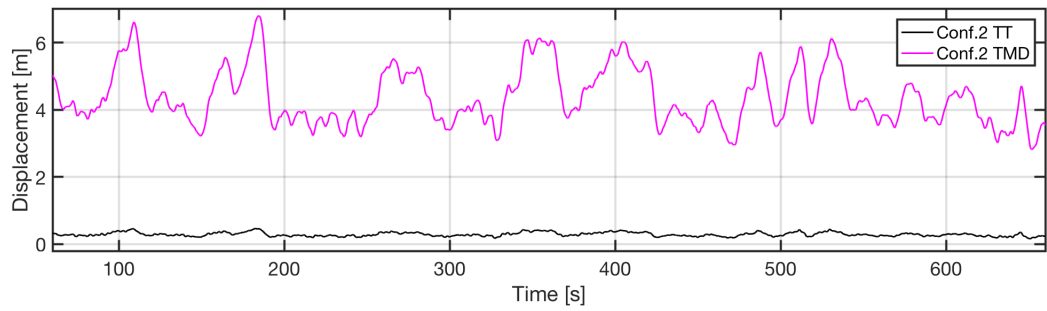


Figure A.22: Displacement of MATLAB Configuration 2 under 14mps wind.

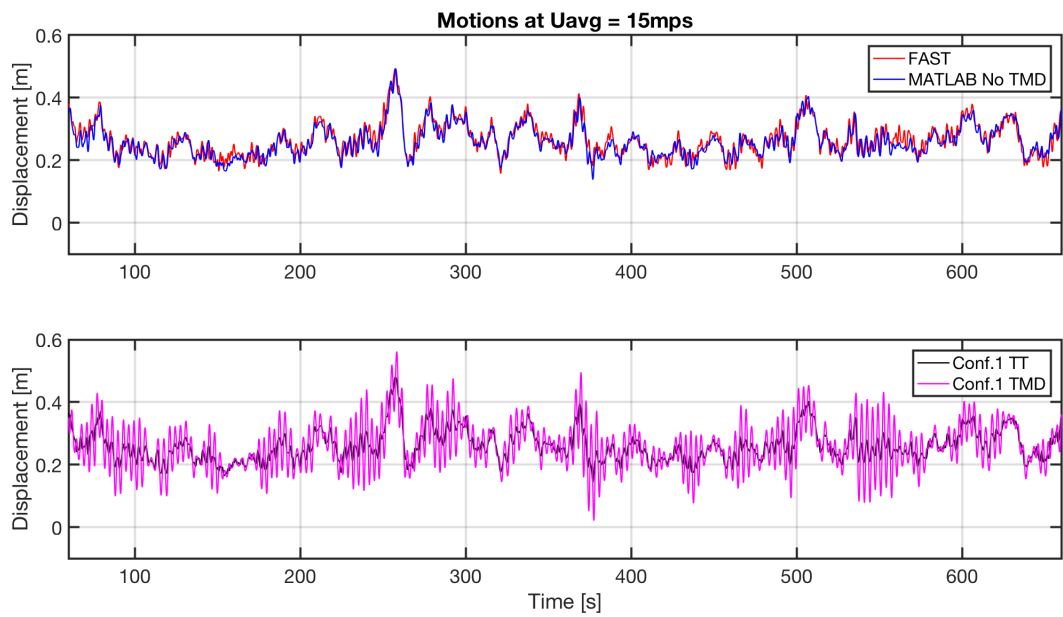


Figure A.23: Displacements of FAST and MATLAB Configuration 0 and Configuration 1 under 15mps wind.

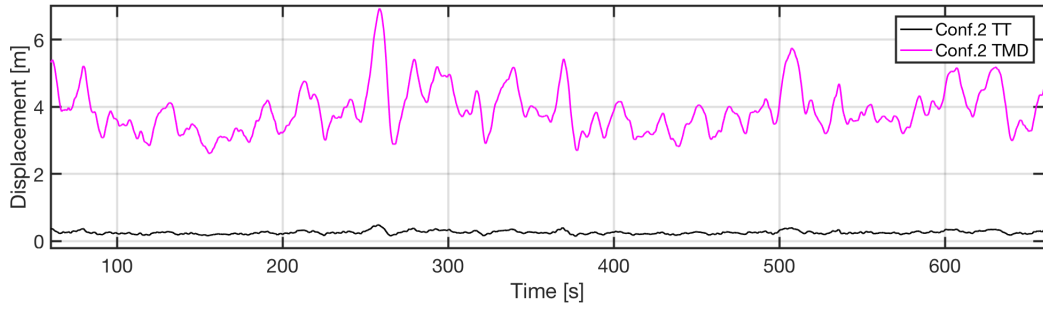


Figure A.24: Displacement of MATLAB Configuration 2 under 15mps wind.

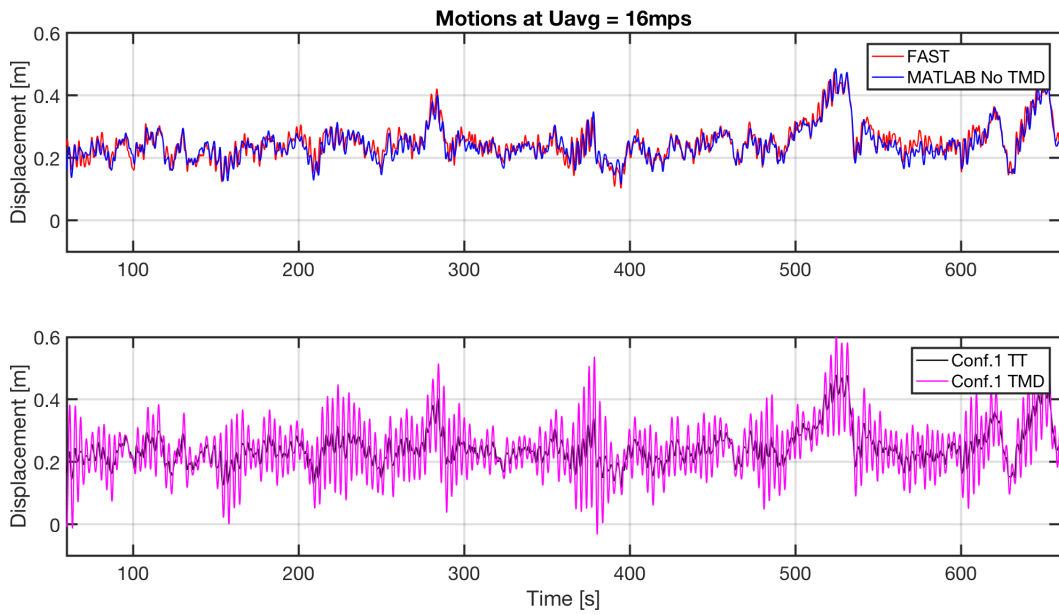


Figure A.25: Displacements of FAST and MATLAB Configuration 0 and Configuration 1 under 16mps wind.

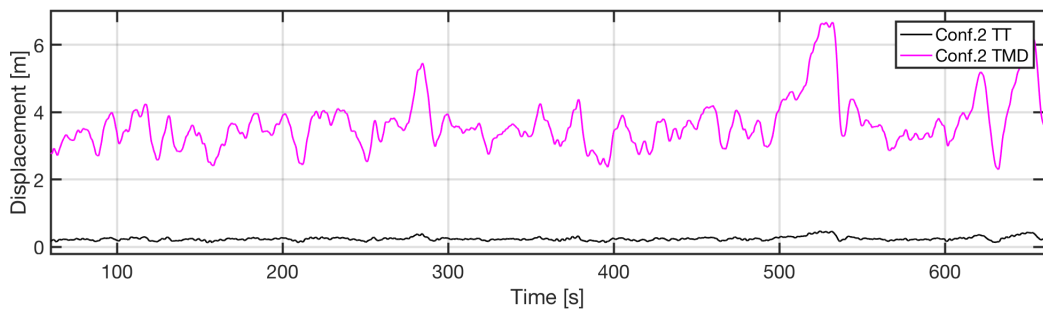


Figure A.26: Displacement of MATLAB Configuration 2 under 16mps wind.

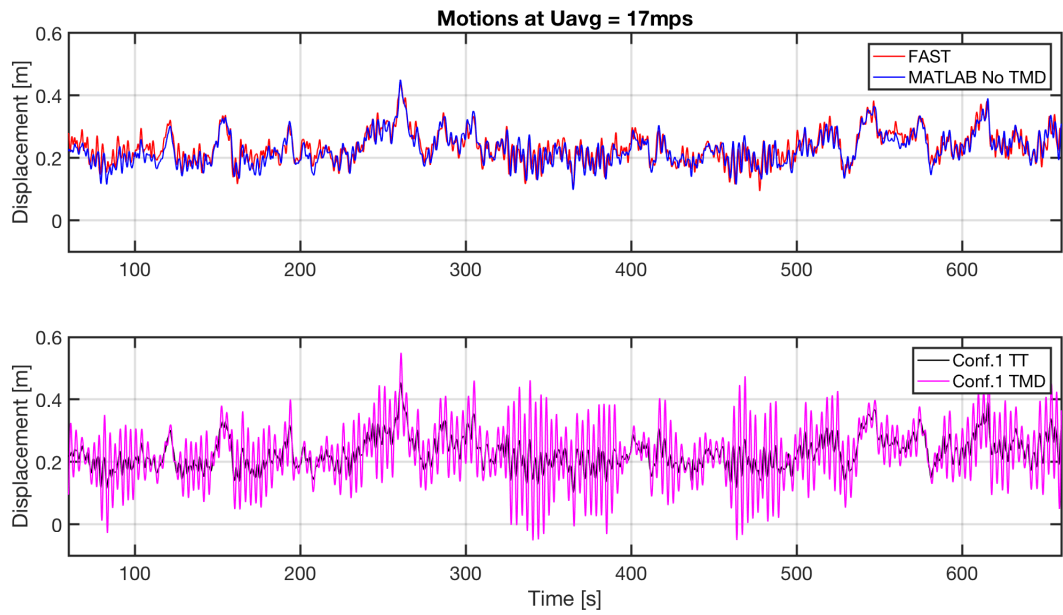


Figure A.27: Displacements of FAST and MATLAB Configuration 0 and Configuration 1 under 17mps wind.

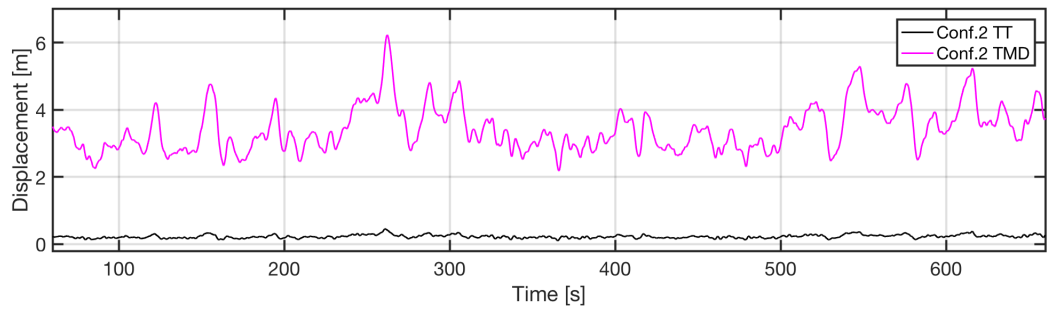


Figure A.28: Displacement of MATLAB Configuration 2 under 17mps wind.

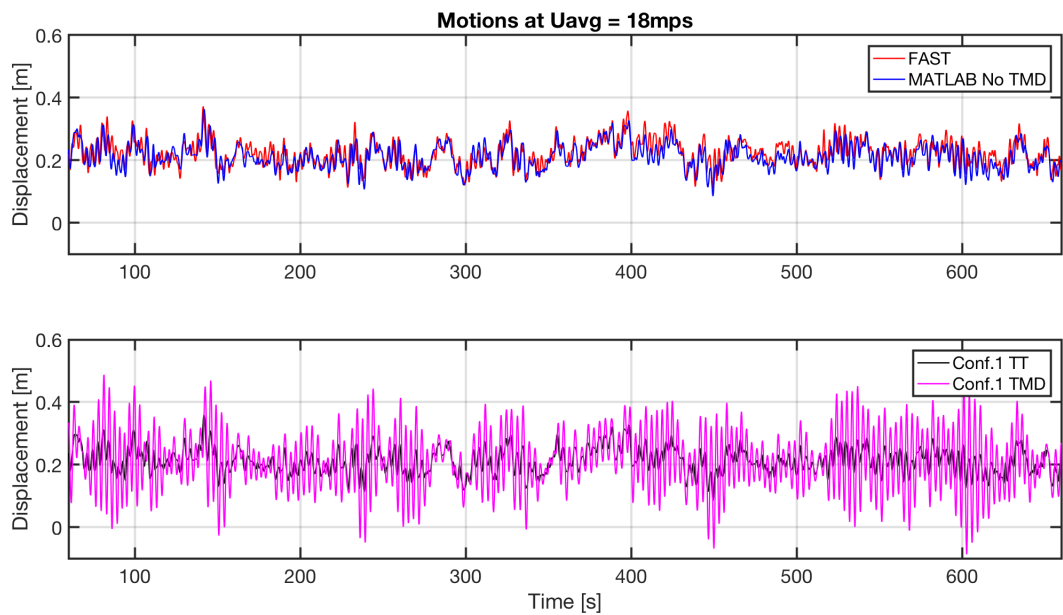


Figure A.29: Displacements of FAST and MATLAB Configuration 0 and Configuration 1 under 18mps wind.

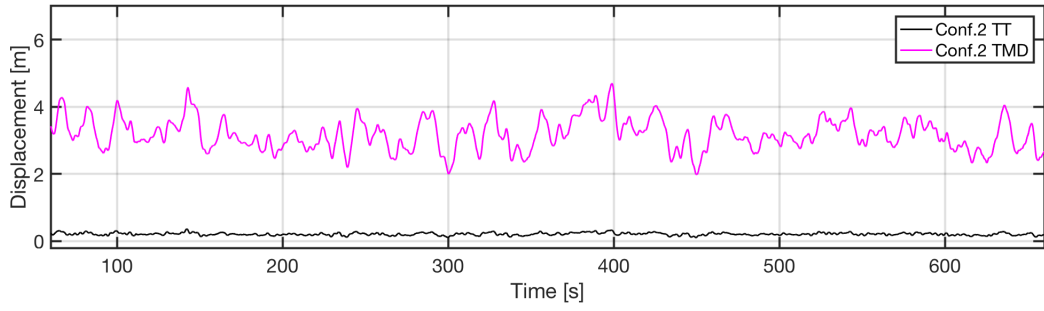


Figure A.30: Displacement of MATLAB Configuration 2 under 18mps wind.

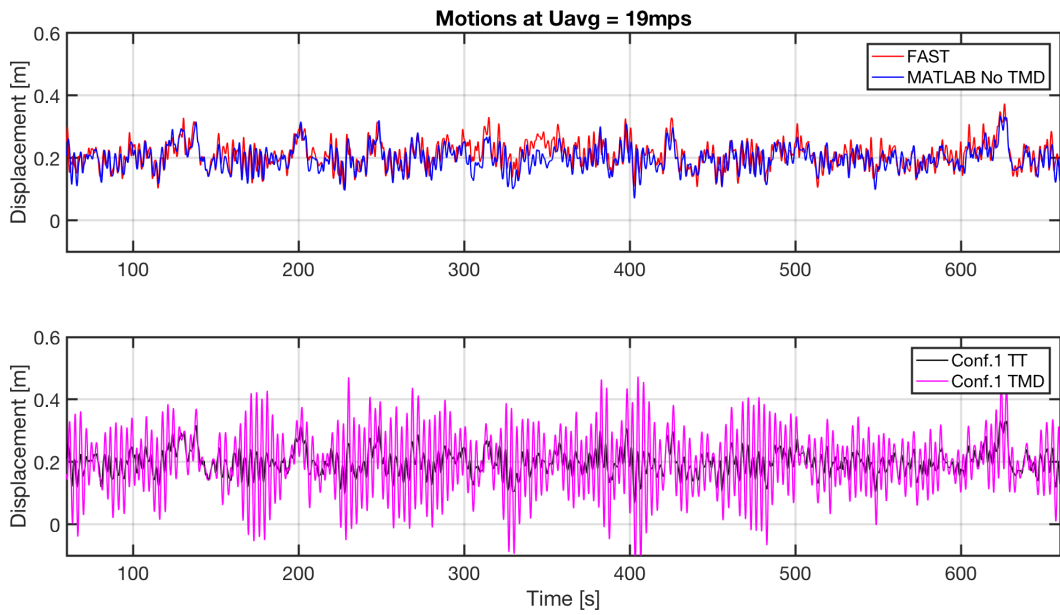


Figure A.31: Displacements of FAST and MATLAB Configuration 0 and Configuration 1 under 19mps wind.

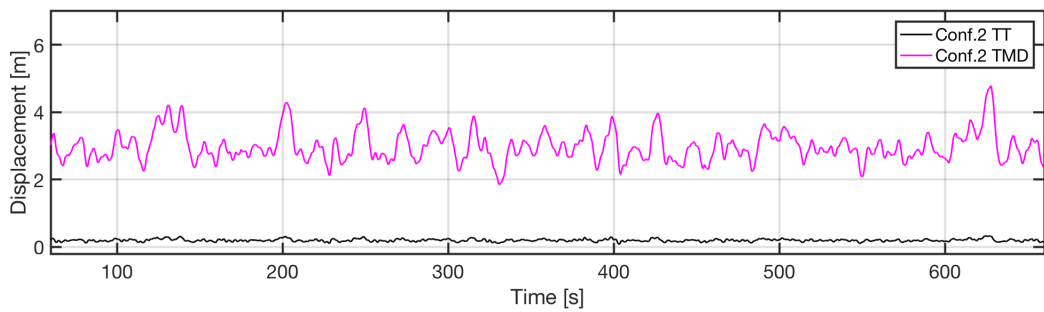


Figure A.32: Displacement of MATLAB Configuration 2 under 19mps wind.

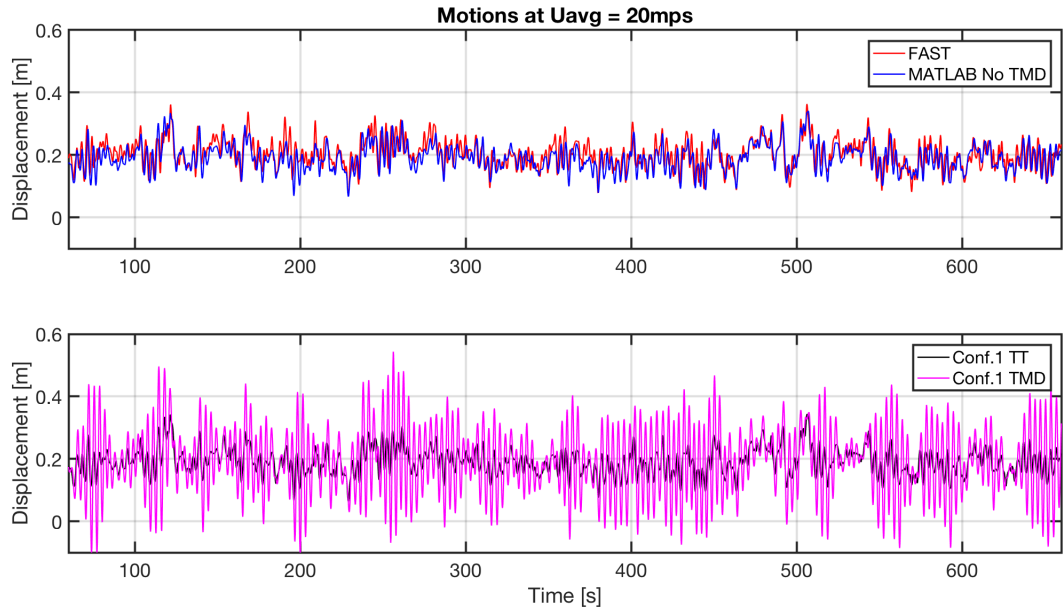


Figure A.33: Displacements of FAST and MATLAB Configuration 0 and Configuration 1 under 20mps wind.

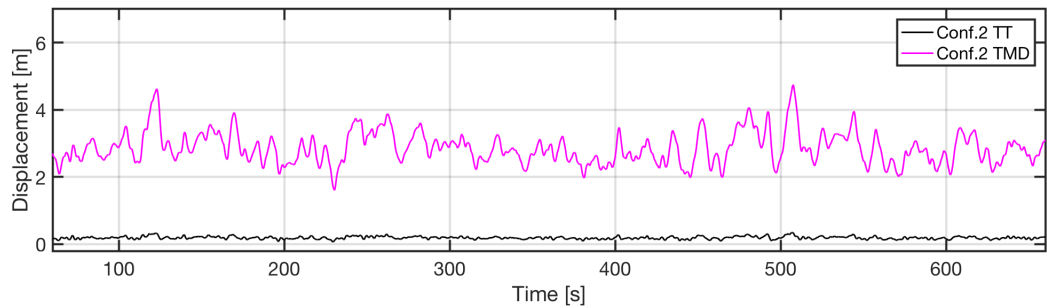
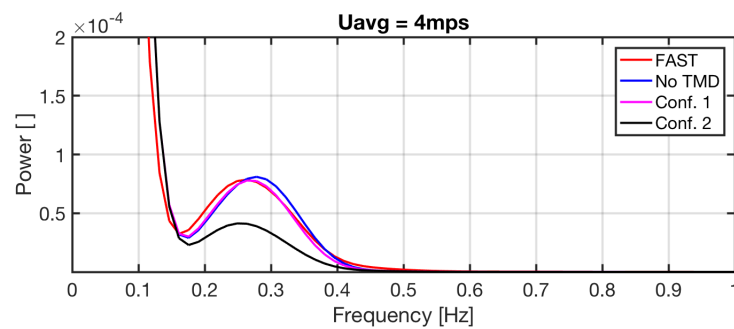
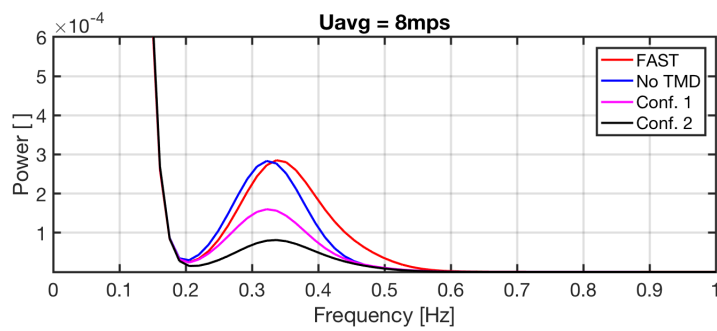
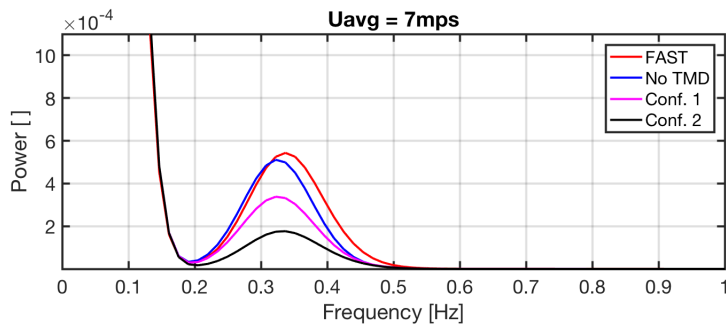
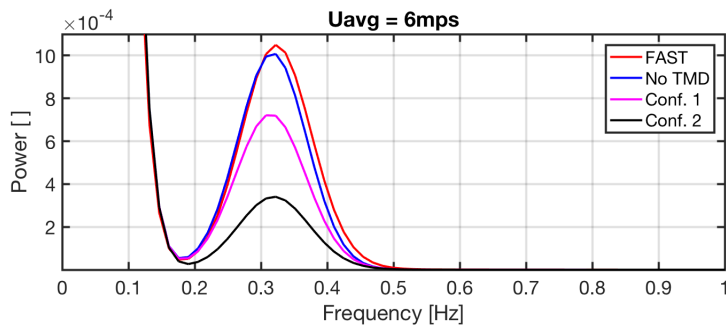
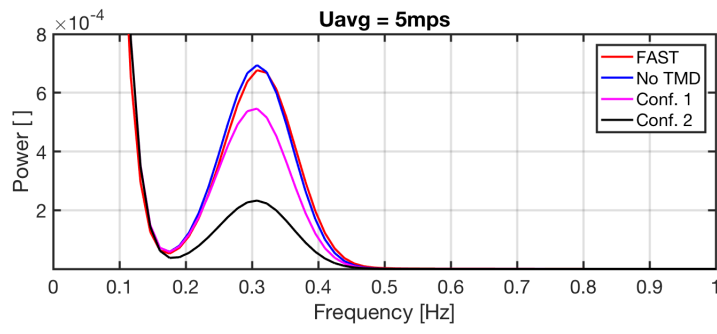
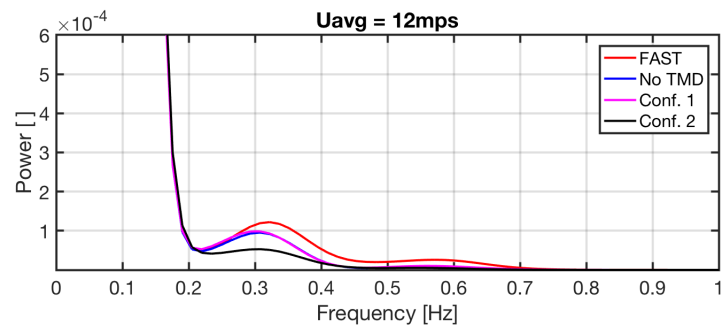
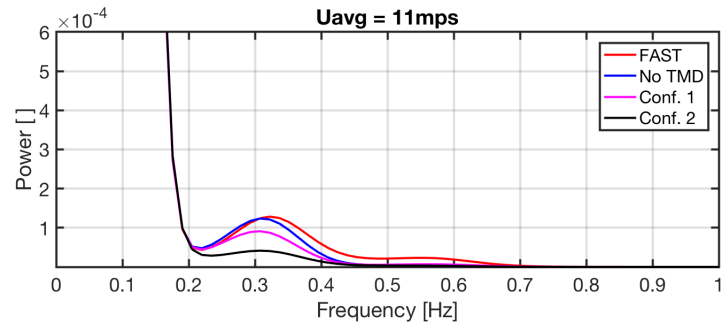
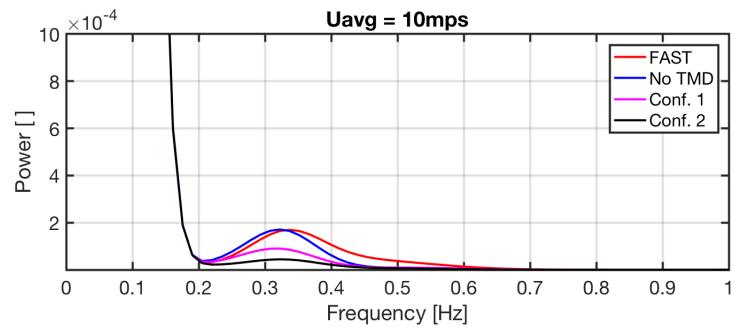
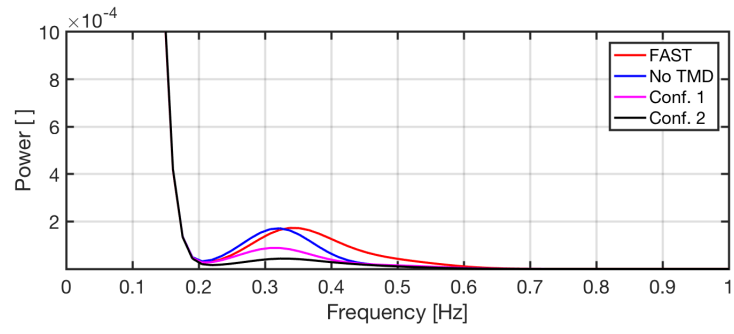


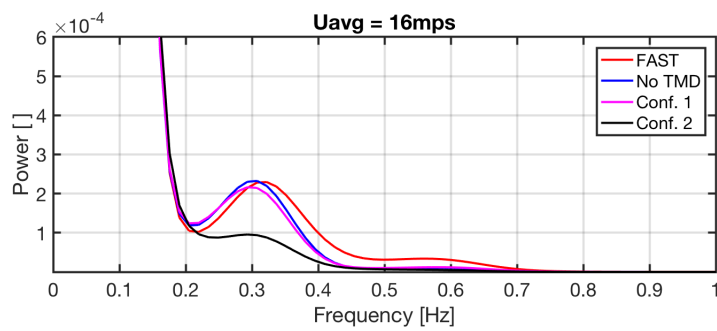
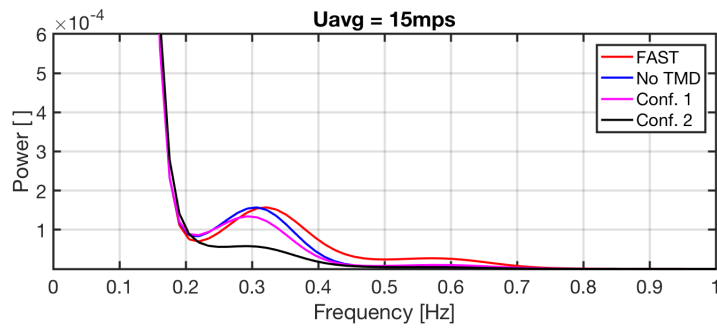
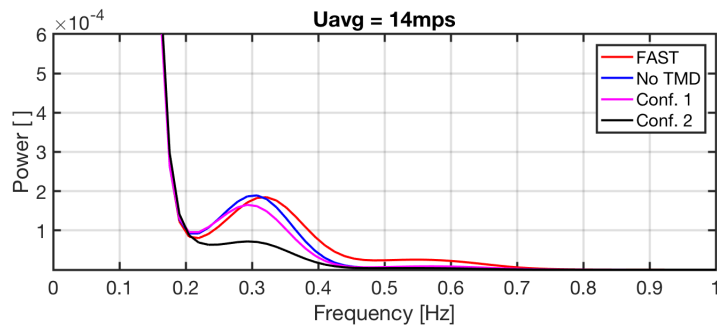
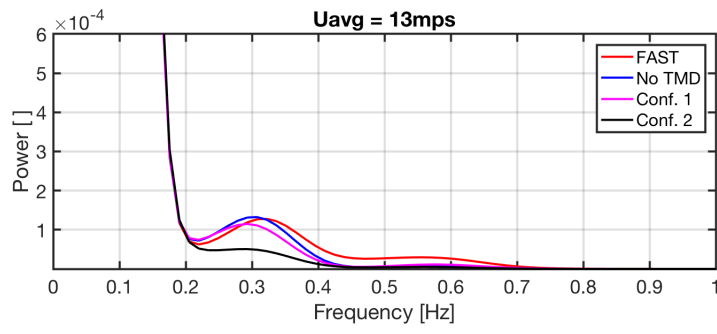
Figure A.34: Displacement of MATLAB Configuration 2 under 20mps wind.

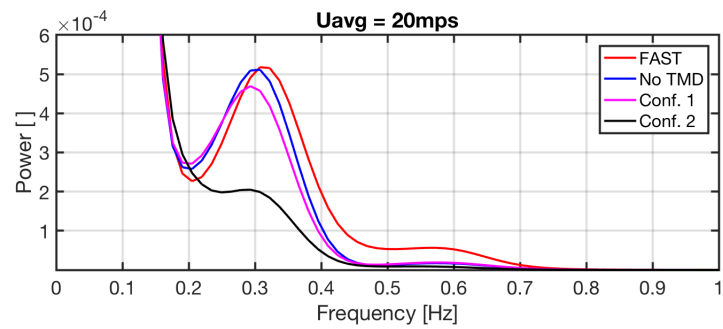
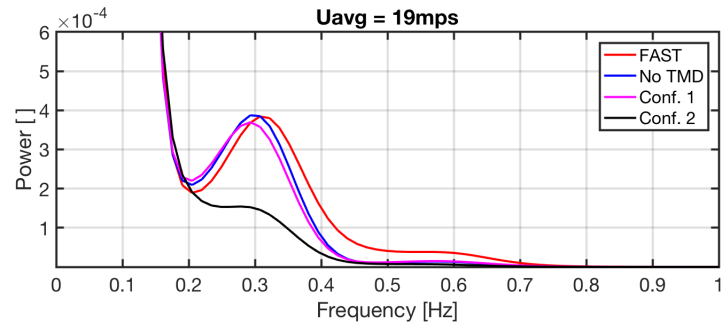
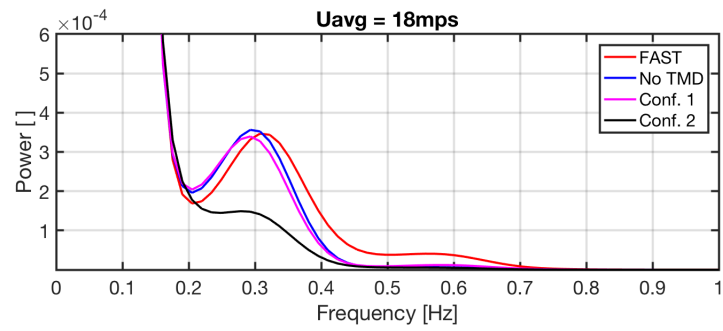
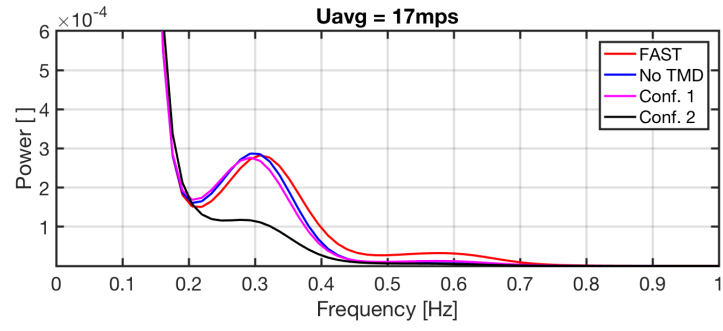
A.2. All PSDs for FAST and MATLAB thrust-excited simulations

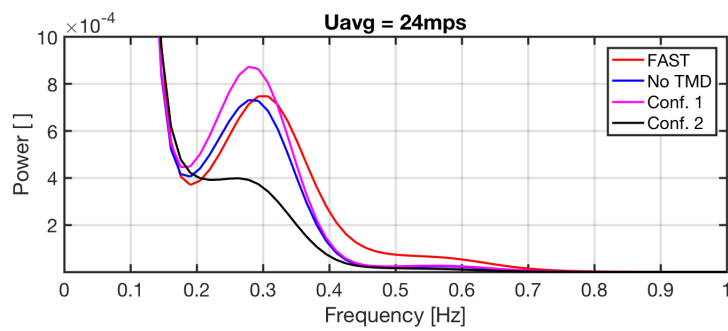
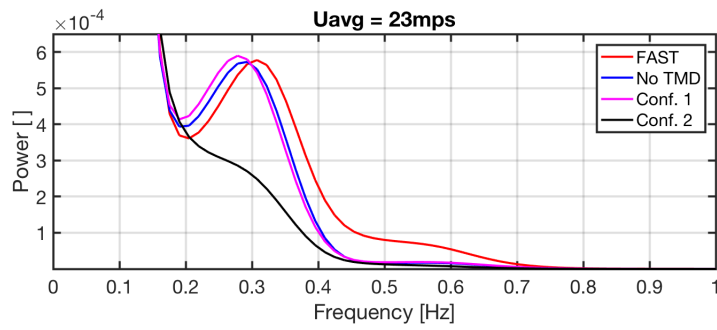
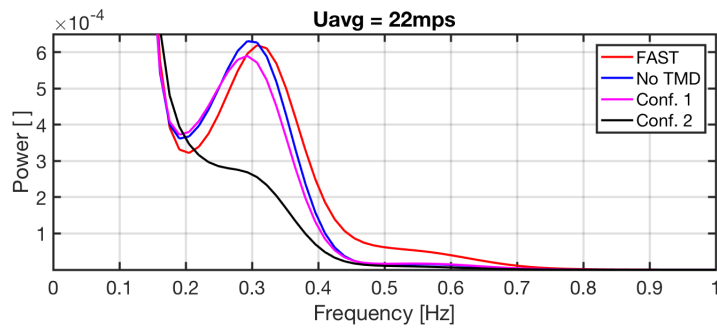
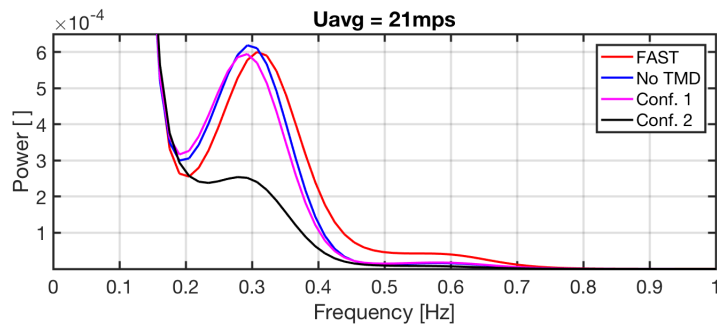


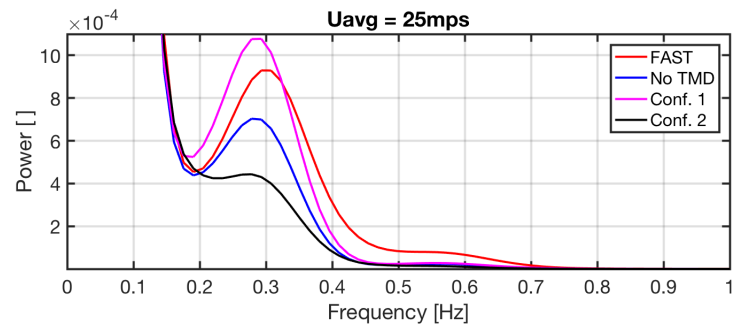












B

Modeling Using Wind Excitations

B.1. Failure of Simulations with Wind Excitation

By using wind to excite the MATLAB model, the simulations bypass the effects of control lag explained in Section 6.2.2, which are present in the thrust signals. The model having instantaneous control response will evidently behave different to the FAST model in the full load region, given that the thrust will follow exactly the given wind speed at each times step, as it does in Figure 6.6. However, in the partial load region, the behaviours should be as similar as possible.

In Figure B.1 the wind signal output from a FAST simulation can be seen in blue. This signal is taken from a single point in the rotor. The red curve is the signal of all data points over the rotor area, averaged at each time step. The two signals are clearly quite different from each other: the averaged signal is much less turbulent. This makes sense, since averaging turbulent signals always smooths out differences.

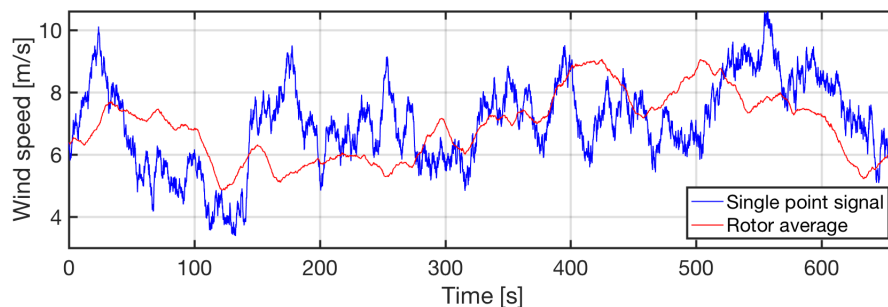


Figure B.1: Normal turbulence model wind signal with $U_{avg} = 7 \frac{m}{s}$

To test these, the MATLAB 1DOF model is excited with each of these wind signals, creating thrust as a time dependent value using the function described in Section 5.3.3. Figure B.2 shows that exciting the MATLAB model with the rotor-averaged wind signal results in a displacement curve very similar in shape to the wind. This makes sense, since forces varying with low frequencies relative to the natural frequency of the model will not cause dynamic excitation. Thus, with little dynamic excitation, the turbine moves essentially following the displacement dictated by Hooke's law, in Equation 6.1.

The displacements of the model excited by the 1-point wind signal, shown in black, resemble the real turbine much more, but not nearly enough to consider them sufficiently accurate for fatigue calculation purposes. Both signals seems to follow the same average, and the amplitudes are much more similar, but in some moments the MATLAB amplitudes become smaller or larger than those from FAST.

The reader must notice, however, that the displacements of the 1-point simulation follow rather well the wind signal that excites it (blue curve in Figure B.1). The high frequency displacement amplitudes are larger, but this is expected since dynamic excitations amplify the response.

Neither of these wind excited simulations emulate the FAST model to a satisfactory extent. Using one point assumes a highly turbulent fully coherent wind signal going through the entire rotor, a wind

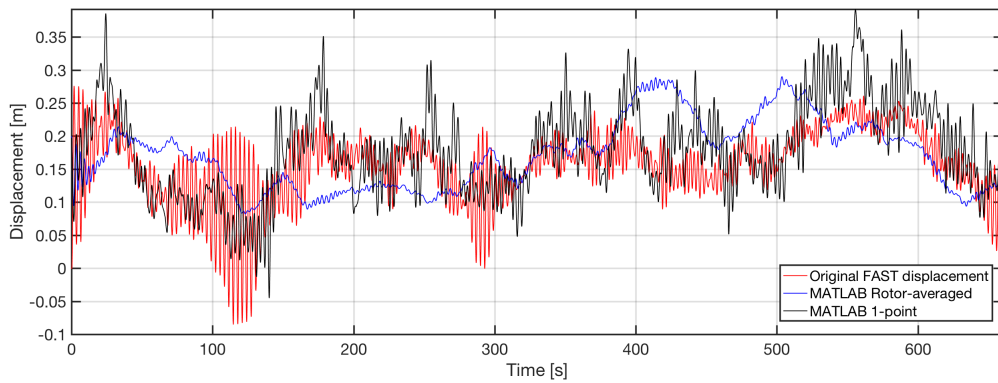


Figure B.2: Displacements of the MATLAB model with a 1-point and rotor-averaged wind signals, compared to original motions from FAST

signal that doesn't fully represent the wind felt by the FAST turbine. Using the full rotor-averaged signal smooths out a lot of the energy in the wind, resulting in a quasi-static response on the MATLAB model.

B.1.1. Rotor point wind averaging

In order to test the similarity between FAST and MATLAB in partial load under turbulent wind conditions, at each wind speed 8 points over the blade areas were chosen. The wind data from those points were averaged at each time step to produce a single-point wind signal that dictates the amount of thrust on the MATLAB model throughout the 660s simulation of a given wind speed.

The grid of wind data points experienced by the FAST turbine model, from which the aforementioned wind data were taken, is shown in Figure B.3. The locations sampled by the turbine in FAST of course change as the blades rotate, but choosing locations on the grid over the blades with Blade 1 at zero-degree azimuth (meaning pointing upwards) was considered to be a good enough approximation. For each blade, 6 points over the radius were chosen.

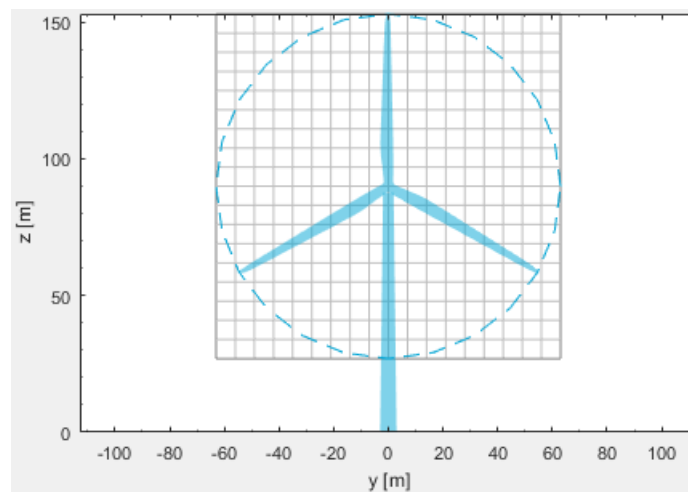


Figure B.3: Grid of wind data points that is sampled by the FAST turbine's rotor.

The accuracy of the MATLAB simulations with the chosen number of wind data points was gauged based on the power spectra of the motions of MATLAB compared to those of FAST. For example, the motions of a FAST simulation are shown in Figure B.4 in red along with the motions of the MATLAB model, in blue, that is excited by the 1-point wind signal output by FAST. By using 8 instead of 1 points over the rotor area to create a new wind signal, and using that to excite the MATLAB model, we get the signal shown in blue in Figure B.5, which behaves with much smaller amplitudes. This method is not giving the correspondence seen on the thrust-excited simulations in the main report. The power spectrum of each of these signals is shown on a linear vertical axis in Figure B.6. In it, we see that the

energy at the first natural frequency of the MATLAB model excited by the 18-point-averaged signal is much lower than the FAST signal.

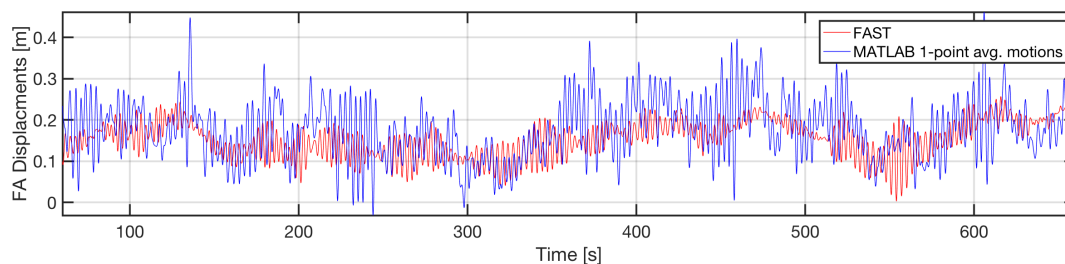


Figure B.4: Displacement of MATLAB model excited by a 7mps 1-point signal compared to original motions from FAST

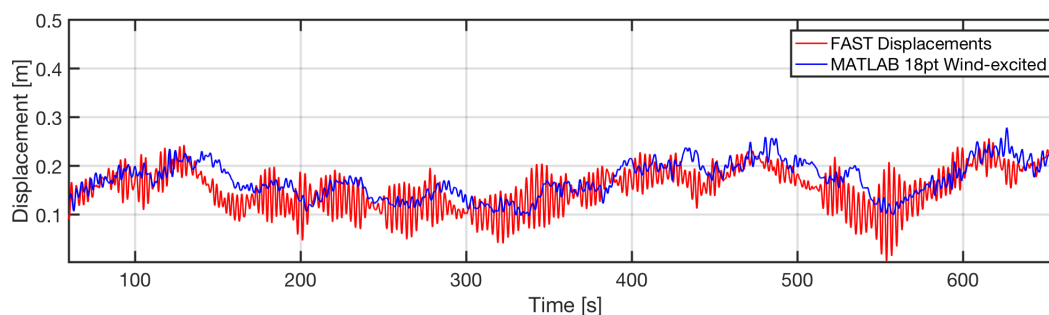


Figure B.5: Displacement of MATLAB model excited by a 7mps 18-point-averaged signal compared to original motions from FAST

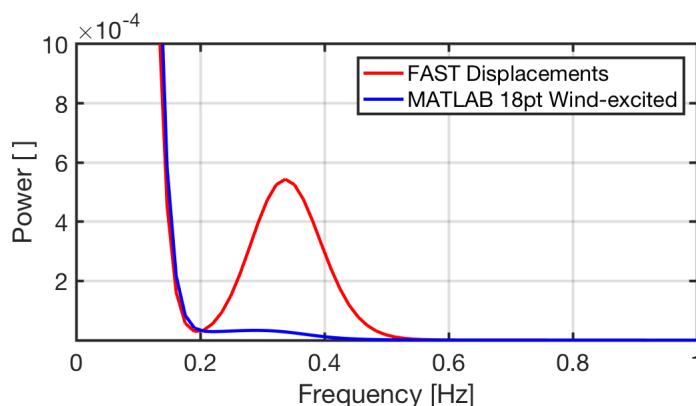


Figure B.6: Power spectral densities of the motion signals of Figure B.5

None of the MATLAB simulations using wind as a source of excitation are able to provide satisfactory correspondence with the FAST turbine. In an attempt to increase similarity, a similar number of wind points were used at different speeds to produce wind signals that would then produce motions in MATLAB that are more similar to those in FAST. Still, none of the simulations provide the level of correspondence seen from the thrust-excited simulations.

Moreover, at wind speeds above rated there is no method to establish what number of wind points are required to properly model the turbine. Since the motions are expected to be different because of instant "control" response, there is no reference for comparison on which to validate the model.

Given the time limitations of the project, the use of wind as an excitation source is left out of the main report text. The study of a super-stiff turbine, or a turbine model with instantaneous control response cannot be completed. Thus, given that meaningful results cannot be drawn, this segment of the project is left out of the Results Chapter.

B.2. Loads on a Super-stiff Turbine

Plotting the thrust signal for the super-stiff turbine "model" at $U = 12 \frac{m}{s}$ in Figure B.7, we can see the distinctive shape given by the wind crossing over the maximum point in the thrust curve. In the graph we see exactly where the thrust peaks, at $7.7e5N$. For comparison, Figure B.8 shows the thrust signal extracted from FAST for the same simulation. Both are shown on the same scale for ease of comparison. They seem to both have the same cycle frequency, and although the real turbine has larger low frequency amplitudes, its clear that the "instant" thrust signal has on average larger cycle amplitude. The lifetime fatigue equivalent load calculated for this turbine is $5.17e05[Pa]$, which is more than a 25% increase as compared to the real turbine.

This method depended on the use of wind excitations to calculate loads on the tower. Unfortunately, given that we cannot rely on the use of wind in the MATLAB model, no meaningful conclusions can be drawn from these calculations. Thus, just as the previous section, this procedure is left out of the main report.

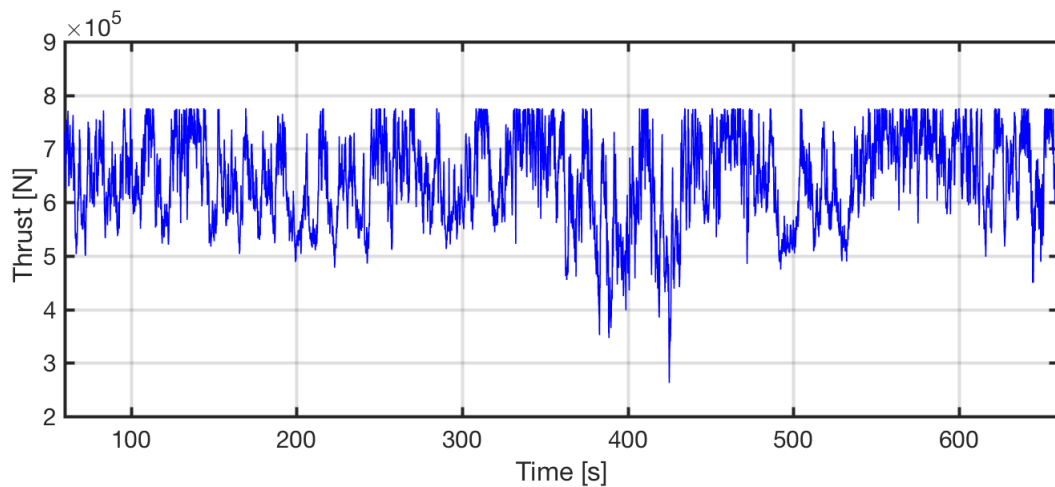


Figure B.7: Thrust on the rotor of "super-stiff" turbine, under 12[m/s] winds.

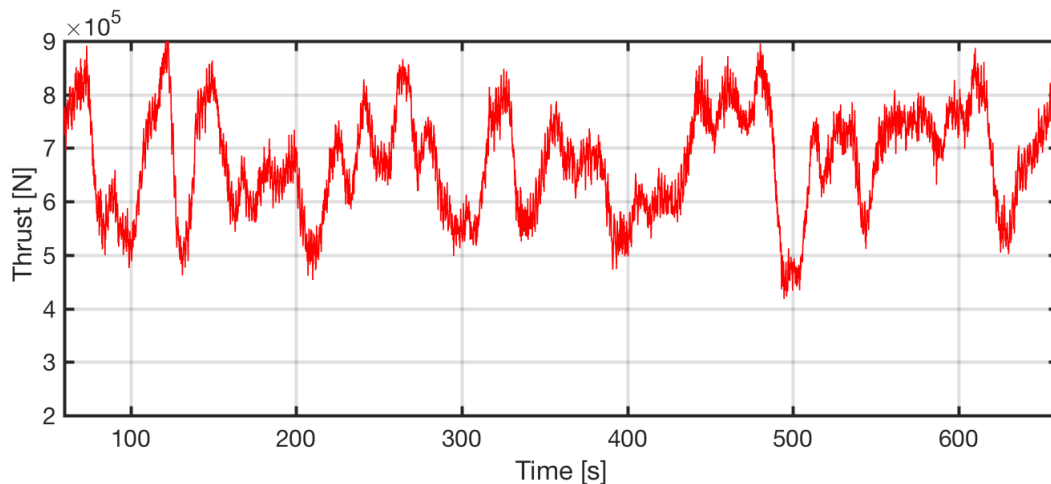


Figure B.8: Thrust on the rotor of the FAST turbine, under 12[m/s] winds.

B.3. Additional examples of wind-excited simulations

This section provides additional examples of the wind-excited MATLAB model. As is clear in the Figures, at none of the speeds here shown does the MATLAB model provide satisfactory behavior.

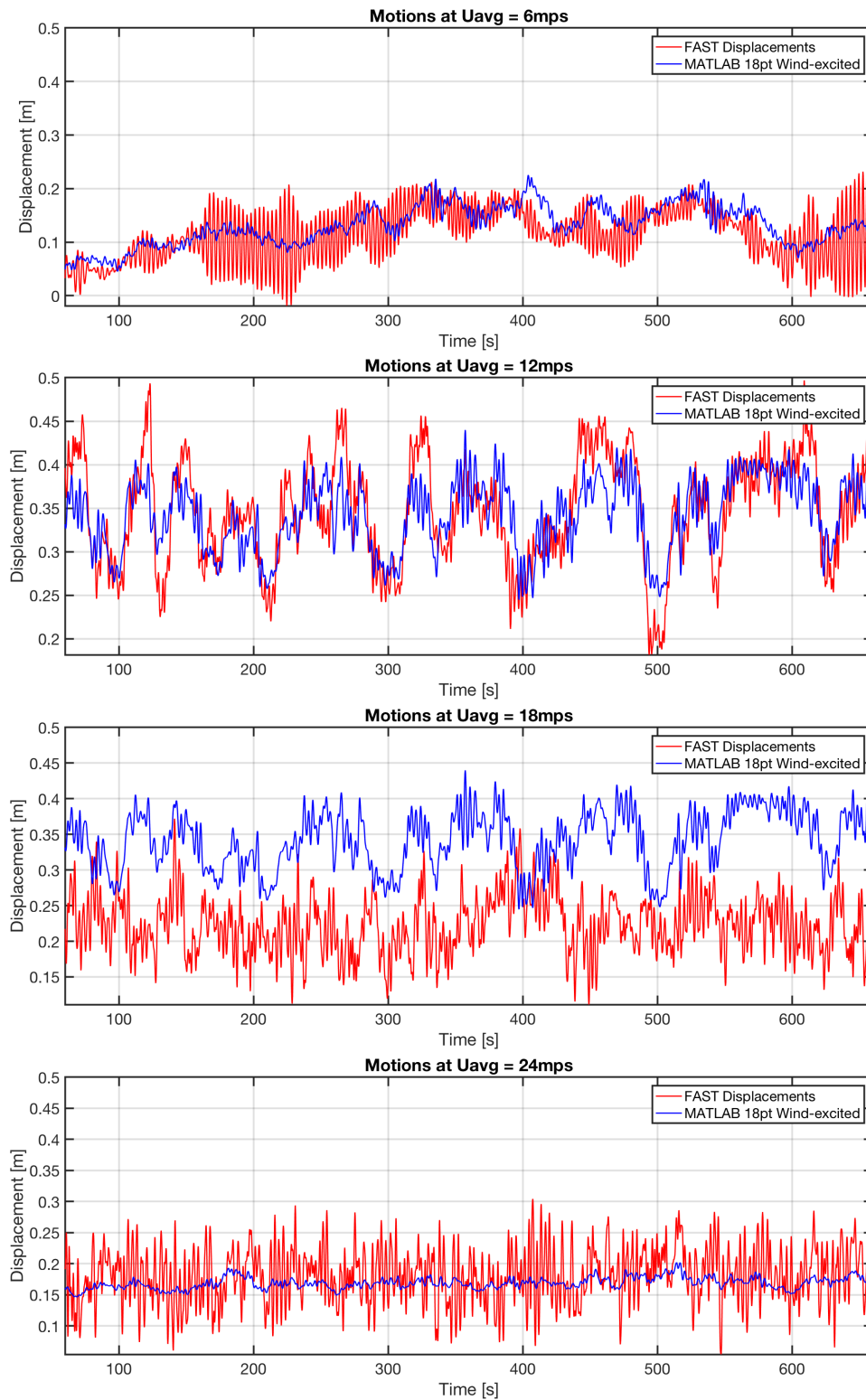


Figure B.9: Motions of the FAST turbine and 18 wind-point-excited MATLAB model.